Assessment of Meteorological Remote Sensing Products for Stream Flow Modelling Using HBV-light in Nyabarongo Basin, Rwanda

MPUNDU IGNACE SENDAMA
March, 2015

SUPERVISORS:
Dr ing. T.H.M. Rientjes
Ir. A.M. van Lieshout

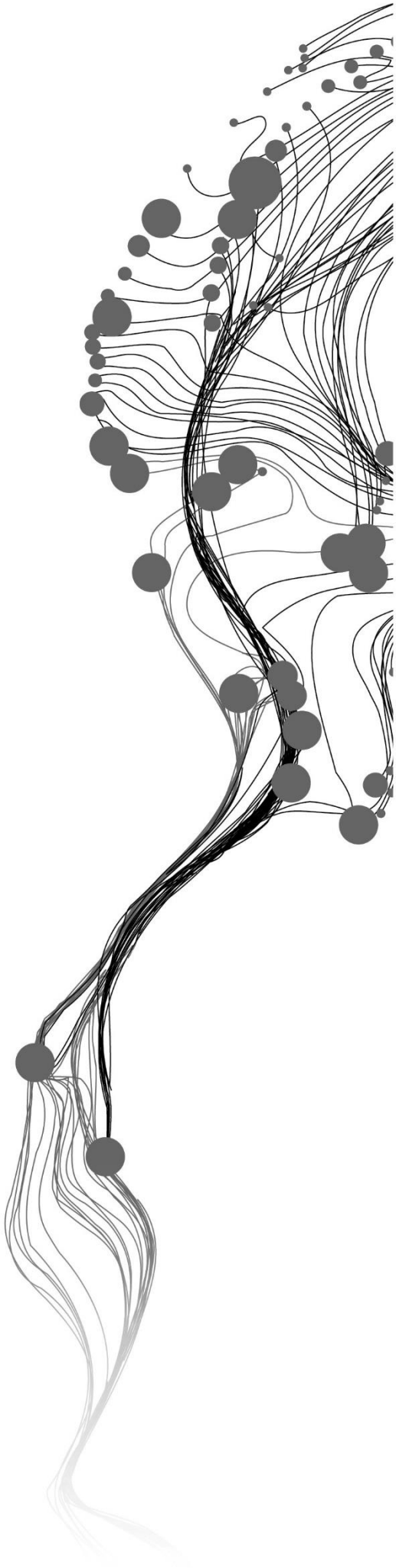

Assessment of Meteorological Remote Sensing Products for Stream Flow Modelling Using HBV-light in Nyabarongo Basin, Rwanda

MPUNDU SENDAMA IGNACE
Enschede, The Netherlands, March, 2015

Thesis submitted to the Faculty of Geo-Information Science and Earth Observation of the University of Twente in partial fulfilment of the requirements for the degree of Master of Science in Geo-information Science and Earth Observation.
Specialization: Water Resources and Environmental Management

SUPERVISORS:
Dr ing. T.H.M. Rientjes
Ir. A.M. van Lieshout

THESIS ASSESSMENT BOARD:
Dr. Ir. C. van der Tol (Chair)]
Prof. Dr. P. Reggiani (External Examiner, University of Siegen - Germany)

ABSTRACT

In hydrology, satellite based meteorological products are used to retrieve the components of the water cycle for water resources assessment and management, as they provide large spatial coverage on regular temporal scale.
Several authors report on systematic and random errors in these products. However, there is a number of methods that can be applied to correct these errors, in specific the systematic errors.

In this study four satellite meteorological products CMORPH 8km, RFE 2.0 and TRMM 3B42 v7 and FEWSNET PET were assessed and corrected for their systematic errors. After bias correction, these products were also evaluated as forcing data for stream flow modelling in HBV-light hydrological model.
This study was undertaken in Nyabarongo, a relatively well gauged basin of 8481.21km^2 located in Rwanda. The reference data was obtained from 21 meteorological stations that are distributed inside or at close distance to the basin. For this study daily time series data for a 5 years period (2009-2013) were used.

The differences between the data retrieved from the satellite based meteorological products and the gauge station measurements were estimated using statistical measures and analysis. The statistical measures involved the Bias measurements, the Mean Error, the Root Mean Square Error and the Coefficient of Regression. In addition, the total bias was split into its three components (Hits rainfall, Missed rainfall and False rainfall), to inspect which was the major source of the bias errors found in the satellite based meteorological products. The rainfall detection capability analysis of the satellite products was conducted by means of the contingency table score components such as the Bias Frequency, the Probability of Detection, the False Alarm Ratio and the Critical Index Success. These analyses were done by point to pixel comparison based to the location of the stations and their counterpart's products images pixels. Also areal representation of the meteorological variables from gauge stations and satellite products, was made to allow assessment at sub-basin scale.

The satellite based rainfall products were found to underestimate the depths of rainfall in the basin with a bias up to 0.67 (CMORPH 8km) and showed a low level of agreement with *in situ* observations with R^2=0.5% for TRMM 3B42 v7 as an example. The FEWSNET product was found to overestimate the PET observations in the basin. However, when used in HBV-light to simulate the Nyabarongo stream flow, the model showed very good performance with NSE=0.958 for the bias corrected data, and NSE=0.918 for the uncorrected product data.
Good model performances were also observed when the bias corrected satellite rainfall time series replaced the *in situ* measurements in the model. On the other hand, the model performances were found not satisfactory with NSE < 0.5, when the uncorrected satellite rainfall products were used as forcing data in HBV-light hydrological model.

Keywords: Satellite meteorological products, Bias correction, Stream flow modelling, HBV-light, Nyabarongo basin.

ACKNOWLEDGEMENTS

First and foremost, all praises and thanks be to the Almighty GOD for His sustenance and protection throughout the duration of my studies in the Netherlands.

I wish to express my sincere appreciation to the Netherlands Governments under the Netherlands Fellowship Programme for granting me the opportunity to study at the University of Twente. A special word of thanks goes to the staff of the ITC/WREM department, for their valuable support and ardent commitment, which gave me a good learning atmosphere.

I am deeply indebted and grateful to my first supervisor Dr. ing. T.H.M Rientjes for his constructive comments, technical advices, patience, guidance and encouragement all through this research. I highly appreciate the devoted time you gave to my work, and I have surely learnt a lot during the entire period of this research. I would like to acknowledge my second supervisor Ir. A.M. van Lieshout for his kind support and constructive comments. I am grateful for the time you dedicated to review my work.

My thanks also go to all offices and personalities who provided the needed data for my research, the Ministry of Natural Resources of Rwanda in particular, through its RNRA and RMA agencies. I extend my gratitude especially to Mr Kabalisa Vincent de Paul, head of the Integrated Water Resources Department, for his support, motivation and encouragement to pursue my studies at the ITC.

I wish to express my deep sense of appreciation to my colleagues Marc, Sonam, Henry, Irene, Fred, Gilbert, and Elias for their good companionship and support throughout the period of my MSc study. May the Heavenly Father continue to guard, guide and grant you all tremendous success in your endeavours.

Last but not least, I wish to express my unreserved and profound gratitude to my family and friends, for their incomparable moral support and constant prayers which kept me motivated.

TABLE OF CONTENTS

LIST OF FIGURES

LIST OF TABLES

LIST OF ABBREVIATIONS

amsl	above mean sea level
AMSRE	Advanced Microwave Sounding Radiometer-Earth Observing System
AMSU	Advanced Microwave Sounding Unit
BF	Bias Factor
CMORPH	CPC morphing technique product
CPC	Climate Prediction Center
CSI	Critical Success Index
DEM	Digital Elevation Model
DMSP	Defense Meteorological Satellite Program
FAR	False Alarm Ratio
FB	Frequency Bias
FEWSNET	The Famine Early Warning Systems Network
GDAS	Global Data Assimilation System
GMS	Geostationary Meteorological Satellite
GOES	Geostationary Operational Environmental Satellites
GTS	Global Telecommunication System
HBV	Hydrologiska Byråns Vattenbalansavdelning model
ILWIS	Integrated Land and Water Information System
IPCC	Intergovernmental Panel on Climate Change
ISOD	*In situ* and Online Data
ITCZ	Inter-Tropical Convergence Zone
LANDSAT ETM	The Landsat Enhanced Thematic Mapper
ME	Mean Error
MSG	The METEOSAT Second Generation
NOAA	National Oceanic and Atmospheric Administration
NSE	Nash-Sutcliffe Coefficient
PET	Potential Evapotranspiration
PMW	Passive Microwave
POD	Probability of Detection
POES	Polar Operational Environmental Satellites
PTQ	Precipitation-Temperature-Discharge
RFE	Africa Rainfall Estimation Algorithm Product
RMA	Rwanda Meteorological Agency
RMSE	Root Mean Square Error
RNRA	Rwanda Natural Resources Authority
RVE	Relative Volume Error
SRTM	Shuttle Radar Topography Mission
SSM/I	Special Sensor Microwave/Imager
TMI	The TRMM Microwave Imager
TRMM	Tropical Precipitation Measuring Mission
USGS	United States Geological Survey
WGS	World Geodetic System
WV	Water Vapor

1. INTRODUCTION

1.1. Background

Water resources have a vast impact on the economic development and environment protection for countries all over the world (Gleick, 2000). Being a cross cutting resource in different activity sectors such as agriculture, energy, domestic use, transport, recreational etc., its planning and management is an important component for development processes. Thus, for a good water assessment, planning and decision making in water management, quantification of the spatial and temporal changes of water balance variables is crucial (Wagner, Kunstmann, Bárdossy, Conrad, & Colditz, 2009).

Water assessment studies require reliable information on the water cycle components. The main aim of water resources assessment is to quantify and to qualify water in a system by means of data collection and other water accounting techniques.
The land-atmosphere boundary is considered to be the start of the water cycle with precipitation as the major input and evapotranspiration as the major output from the surface view (Brutsaert, 2005). On the land surface, flow measurements in river channels are the common way to assess surface water availability for a given area.

Water resources management in Rwanda is a sector still under development. The Integrated Water Resources Management Department was established in 2011, with the mission to manage and resolve all the matters regarding the water resources in the country. In 2013 the Water Resources Master Plan in Rwanda was developed to serve as a baseline for sustainable water resource management.
During its exploratory phase, the developers of the Rwanda Water Resources Master Plan, raised many queries related to the hydrological infrastructures and data availability within different catchments in the country (SHER Ingénieurs-Conseils s.a., 2012). In addition, insufficient meteorological data was observed due to deteriorating *in situ* stations and poor data collection procedures, as it has been reported by Mikova, Garba, & Nhapi (2010).

The information on precipitation and evapotranspiration, which is referred here as meteorological information, can be collected from ground stations but also from remote sensing. Thiemig, Rojas, Zambrano-Bigiarini, Levizzani, & De Roo (2012) and Sun et al.(2012) have explored the usability of satellite based meteorological products, respectively precipitation and evapotranspiration, over Africa. As investigated by Dinku et al.(2007), most often in developing countries the distribution of ground stations is sparse, and available data are insufficient to describe the highly spatial variability of meteorological variables. Therefore on the inclusion of a remotely sensed meteorological variables might be necessary to substantially improve the description of the water cycle components.
Satellite based meteorological products are abundantly available with a sufficient level of accuracy on a global scale (Ebert, Janowiak, & Kidd, 2007). But when used on a regional or local scale, these products need to be handled with caution as algorithms associated to each product, have their strengths and weaknesses that affect their accuracy (Huffman, Adler, Bolvin, & Nelkin, 2010). For that reason, it is essential to evaluate these products before using them in water resource assessment studies.

As aforementioned, in hydrology, surface water assessment can be done by Gupta (2010) water flow measurements which requires onsite gauge stations. In poorly gauged basins, hydrological models can be

used to provide a good understanding of the hydrological processes. Hydrological models are defined by Beven (2011) as simplified conceptual representation of a part of the hydrologic cycle that simulates the input-output response behavior of the real-world system. And as defined by hydrological models ordinarily incorporate hydrological and meteorological data coupled with the real world characteristics such as initial and boundary conditions, and the hydrologic stresses of the area understudy to simulate the its hydrological processes.

1.2. Study Releavance

To date, the development of water resources management in Rwanda is still facing challenges as partly caused by lack of reliable hydro-meteorological information. To overcome this shortage of *in situ* measurements, remotely sensed meteorological data can be used as alternative data source as shown in recent studies by Thiemig (2014) Considering Rwanda's complex topography, for hydrological modelling these remotely sensed meteorological data need to be reliable in representing the meteorological conditions both gauged and ungauged catchments in the country. Nyabarongo basin, being one of the most gauged catchment in Rwanda, was considered suitable for the validation of the satellite products. Hence, this research focusses on assessing the usefulness of meteorological remote sensing products as model inputs to simulate the stream flow of Nyabarongo River.

In addition the same Nyabarongo basin, urgently calls for proper management in order to resolve conflicts related to water allocation for different sectors such as agriculture and water supply (ENTREM Ltd, 2012). It is also the most populated and the most urbanized basin in Rwanda as it includes the capital city Kigali, where the water demands of intensified social-economic development is very high. Furthermore, floods are becoming a threat in its downstream during rainy seasons as it has been investigated by Bizimana & Schilling (2010). A better hydrological characterization of the catchment can contribute to better water resources management plans of this basin.

1.3. Problem Statement

Remotely sensed data can be used for data retrieval in areas where there are insufficient *in situ* measurements or limited accessibility to available data. However, satellite data should be assessed for their accuracy, which is done by verifying the satellites estimates against *in situ* measurements. It is assumed that *in situ* measurements give the true representation of the real world (Ebert, 2010). This verification is done because a variety of potential errors, originate in the satellite data from e.g. irregular revisit times of observing sensors, and defaulting algorithms for specific products (Thiemig, 2014)

The potential use of meteorological satellite data to overcome the shortage of *in situ* data in hydrological domain, found promising in some other parts of the world (Artan et al., 2007), has not yet been explored in Rwanda. Though, knowing that the usefulness of satellite based hydrological applications is, to some degree, determined by the accuracy of the collected meteorological information, this study assesses the most commonly used remotely sensed meteorological products over one of the relatively well gauged basins in Rwanda.

For this study, 3 satellite based rainfall products and 1 evapotranspiration product were selected. The meteorological satellite products were selected according to their availability over the basin with sufficient long time series, and good temporal and spatial resolution. Moreover, the fact that these images are freely available, widely used and their algorithms are considered to be the state of the art (Dinku, Connor, & Ceccato, 2010) was taken into account as well. Therefore, the Climate Prediction Center morphing technique product (CMORPH), the Africa Rainfall Estimation algorithm product (RFE) and the Tropical Rainfall Measuring Mission TRMM 3B42 product were selected for the precipitations component. And

the Famine Early Warning Systems Network Global PET product was selected for the evapotranspiration component.

1.4. Objectives and Research Questions

1.4.1. Objectives

The main objective of this research is to assess various satellite based meteorological products as input for stream flow modelling in Nyabarongo basin using HBV-light.

The specific objectives are;

- To evaluate the precipitation and potential evapotranspiration satellite based products in reference to the *in situ* data.
- To correct the systematic errors in the precipitation and potential evapotranspiration satellite based data.
- To define the basin's elevation vegetation zones to serve as inputs for stream flow modelling in HBV-light model.
- To simulate Nyabarongo daily stream flow using bias corrected satellite based data.
- To determine the most accurate meteorological satellite products for Nyabarongo stream flow modelling.
- To compare the model water balance components in the basin, when satellite based meteorological data and in *situ* observations are used in the model.

1.4.2. Research Questions

- How well relate satellite observations to *in situ* data?
- What is the magnitude of the error for the meteorological remote sensing products, at the stations and on a sub-basin scale?
- What are the land cover classes and elevation zones to represent the basin for stream flow modelling in the HBV-light model?
- What is the performance of HBV-light model combined with bias corrected satellite based meteorological data in simulating Nyabarongo daily discharge?
- Which satellite products are most reliable for Nyabarongo stream flow modelling in HBV-light?
- What are the differences in the water balance components based on the model outputs, when *in situ* and the satellite meteorological products are used in the model?

1.5. General Methodology

This research can be separated in 3 distinct periods, the pre-field work, the field work and the post-filed work phase.

1.5.1. Pre-field Work

Before the field work, the activities regarding this research consisted of literature review. Gathering knowledge on the techniques and methods needed to conduct this study from previous studies and discussions with the supervisors. HBV-light model was acquired and installed, the process of downloading the satellite based data was initiated.

Also during this period, preparations of the field work started. Here contacts with offices where *in situ* data were to be collected were made, and a work plan for the period in the field was developed.

1.5.2. Field Work

In this phase, data to conduct this study were collected from different institutions in Rwanda.
Water levels of Nyabarongo River at Ruliba station; the outlet of Nyabarongo Basin, were collected from Rwanda Natural Resources Authority.
Meteorological data for the whole country, such as daily rainfall, temperature, and evaporation were collected from Rwanda Meteorological Agency.
Site visits in the basin were done in order to gather more information on the study area and its hydrological characteristics, as well as to inspect on the state and the locations of the hydro-meteorological stations.

1.5.3. Post-field Work

After field work, the infilling of the *in situ* data and data analysis followed. Then the assessment of the remotely sensed meteorological products took place in in reference to the *in situ* data. After that, the bias error in the satellite data was corrected to improve the remotely sensed data for hydrological modelling. Finally the results of the modelling with respect to different satellite products were analysed.
In general, the steps followed in this research can be summarized in the diagram shown in Figure1-1.

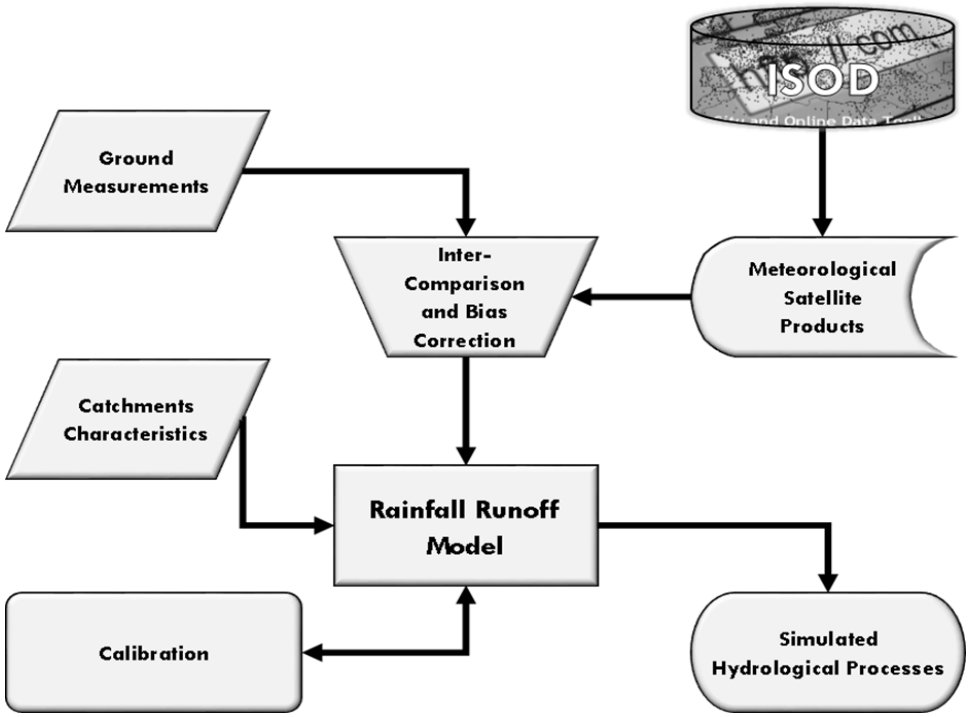

Figure 1-1: Diagram showing the steps followed in this study

1.6. Thesis Outline

This thesis is has six chapters. The first chapter introduces the research topic and a brief background on the use of meteorological remote sensing products in hydrological modelling. In the same chapter, the problem statement, the research objectives, and the research questions are presented as well. The second chapter describes the available data and the study area with its location, topography, climate and land cover. A literature review on which this study is scientifically based on is presented in Chapter 3. Chapter 4 addresses the materials and methods used to conduct this research. The results obtained by the study and their discussions are in Chapter 5. Chapter 6 concludes this study with recommendations for future studies.

2. STUDY AREA AND DATA AVAILABILITY

2.1. Study Area

2.1.1. Location

The study area of this research, Nyabarongo basin, is part of the Nile basin in Rwanda and it is recognized to be the source of the Nile River. Nyabarongo basin covers three sub-basins of the nine major sub-basins covering the country. Nyabarongo basin is made of Mukungwa sub-basin in the North, Nyabarongo upstream sub-basin in the South and Nyabarongo downstream sub-basin at the East. Nyabarongo basin is entirely located within Rwanda between 1° 18' S to 2° 34'S latitude and 29° 15' E to 30° 35' E longitude with a total area of 8481.21km². Nyabarongo River is the largest river in the country.

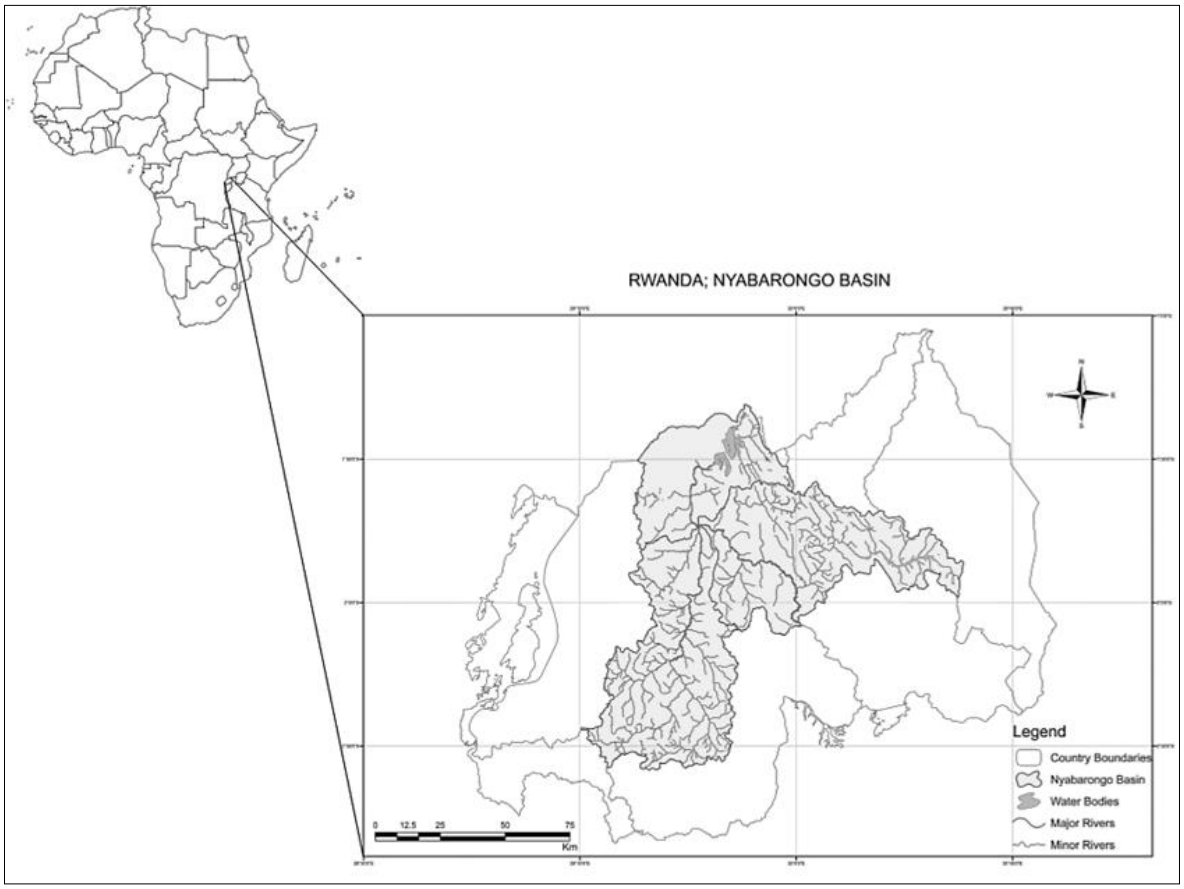

Figure 2-1: Location of the study area with the water bodies and the river network added.

2.1.2. Climate

At the website of the Rwanda Meteorological Agency (RMA) (http://www.meteorwanda.gov.rw/), it is described that Rwanda has a bimodal pattern of rainfall, which is driven mainly by the progression of the Inter-Tropical Convergence Zone (ITCZ)

Rwanda has a moderate tropical climate due to its high altitude. The average rainfall in the study area is slightly above 1200mm per year distributed in two distinct rainy seasons; the long rains season from March to May with about the half of the total year rainfall and the short rains season from September to

December. The average temperature in the study area is between 17 and 20°C. The spatial distribution of the temperature and the rainfall varies with the topography in the Basin.

2.1.3. Topography

The elevation of Nyabarongo basin varies from 1342m to 4480m (a.m.s.l) as shown below in figure 2-2. It covers a mountainous area with steep slopes in the volcanic region in the north and at the Congo-Nile divide in the west. Nyabarongo basin has a rugged relief made of steep hills separated by deep valleys. The eastern part has more moderate slopes with a broad valley in the downstream of the basin where floods have, in the recent years become a serious issue.

2.1.4. Land Cover

As in most of the regions in Rwanda, rain-fed agriculture is the major economic activity in Nyabarongo basin. Natural forests, forest plantations and scattered woodland cover a considerable portion of the basin as well, mostly on the top of the hills. The built up area is considerable as Nyabarongo basin includes a large part of the capital city, Kigali along with some other major cities in Rwanda namely, Musanze, Huye and Muhanga.

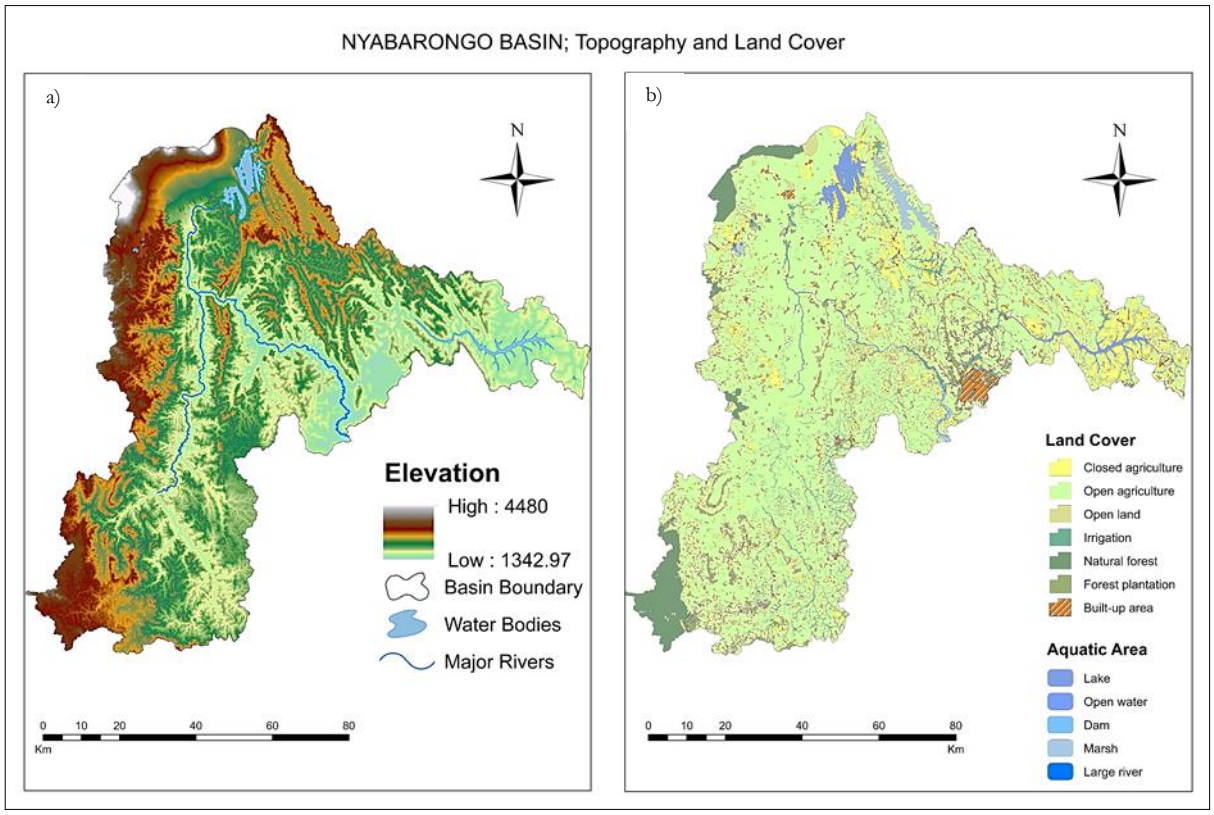

Figure 2-2: Maps showing the Topography (a) and the Land cover (b) of the study area of Nyabarongo basin (This study)

2.1.5. Hydrology

Nyabarongo basin has a dense network of rivers, several wetlands and lakes, next to some small scale irrigation agriculture. In the basin several hydropower plants are present and others are to be constructed. For example, Ntaruka hydropower located between Lake Burera and Ruhondo in the North, Nyabarongo 1 hydropower in is Nyabarongo upstream sub-basin and Nyabarongo 2 hydropower which is planned to be built in Nyabarongo downstream sub-basin.

2.2. Data Availabily

2.2.1. Meteorological Data

In Rwanda meteorological data have been collected since 1907. Up to date, 183 stations were counted in the country, unfortunately a big number of them are not operational anymore and also few of them were installed very recently.

Those meteorological stations are manually operated, and they are classified in 3 types:

- The Agro Synoptic Stations are only 12 in the whole country. They are called 'main stations' as they measure a large number of meteorological parameters such as rainfall, minimum and maximum temperature, soil temperature, wind speed and direction, relative humidity, sunshine hours, evaporation, soil moisture deficit, atmospheric pressure, solar radiation; etc. They are operated by permanent staff of RMA on a daily basis. For this study they were considered as reference stations.
- The Climatological Weather Stations measure rainfall as well as surface air temperature only. Those are followed up by voluntary observers under the supervision of RMA.
- Rainfall Weather Stations which measures only rainfall are followed up by voluntary observers as well and some of them are owned by private people who send records to RMA.

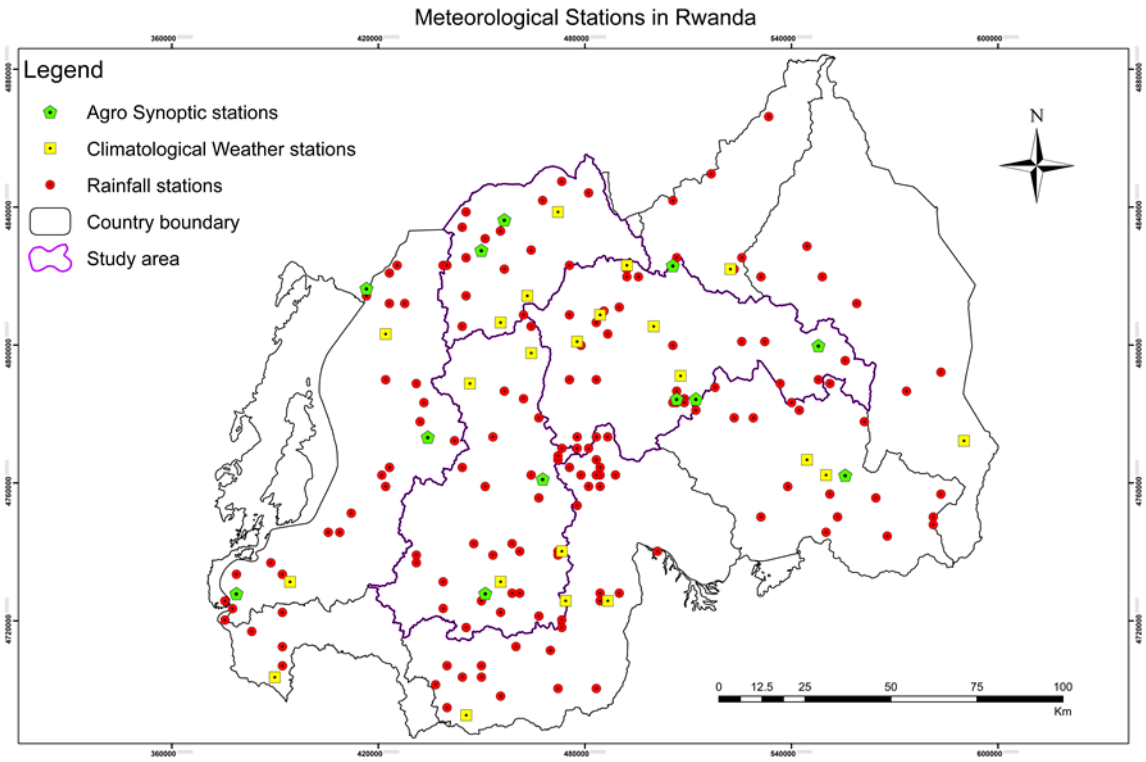

Figure 2-3 Figure 2 3: Meteorological stations in Rwanda. (This study)

Rainfall Station Data

Screening of the rainfall time series covered the period 2009-2013 based on the period the satellite rainfall products; were available. For this study 87 rainfall stations were suitable for further use. As many stations showed big data gaps, screening also served to identify stations with at least two complete years and resulted in 37 stations which covered the whole country.

Evapotranspiration Station Data

Only Agro Synoptic stations measure Evaporation in Rwanda. At those stations the evaporation is measured by use of "Class A" evaporation pans, for the determination of the quantity of evaporation at a given location. Measurements are assumed to be equivalent to the Potential Evapotranspiration (PET), as by definition PET is the amount of evaporation that occurs when a sufficient water source is available.
Among the 12 Agro Synoptic stations, 10 had the evaporation data. For the period of 2009-2013 only 6 stations were operational. This set of stations was considered sufficient to estimate PET for this study as PET is not characterized by very large spatial variability as rainfall is.

Temperature Station Data

As aforementioned, in Rwanda air temperature is measured by Agro Synoptic stations and Climatological Weather Stations. The minimum and maximum daily temperature has been measured by 100 stations which are distributed over the country. The two measurements are used to estimate the mean daily temperature by simple arithmetic averaging. For the period of 2009 to 2013, 26 stations were selected based on time series completeness.

2.2.2. Hydrological Data

For rainfall-runoff modelling in Nyabarongo river basin, discharge measurements recorded at the outflow of Nyabarongo downstream catchment and known as Ruliba station were collected during fieldwork. Daily water levels have been recorded from Ruliba station since 1955, by various organizations during different periods (Also at certain dates Nyabarongo river discharge was measured directly at the same location using current meters.)
Voluntary observers used to record water level three times a day which are kept by Rwanda Natural Resources Authority. Since 2012 gauge measurements are automated by a data logger which records hourly water levels at Ruliba station.

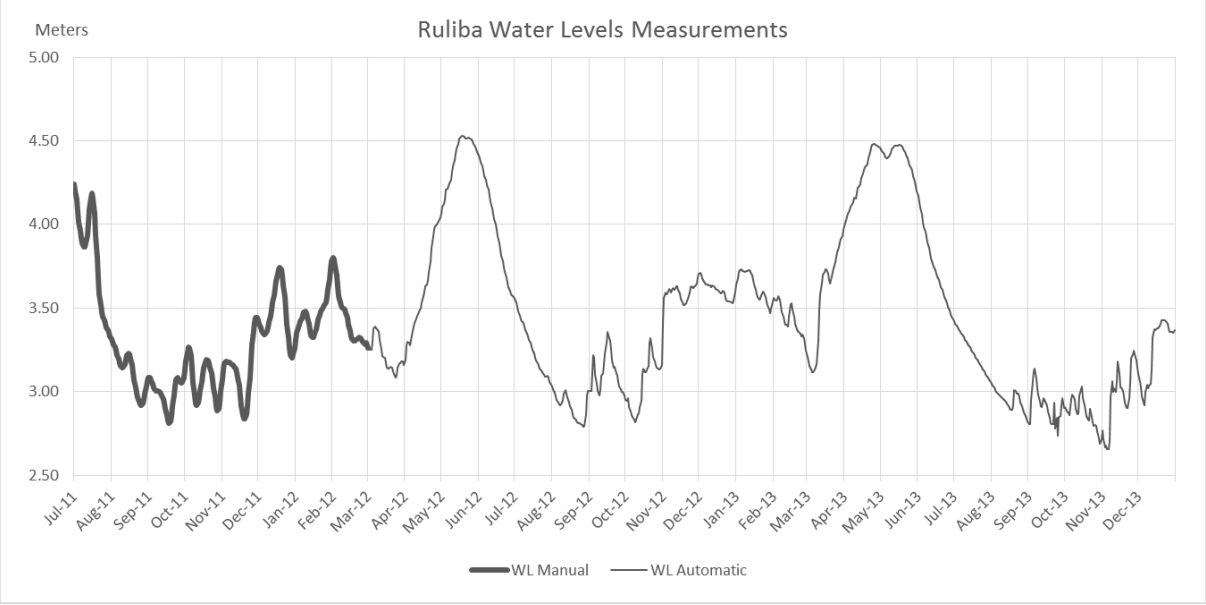

Figure 2-4: Water levels measurements at Ruliba Station (July/2011 to December/2013)

3. LITERATURE REVIEW

3.1. Meteorological Remote Sensing and Reliability

Remote sensing data has been used in hydrological studies for decades now. Ever since the 1960's when the first meteorological satellites were launched, methods for deducing water cycle variables from space rather than gauge measurements were improved from time to time.

Water cycle dynamics takes place at a wide range of spatial and temporal scales which makes it complex to observe and stresses to explore applicability of satellite based observations available from various platforms. Satellites may be geostationary or in a polar orbit and use a range of spectral bands to retrieve meteorological data from space.

Rainfall being a very important component of the hydrological cycle, is a main input to hydrological modelling and in particular rainfall-runoff modelling. Hence, understanding rainfall is the underlining process for various hydrological research studies. Rainfall happens when humid air raises, cools down and condense to form cloud droplets, several millions of cloud droplets are required to make one raindrop, the latter will grow till its fall velocity exceeds the rate of uplift and fall from clouds to the earth (Brutsaert, 2005).

In order to improve spatial rainfall estimation product from, satellite rainfall algorithms which incorporate the physical basics of rainfall formation and evolution, were developed for different time and space resolution.

The main aim of rainfall monitoring using satellite is to derive data on the occurrence, amount and distribution of rainfall on the earth for different purposes.

Various methods have been developed for rainfall estimation, which rely on the visible (VIS), infrared (IR), near infrared (NIR), water vapor (WV) and microwave (MW) bands of the electromagnetic spectrum (Kummerow & Giglio, 1994). Both IR and MW will be discussed in the following subsections as they are the most used.

Geostationary weather satellite commonly rely on VIS and IR sensors. They have a large space coverage to capture the growth and decay of precipitating clouds at small time intervals up to 15 minutes. Polar orbiting satellites commonly rely on MW sensors and provide images at low temporal resolution but with higher spatial resolution resulting in more direct observation of cloud profiles.

3.1.1. Infrared Based Methods

The IR band sensors commonly are mounted on geostationary satellites such as MSG, GOES and DMSP. IR observations observe the different cloud stages and form the basis of rainfall intensity estimates at the land surface. Various techniques use IR images to estimate precipitation, whereby algorithms are based on thresholds with seasonal or regional dependence and the cloud top temperature. The IR precipitation estimate is a simple "colder clouds precipitate more" approach (Huffman et al., 2010). The colder clouds occur at higher altitudes and their temperature provides information about their top height. Therefore higher cloud tops are assumed to be also thick and are positively associated with precipitation for convective clouds which governs precipitation accumulations except for high cirrus clouds which don't rain as they are not thick even though they are very cold. This technique is based on cloud indexing, bispectral analysis, cloud life history and cloud models (Levizzani et al., 2001).

The IR band is very useful for rainfall detection and delineation but it show a relatively low accuracy in estimating the depth of rainfall.

3.1.2. Microwaves Based Methods

For rainfall estimation, observations done by MW bands consider the hydrometeor particles directly themselves. Using the visible and infrared spectral ranges, can be limiting since the cloud usually appear opaque and rainfall is deduced from cloud top structure, hence the use of MW approaches which are based on the concept of Planck's radiation law (Kidd & Kniveton, 2003). The emitted radiation in MW frequencies is affected by atmospheric hydrometeors such as clouds and precipitations droplets. Therefore, the surfaces emit about a half of microwave energy and therefore half of their temperature can be recorded which makes water surfaces look very cold. However, precipitation droplets appear with their real temperature, as result of the scattering of the radiation by the raindrops. So the more raindrops in the cloud profile, the warmer the scene appears. With Microwave radiometers, more reliable information concerning instantaneous precipitation rates can be obtained due to their ability to see through the cloud tops and detect directly the presence of actual precipitation particles within and below the clouds.
The MW bands allow fairly accurate rainfall rates estimation but they are limited since the MW sensors are exclusively mounted on board of low earth orbiting satellites with their poor spatial and temporal resolution such as TRMM and POES.

3.1.3. Combined Infrared and Microwave Methods

Thermal IR based techniques benefits from a degree of simplicity together with a 24 hour availability of data. It has been noticed that IR methods overestimate rainfall and show a maxima in its estimation much later than actually observed on ground (Bell & Reid, 1993). On the other hand, MW methods estimate rainfall with a low temporal resolution. Combining measurements from different satellite sensors such as IR and MW, is a technique that overcomes the drawbacks of rainfall estimation from a single data source. This blending approach of both IR and MW usually benefit from the availability of IR images at high temporal resolution and from direct information on cloud and rainfall characteristics from MW images (Levizzani, 2003). Many satellite based rainfall products such as TRMM 3B42, CMORPH and RFE use this technique. This blending method make use of the superior performances of MW sensors in terms of their rainfall estimation accuracy to calibrate the IR temperatures of the geostationary imagery.

3.1.4. *In Situ* and Online Data (ISOD)

ISOD is a toolbox developed in ILWIS to acquire data on various environmental data resources through the internet, especially time series of data. The toolbox is an open source software tool for archived time series data. This service is free of charge to the user community so it helps out developing countries, which can't afford to spend the little they have in measuring meteorological variables on small temporal or spatial scale with expensive automatic instruments.
ISOD toolbox automatically retrieves and processes different data resources including near real time climatological *in situ* observations, gauge and satellite derived precipitation products, weather and pressure forecasts, potential evapotranspiration, normalized difference vegetation indices and elevation information (Maathuis & Mannaerts, 2012). Even though a large number of these resources have a global dimension, the current focus is on data provision for Africa.

3.2. Bias Error Correction

As aforementioned some errors from different sources are found in satellite based meteorological products. These errors can be classified as systematic or random and require assessment and correction before products can be used in hydrological modelling.
This research emphasis is on correcting systematic errors also called the bias, since they are repetitive differences between *in situ* measurements and the estimations given by algorithms to retrieve meteorological variables. The random errors on the other side are short-term deviation from the measurement's true value and they cannot be corrected on a singular measurements basis.
Systematic errors error normally persist when the estimates are aggregated over time and can cause abundant uncertainties in hydrological modelling (Habib, Haile, Sazib, Zhang, & Rientjes, 2014).

The sources of the repetitive differences between observations by the satellite sensor and the observation by gauge stations are multifold. These differences may occur from the algorithms used to retrieve meteorological variables themselves, or caused by the observation scale and interpolation (temporal and spatial resolution) because of the discretization of the time and the area covered. The rounding off of the meteorological estimation values can also cause bias errors by accumulation over time.

Therefore before use in hydrological applications the bias in the remote sensing products ought to be assessed and corrected. For that purpose, a period of accumulation also called time window is used. In the aspect of time, the bias can be corrected by applying a sequential or a moving time window. For the sequential window the selected time window is displaced as a whole consecutively over the time series while for the moving window the selected time window is displaced time step by time step within the same time window repetitively over the time series.
For daily meteorological products the time window for bias assessment is commonly larger than 2 but shorter than 10 days.
The satellite data are bias corrected by multiplying the ratio between gauge and satellite observations, called bias factors (BF), with the uncorrected satellite data.

Habib et al. (2014) presented various schemes for bias correction. Correction algorithms are to correct the bias in time, in space and in time-space as shown in the expression below:

The time and space variant (TSV) bias correction scheme where the bias factor (BF) is pixel based at daily scale:

$$BF_{TSV} = \frac{\sum_{t=d}^{t=d-l} S_{(i,t)}}{\sum_{t=d}^{t=d-l} G_{(i,t)}}$$

The time and space fixed (TSF) bias correction scheme where the BF is lumped over the entire domain and the whole period of the sample:

$$BF_{TSF} = \frac{\sum_{t=1}^{t=T} \sum_{i=1}^{i=n} S_{(i,t)}}{\sum_{t=1}^{t=T} \sum_{i=1}^{i=n} G_{(i,t)}}$$

And the time variable (TV) bias correction scheme where the BF is lumped over the entire domain but for each day:

$$BF_{TV} = \frac{\sum_{t=d}^{t=d-l} \sum_{i=1}^{i=n} S_{(i,t)}}{\sum_{t=d}^{t=d-l} \sum_{i=1}^{i=n} G_{(i,t)}}$$

For the previous formula, *G* and *S* represent daily ground measurements data (i.e. station) and satellite estimates data respectively. *t* refers to Julian day, *l* is the length of a time window for bias calculation and *i* denotes the gauge location.

3.3. Hydrological Modelling

In poorly gauged river basins, hydrological modelling may serve to better understand hydrological processes in their spatial and temporal patterns and often serves to improve water resources management practices. Depending on the amount of details in terms of input data provided for a given basin, so we use lumped, semi distributed and fully distributed model approaches for the spatial aspect, in order to quantify water resources. In other words limitations of hydrological measurements techniques and limited range of measurements in space and time are the main reasons to model the hydrological processes (Beven, 2011).

Various types of hydrological models can be distinguished based on their model approach, model structures and core mathematical equations.
The physically based rainfall-runoff models are based on equations which define the physics that governs nature. They are based on conservative equations of mass and momentum, and in certain cases, also energy and entropy. While Empirical (or transfer) models are based on a set of equations that only is able to simulate input/output patterns (Rientjes, 2014).

3.3.1. Conceptual Rainfall Runoff Model

Conceptual rainfall runoff models are designed to approximate within their structures the general physical mechanisms which govern the hydrologic cycle. They rely on simple mathematical relations and water balance equations to simulate the observed real world behavior.

Conceptual rainfall-runoff models serve to provide quantitative information on a catchment runoff and inherent characteristics. This is done by using realistic functions to describe internal operations of several interconnected subsystems, each representing a certain component in the main output which is a hydrograph (Duan & Gupta, 1992). They can be lumped on the entire domain, semi-distributed or totally distributed.
Hydrograph (see Figure 3.1), which is a graph that shows the rate of water flow (often in volume units) over time at a specific point in a river, is interpreted as integral response function of rainfall-runoff processes. Hence, the stream flow hydrograph being the main output of the model, gives various information on the hydrological processes in the area understudy such as the base flow of the drained area and the direct runoff or effective rainfall of the area. Other information that can be delivered from a hydrograph especially from its rising limb and falling limb are the water concentration time or lag time of a catchment area in response to a rainfall event, and the highest discharge in the channel called peak discharge.
The successful application of a conceptual rainfall-runoff model depends on how well the model is calibrated, what consist in finding the parameter set values allowing the best fit between the observed and the simulated discharge at the outlet of a catchment.

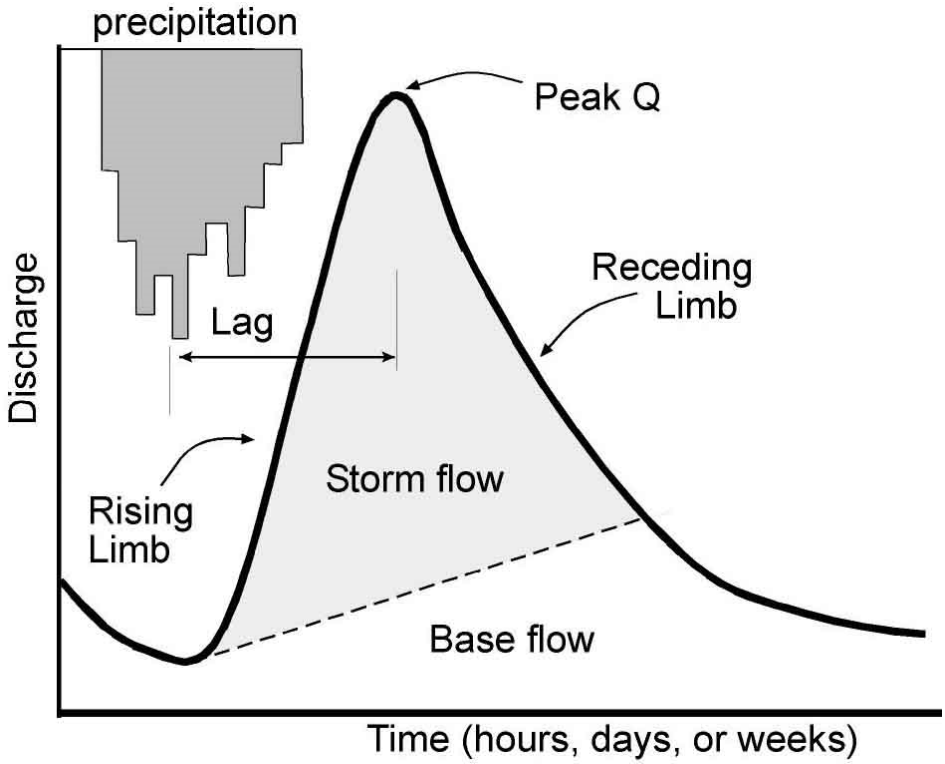

Figure 3-1: Hydrograph sections (from public resource GeogOnline/storm hydrograph)

4. MATERIALS AND METHODS

4.1. MATERIALS

4.1.1. Remote Sensing Products

For this study satellite rainfall products and a satellite evapotranspiration product were used. Other products from remote sensing used are a digital elevation model of the Shuttle Radar Topography Mission (SRTM) from (http://droppr.org/srtm/v4.1/6_65x5_TFIs/) and a land cover map classified from a LANDSAT TM and ETM scenes (http://landsatlook.usgs.gov/).

CMORPH rainfall product

The CMORPH rainfall products are based on a morphing approach for high resolution precipitation product generation. CMORPH merges passive microwave (PMW) data, on which the precipitation estimates are quantitatively based, and infrared (IR) data to interpolate between two PMW-derived rainfall intensity fields. This is done in two steps: (1) Atmospheric motion vectors from two successive IR images are generated at 30-minute intervals. (2) The derived motion field is used to propagate the precipitation estimates derived from the different PMW sources (Joyce, Jonowiak, Arkin, & Xie, 2004).

The main inputs for the Climate Prediction Center (NOAA-CPC) MORPHing technique (CMORPH) are geostationary IR data from the US Geostationary Operational Environmental Satellites GOES-8/10, the European Meteosat-5/7and the Japanese Geostationary Meteorological Satellite GMS-5, PMW derived precipitation data from the TRMM Microwave Imager (TMI), the Special Sensor Microwave/Imager (SSM/I), and the Advanced Microwave Sounding Unit (AMSU)(Thiemig, 2014).

RFE rainfall product

The RFE 2.0 rainfall product is provided by the NOAA African Precipitation Estimation Algorithm which is based on IR (Meteosat-7 every 30 minutes) and PMW (SSM/I every 6 hours and AMSU every 12 hours) data as well as on Global Telecommunication System (GTS) rain gauge station data which are taken to be true rainfall within 15-km radii of each station (Thiemig, 2014).

Rainfall estimates are generated in two steps as well: first, satellite data sources are linearly combined through a Maximum Likelihood (ML) estimation method to eliminate data gaps and to decrease random errors and systematic bias. Secondly, bias correction is implemented on a grid-to-grid basis using the GTS rain gauge stations to correct for quantitative deviations (Herman, Kumar, Arkin, & Kousky, 2010).

TRMM rainfall product

The Tropical Rainfall Measuring Mission provides good estimates of global precipitation from a wide variety of modern satellite born precipitation related sensors. The algorithm of TRMM 3B42 v7, which is currently the most commonly used among the TRMM rainfall products, is executed in four steps: (1) PMW precipitation estimates are calibrated and combined, (2) IR precipitation estimates are generated using the calibrated PMW data, (3) both IR and PMW data are then combined, and (4) rescaled on a monthly basis using rain gauge data

Hence, the main input sources for the TRMM are IR data from geostationary satellites, PMW data from TMI, SSM/I, AMSU and the Advanced Microwave Sounding Radiometer-Earth Observing System (AMSRE)(Thiemig, 2014).

FEWSNET global evapotranspiration product

The FWESNET global evapotranspiration (PET) is estimated from climate data extracted from the Global Data Assimilation System (GDAS) every 6 hours. These data consist of meteorological parameters from NOAA such as air temperature, atmospheric pressure, relative humidity, solar radiation and wind speed. The daily PET are obtained by summing up the 6 hours computed Global PET (Maathuis & Mannaerts, 2013).On spatial basis, The FEWSNET Global PET is calculated by use of the Penman–Montheith equation.

$$\lambda ET = \frac{S(R_n - G) \times \rho_a C_p \frac{(e_s - e_a)}{r_a}}{S + \gamma \times \left(1 + \frac{r_s}{r_a}\right)}$$

where Rn is the net radiation, G is the soil heat flux, $(e_s - e_a)$ represents the vapour pressure deficit of the air, r_a is the mean air density at constant pressure, c_p is the specific heat of the air, D represents the slope of the saturation vapour pressure temperature relationship, g is the psychrometric constant, and r_s and r_a are the (bulk) surface and aerodynamic resistances.

The psychrometric constant is given by $\gamma = \frac{Cp \times Pa \times Ma}{(\lambda \times Mw)}$ in which Ma and Mw are the molecular masses of dry air and wet air, respectively, and Pa is atmospheric pressure

Table 4-1: Summary of Satellite meteorological variables products

Product	Geographic coverage	Period coverage	Spatial resolution	Temporal resolution	Source
CMORPH 8km	Lat: 60°S - 60°N Lon: 180°W - 180°E	since 2002	0.07° (8km)	30min	ftp://ftp.cpc.ncep.noaa.gov/precip/CMORPH_V1.0/CRT/8km-30min
RFE 2.0	Lat: 40°S - 40°N Lon: 20°E - 55°E	since 2001	0.1°	24h	ftp://ftp.cpc.ncep.noaa.gov/fews/fewsdata/africa/rfe2/bin
TRMM 3B42 v7	Lat: 50°S - 50°N Lon: 180°W - 180°E	since 1998	0.25°	3h	http://disc2.nascom.nasa.gov/opendap/TRMM_L3/TRMM_3B42/
FEWSNET PET	Lat: 90°S - 90°N Lon: 180°W - 180°E	since 2001	1°	24h	http://earlywarning.usgs.gov/ftp2/bulkdaily%20data/global/pet/years/

4.1.2. HBV-light Hydrological Model

HBV-light was selected for hydrological modelling in this study for its availability and being one of the most used rainfall-runoff model. HBV model input data requirement is moderate, and its demands in terms of parameters are not exhausting. Through its automatic calibration option it is also relatively easy to calibrate.

HBV-light is a version of HBV model, which was developed to provide an easy to use Windows-version for research and education (Seibert & Vis, 2012).

General Description

HBV is a mathematical model which was designed to apply runoff simulation, hydrological forecasting. The model can also be also used for water balance studies(Lindström, Johansson, Persson, Gardelin, & Bergström, 1997). The model can be classified as a conceptual hydrological model with either semi-distributed or lumped model domain. The approach has most applications in operational and strategic water management. The model incorporates different sub-basins characteristics such as the elevation and the land cover alongside with the sub-basins' meteorological data regime to simulate the dominant hydrological processes in the catchment.
The model general water balance can be described as:

$$P - E - Q = \frac{d}{dt}[SP + SM + UZ + LZ + LAKES]$$

Where: P is precipitation, E is Evapotranspiration, Q is runoff, SP is snow pack, SM is Soil moisture, UZ is upper ground zone, LZ is lower ground zone and $LAKES$ is lakes water storage.

Model Structure

The model structure description has been adapted from Lindström et al., (1997)
The model uses sub-basins as primary hydrological units. The sub-basins can further be subdivided into zones based on elevation and land use classes. The stream flow modelling using the HBV model consists of three main conceptual subroutines:

(1) the snow accumulation and melt subroutines,
(2) the soil moisture accounting subroutines,
(3) and the response and river routing subroutines.

Normally the major inputs of water in the model are precipitation and snow melt but in this case there is no snow melt in the catchment understudy. Hence the first subroutine can be ignored in this study.

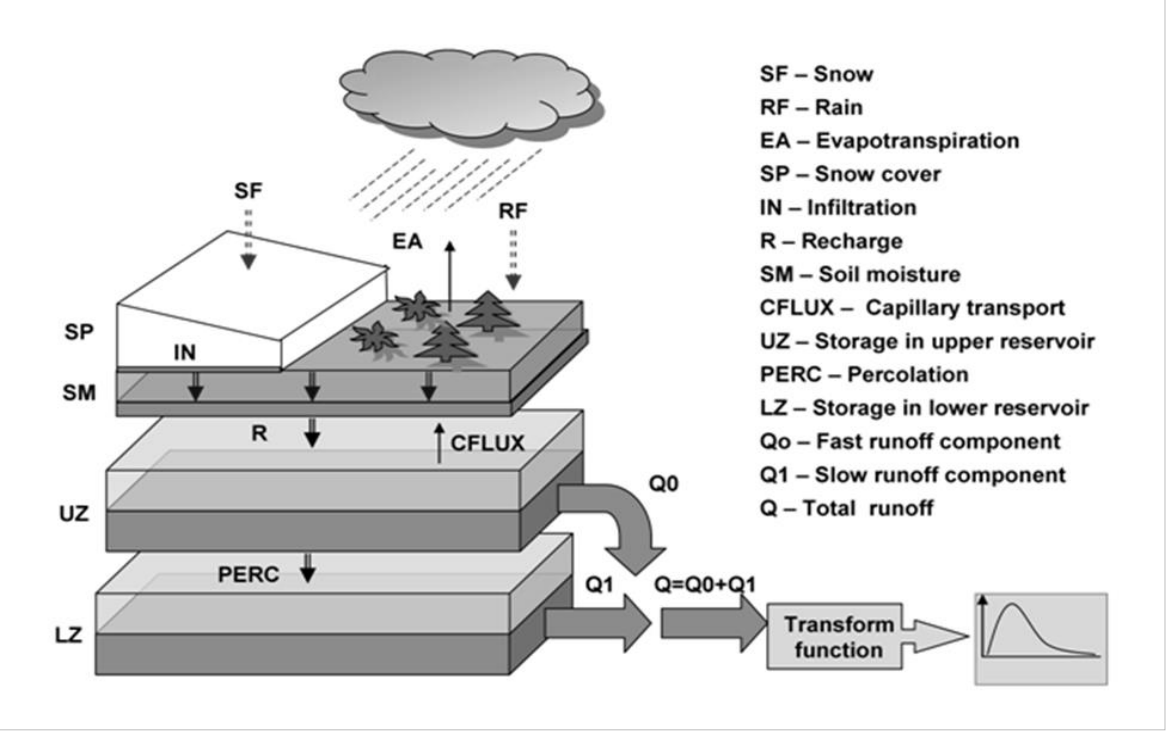

Figure 4-1: Schematic representation of the HBV model. From Solomatine & Shrestha (2009)

It is in the soil moisture subroutine that runoff formation occurs alongside with the actual evapotranspiration. This total runoff comprises a fast runoff and a slow runoff.
The fast runoff is governed by the exceedance of water in the soil moisture reservoir of the catchment to the maximum soil moisture storage indicated by the *FC* parameter. When the soil moisture saturation is not reached, the precipitation infiltrates (*IN*) in the soil moisture reservoir first it refills the soil moisture reservoir and then seeps through the soil layer as represented by *R* in figure 4-1.

$$R = IN\left(\frac{SM}{FC}\right)^{\beta}$$

where β is an empirical coefficient.

The slow runoff is to be determined according to the amount of recharge water flowing through the soil layer.
The actual evapotranspiration (*Ea*) is determined by the *LP* parameter which is the limit for potential evapotranspiration (*Ep*) in the following expression:

$$Ea = Ep\left(\frac{SM}{LP * FC}, 1\right)$$

where (*Ep*) is the potential evapotranspiration and (*Ea*) can't be superior to it.

In the upper zone several hydrological processes can be distinguished, the percolation which is denoted by the *PERC* parameter, and expressed as a constant rate of available water, it takes place only when extra water is available in this zone. The capillary flow is governed by the *CFLUX* parameter and occur when the soil moisture is less than the available water in the upper zone.

$$C_f = CFLUX\left(\frac{FC - SM}{FC}\right)$$

when the recharge water is more than the amount of water which percolates to the groundwater, the fast runoff flows from this zone and it can be expressed as

$$Q_0 = K_f.UZ^{(1+\alpha)}$$

where *UZ* is the actual storage in the upper zone reservoir, α, a non-linearity measure of the fast flow and K_f, a recession coefficient.

In the lower zone, the slow flow of the catchment is simulated in the base flow routine and can be conveyed as shown in this expression

$$Q_1 = K_s.LZ$$

in which *LZ* is the actual storage in the lower zone reservoir from the upper zone through the percolation, and K_s is the recession coefficient for that zone.

The proper shape of the hydrograph is defined during the transformation routine where the discharge of each sub-basin is routed by a triangular distribution function.
As shown above the model relies on simple equations and only dominant hydrological processes are simulated. Here, small scale processes such as macro-pore flow and perched surface flow are somehow are ignored. The water balance is solved for every simulation in each reservoir at each time step and for the entire simulation period as well.

4.2. METHODS

The methods used in the first part of this study which is the data pre-processing, assessment of the satellite based meteorological data and bias correction can be summarized in the following flow chart.

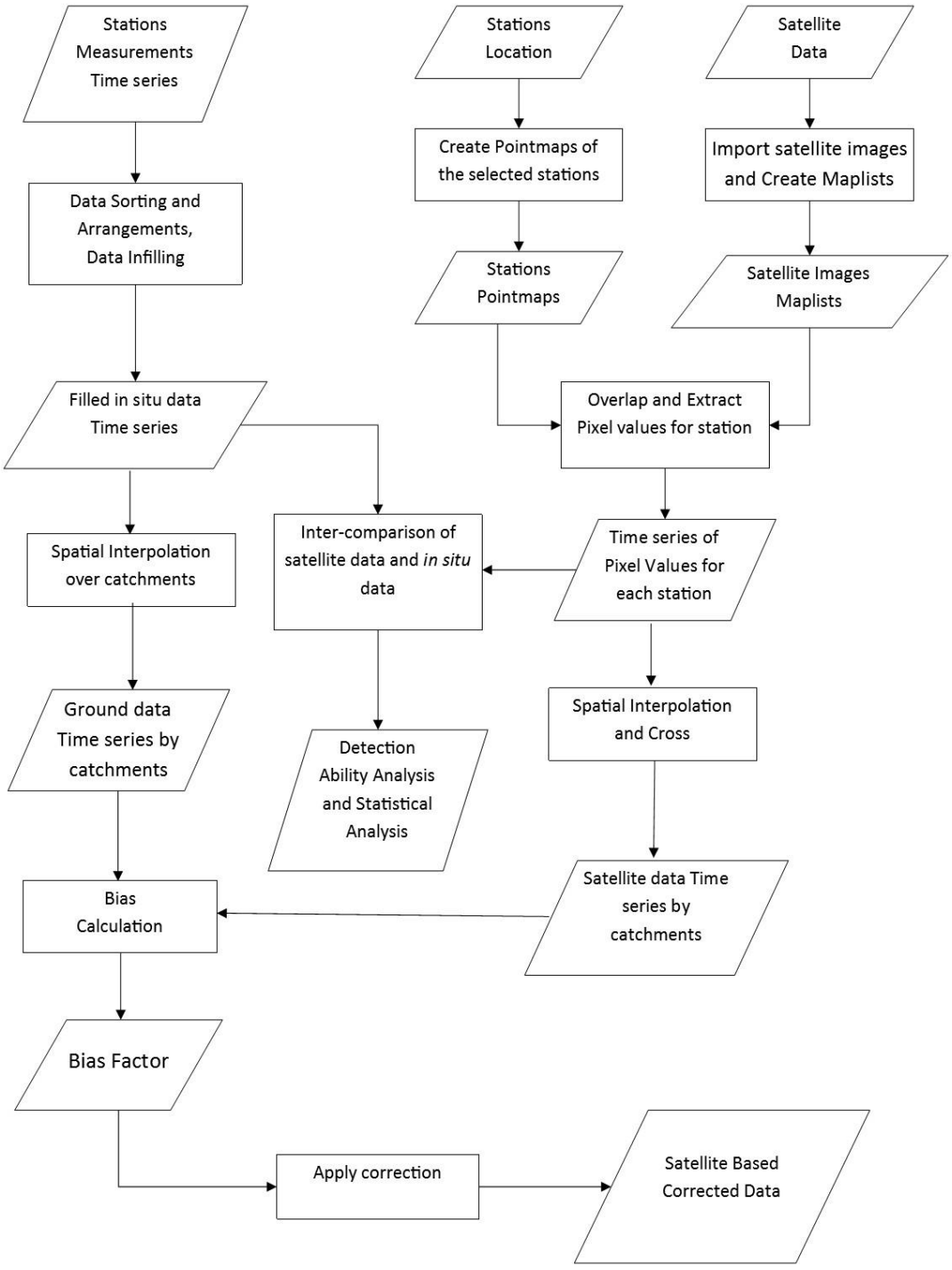

Figure 4-2: Followed steps from data processing to satellite products assessment and bias correction

4.2.1. *In Situ* Meteorological Data Pre-processing

Meteorological Data Completion and Consistency Check

As aforementioned, screening of *in situ* measurements to be used in this study was based on stations with at least two years with complete data, the following step was to infill missing values, to identify and remove unrealistic values (overshoot) which are considered as erroneous data. These overshoot data were noticed when the meteorological data were plotted over time and each station compared to the neighboring stations recordings.

The data infilling method selected was the spatial interpolation method within which the normal ratio method is applied (DHV Consultants BV & Delft Hydraulics, 1999a). The choice of this data infilling method among the existing ones was guided by various aspects such as the fact that the method takes into account the potential heterogeneity of the station locations and its user friendliness as well as adequateness for the type of data collected on the field.

This method is used for cases where the average annual meteorological data of the station under consideration differs from the average annual meteorological data at the neighboring stations by more than 10% mainly due to distance or difference in altitude. In a case that the normal annual meteorological data at the neighboring stations is within the 10% of the normal annual meteorological data at the target station, then the missed values were estimated using arithmetic mean of the neighboring stations.

Hence, the first step regarding this matter was to group the screened weather stations in order to ensure effective completion of estimating missing data. The grouping was done based on the stations proximity to ensure that the stations are located within the same climatic conditions zone as possible according to the agro climatic zones of Rwanda (see Appendix 1).

The erroneous or missing meteorological data at the target station are estimated as the weighted average of the neighboring stations. This method requires at least three adjoining stations to produce acceptable estimates of these meteorological data. This method can be expressed as:

$$Y_{tg} = \frac{1}{M}\left(\frac{N_{tg}}{N_{neigh,1}}X_{1neigh.} + \frac{N_{tg}}{N_{neigh,2}}X_{2neigh.} + \cdots + \frac{N_{tg}}{N_{neigh,M}}X_{M,neigh.}\right)$$

where $\boldsymbol{Y_{tg}}$ is the retrieved data at the target station, $\boldsymbol{X_M}$ is a record of meteorological variable at a neighbouring station, $\boldsymbol{N_{tg}}$; the Annual normal meteorological variable at the target station and $\boldsymbol{N_M}$, the annual normal meteorological variable at the neighbouring stations and $\boldsymbol{M}$ the number of used neighbouring stations.

For the stations which had not enough (<3) neighbouring stations with complete data, closer Agro Synoptic stations were allocated to it as they are considered to be accurate and have more or less complete time series.

After the data infilling, the data quality control and consistency check was done by double mass curve graphical analysis on all the stations with influence on the study area. The technique is used for long time series to check the consistency and accuracy of the data between data from one station and its surrounding stations (Searcy & Hardison, 1960). For this, the cumulative data of the target station is plotted against the cumulative average data of the surrounding stations, starting from the latest year.

The double mass curve is expressed in a linear equation form;

$$Y = \alpha X$$

with $\boldsymbol{Y}$ as target station cumulative data, $\boldsymbol{X}$ the cumulative average of other stations inside or at close distance to the area understudy and α being the slope of the plot.

The method is based on the principle that a plot of two cumulative quantities measured for the same time period should be a straight line and their proportionality, which represents the slope, remains unchanged. Therefore on the cumulative plots a trendline is drawn and any deviation from the later indicates data inconsistency of the target station. If the inconsistency is only observed on a short period, the data can be corrected again by multiplying the affected part of the data by the ratio of the two slopes (the trendline and the scatter plot line).

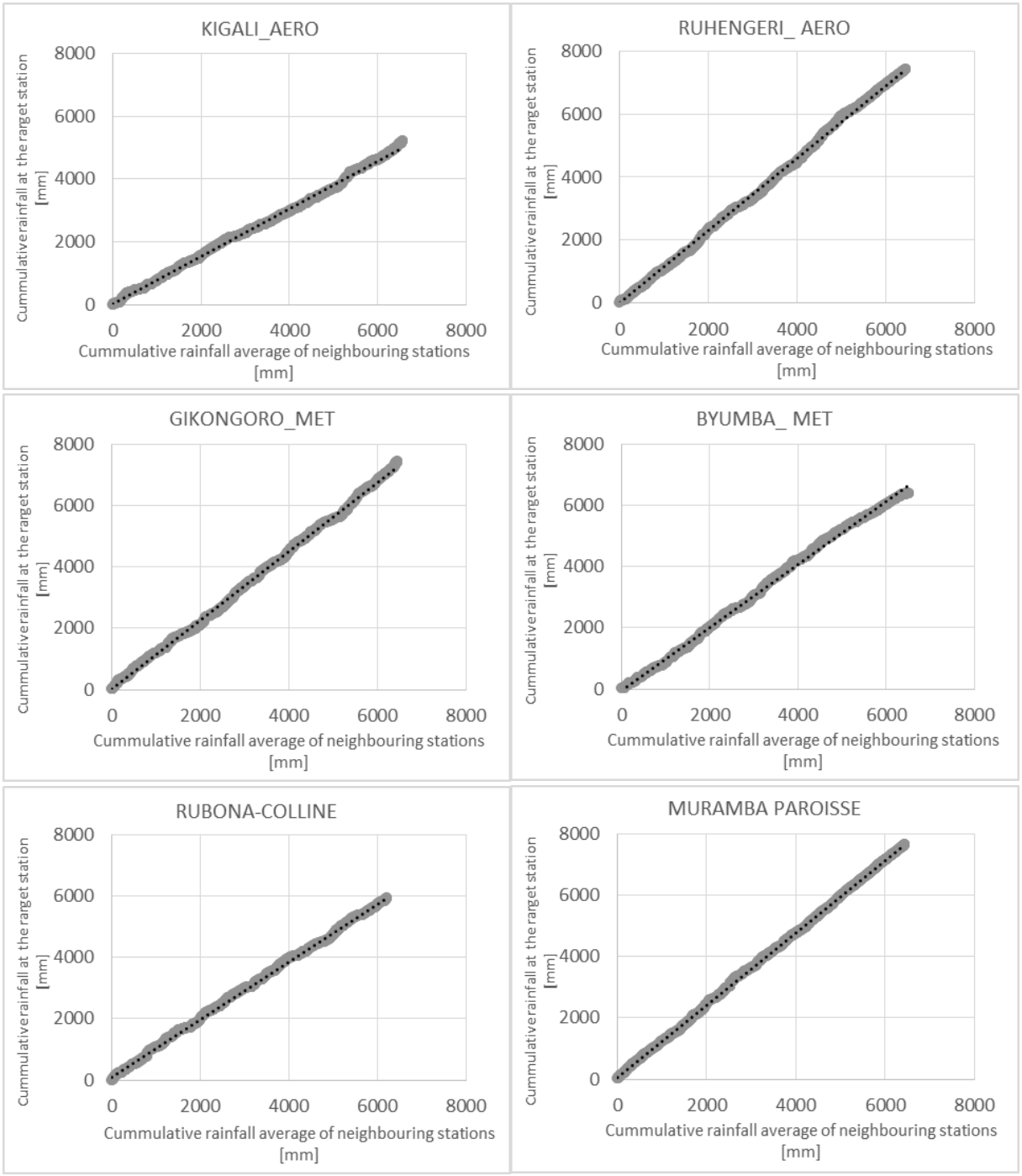

Figure 4-3: Rainfall data double mass curves (a pair for each category of Meteorological stations: Agro Synoptic stations, Climatological Weather stations and Rainfall stations.

Spatial representativeness of the *in situ* meteorological data

Semi distributed Rainfall-runoff modelling in HBV model requires single time series of each meteorological variable for every sub-basin represented in the model. Hence, as the meteorological stations are unevenly spread with no clear network design over the area understudy, the meteorological variables representation in the basin required first of all screening of which stations with measurements were found inside or at close distance to the study area.

The Thiessen polygon method, being one among other approaches of representing areal meteorological measurements, was used in this study to spatially estimate different meteorological variables over Nyabarongo sub-basins.

This method gives weight of each station data in proportion to the area covered by the whole basin. But apart from that, it clearly shows which station measurements are considered to have power in the basin whether the stations are located inside the later or not. Any location inside a polygon is closer to the station gauge at its center than any other station gauge. So, in this method an assumption is made that measured meteorological variable at the center of the polygon applies over the entire polygon (Barbalho, Silva, & Formiga, 2014). Calculating the ratio of each polygon area and the entire basin gives the weight of station gauge at the center of the polygon (see appendix 2). There the spatial representation of the meteorological data over the entire basin or a sub-basin is calculated as follow:

$$\bar{Y} = \frac{1}{A} * \sum_{j=1}^{k} A_j X_j$$

where $\boldsymbol{Y}$ is the representative meteorological variable value, $\boldsymbol{X_j}$ measured value at each station gauge, $\boldsymbol{A_j}$ the area of each polygon inside the basin or sub-basin and $\boldsymbol{A}$ the area of the sub-basin or the total area of the entire basin.

After applying the Thiessen polygon, it was found that 24 rainfall stations out of the 37 stations screened in the whole country, 5 evapotranspiration stations out of 6 screened in the whole country and 9 temperature stations out of 26 screened in the whole country were inside or at close distance to Nyabarongo basin.

Table 4-2: Meteorological stations inside or at close distance to Nyabarongo basin

Stations	Elevation	Evapotranspiration	Temperature	Rainfall
Kigali airport	1462m	Yes	Yes	Yes
Kawangire	1524m		Yes	Yes
Gisenyi airport	1540m	Yes		
Gitega	1554m			Yes
Rubengera meteo	1629m		Yes	Yes
Janja	1636m			Yes
Rubona colline	1680m			Yes
Byimana	1786m		Yes	Yes
Nyagahanga EFA	1839m			Yes
Rukozo	1888m			Yes
Gikongoro meteo	1902m	Yes	Yes	Yes
Muganza	1939m			Yes
Ruhengeri airport	1977m	Yes	Yes	Yes
Ntaruka	2021m			Yes
Muramba parish	2023m		Yes	Yes
Cyinzuzi	2039m			Yes
Nemba	2175m			Yes
Busogo ISAE	2191m	Yes	Yes	Yes
Byumba meteo	2198m		Yes	Yes
Butaro	2256m			Yes
Kabaya	2443m			Yes

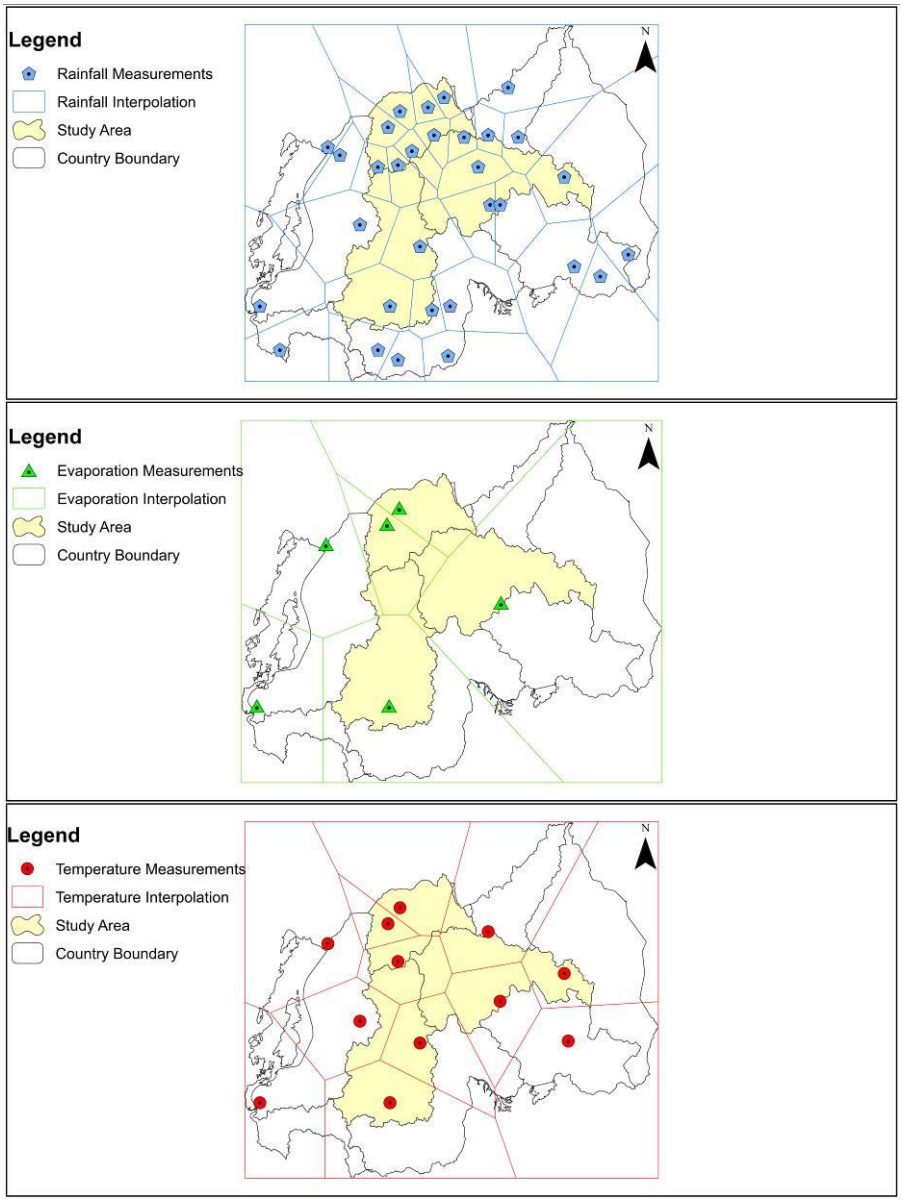

Figure 4-4: Areal representation of meteorological variables in Nyabarongo basin using Thiessen polygons

The meteorological variables were interpolated over each sub-basin and also the entire basin, by using respective Thiessen polygons as shown in figure4-4. This was done in ILWIS, where the Thiessen weight for each station was calculated in every sub-basin.

4.3. Hydrological Data Processing

The water stages collected at Ruliba station were related to water flow discharge of Nyabarongo River using stage-discharge rating curve method. The stage-discharge relation was developed based on the regular equation of the most commonly used stage-discharge rating curves which is the power form equation:

$$Q = c * (h + a)^b$$

where $\boldsymbol{Q}$ is the discharge in m^3/s, $\boldsymbol{h}$; the water stage in m, and $\boldsymbol{a}$; the water stage corresponding to zero flow. $\boldsymbol{c}$ and $\boldsymbol{b}$ are calibration coefficients, $\boldsymbol{c}$ is the discharge when the effective depth of flow ($\boldsymbol{h+a}$) is equal to 1 and $\boldsymbol{b}$ is the rating curve logarithmic slope.

The parameter ***a*** is estimated by the Johnson method which assumes that the medium flow discharge is equal to the square root of the product of the high flow and the low flow discharge.
The value of ***a*** is optimized by 'trial and error' method in a manner that the double logarithmic plot of the rating curve should be a straight line (see Appendix 3). If it is a curved line, the value of ***a*** is increased or decreased depending on if the concavity of the curved line is negative or positive respectively (DHV Consultants BV & Delft Hydraulics, 1999b). On the other hand, the calibration coefficients are determined by the least square method which minimizes the sum of square of deviations between the logarithms of measured discharges and the computed discharges obtained from the fitted rating curve.

$$Error = \sum_{i=1}^{N} (Y_i - Y_i')^2 = \sum_{i=1}^{N} (Y_i - \alpha - \beta X_i)^2$$

where Y_i measured discharges and Y_i' computed discharges from the fitted rating curve

The discharge measurements at Ruliba station were taken directly using current meters and were used to produce the rating curve of Nyabarongo River. As shown in figure4-4.

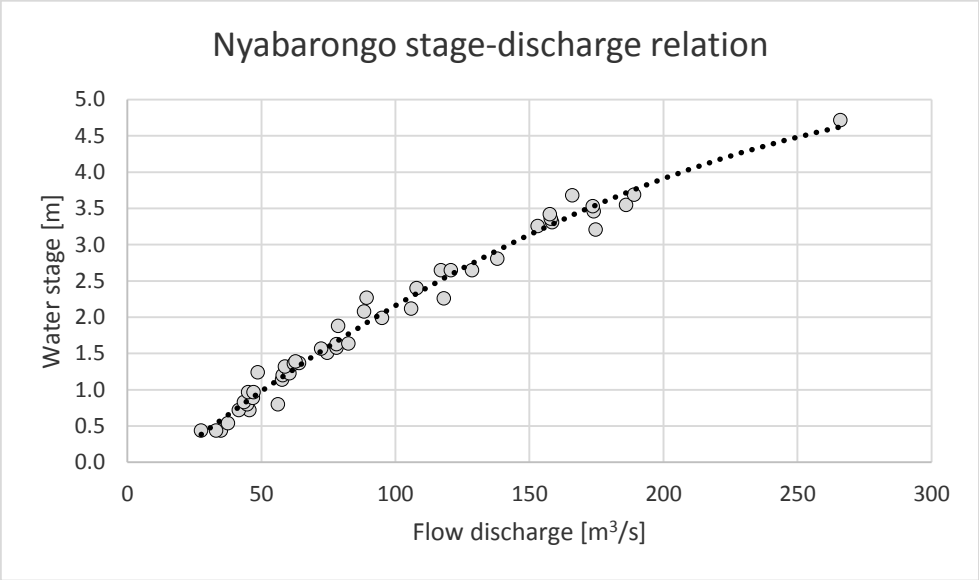

Figure 4-5: Nyabarongo stage-discharge rating curve relation

The water stage at zero flow symbolized by ***a*** was estimated using the Johnson method as aforementioned and a 'trial and error' optimization was used.

$$a = \frac{h^2 - h_1 h_3}{h_1 + h_3 - 2h_2}$$

where h_1 is water stage at low flow, h_2 ; water stage at median flow and h_3 is the water stage at high flow.

We found the water stage at zero flow at 1.5 m so after determining the coefficient ***b*** and ***c*** by the least square method the rating curve was defined as follow:

$$Y = 7.826 * (h + 1.7)^{1.88}$$

With this formula the water stages at Ruliba station were turned into Nyabarongo stream flow discharge at the outlet of the entire basin.

4.4. Meteorological Remotely Sensed Data Processing

Satellite based rainfall and evapotranspiration products at daily base were downloaded from the ISOD toolbox via the Integrated Land and Water Information System (ILWIS). Product's images were download in ILWIS as raster images with the georeference files for a period of five years from 2009 to 2013 on a daily basis apart from CMORPH 8km which was download on an hourly basis.
In the data processing, the hourly CMORPH 8km estimates were aggregated to daily rainfall estimates by stacking 24 CMORPH 8km for raster maps for one day in a maplist. Furthermore, inside each maplist for every day, the 24 images were summed to aggregate the CMORPH 8km hourly product to a daily product.

For each satellite meteorological products, a maplist for the same period of 5 years was created to facilitate the retrieval of satellite daily data time series at the meteorological gauge stations' locations for comparison purposes between the satellite based data and *in situ* measurements.

Rwanda's hydrological and meteorological shapefiles including stations' locations and Nyabarongo basin extent with its sub-basins, were imported to ILWIS. A LatLon WGS84 georeference for the study area was created to visualize them. As the images loaded up in each maplist had the same georeference, the raster maps were stack together and pixel values were extracted as data time series, pixel by pixel for the stations' locations. These satellite products data times series were imported to the excel spreadsheet containing the *in situ* measurements for further assessment.

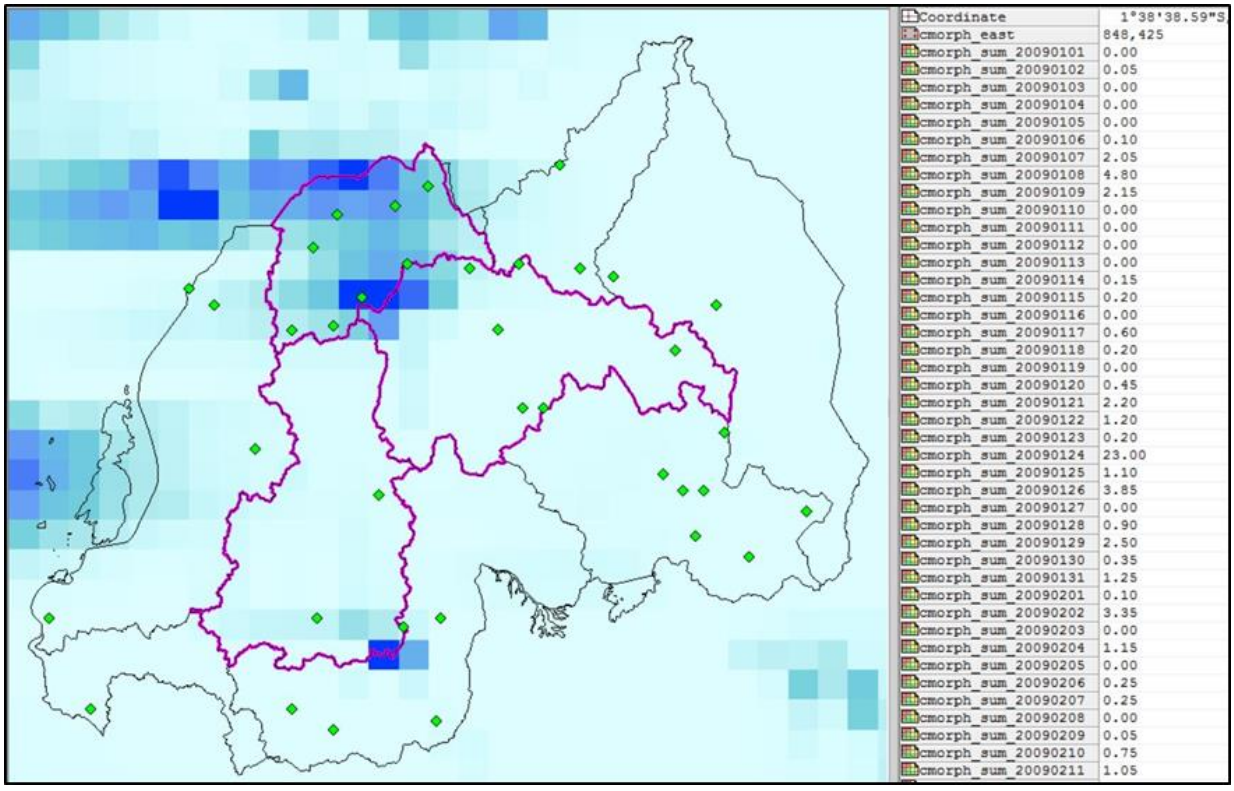

Figure 4-6: CMORPH 8km maplist for 2009-2013

4.5. Inter Comparison Between Gauge Stations And Satellite Based Data

To assess the reliability of satellite meteorological estimates, a first analysis aimed at comparing *in situ* measurements to pixel values for those pixels which overlap station based meteorological variables. 'Point to pixel' analysis was applied to compare time series of respective stations meteorological variables with remotely sensed counterparts. The second analysis aimed at evaluating the satellite meteorological products at a sub-basin wide level. These analyses are based on the depth and the timing (number of days) of rainfall and evapotranspiration estimates.

4.5.1. Statistical Analysis

Statistics analysis served to identify differences found in the satellite based meteorological estimates. Statistical measures selected for this study include the bias, the mean error (ME), the root mean square error (RMSE) and the correlation coefficient (R^2).

The bias and the mean error measure systematic differences where a bias inferior to 1 and a mean error with a negative sign shows underestimation and the inverse shows overestimation of meteorological variables in the satellite products.

The root mean square error measures the magnitude of accumulated errors and the accuracy of satellite rainfall estimates in reference to the *in situ* measurements. Its values vary from 0 to ∞, with 0 meaning an excellent accuracy.

The correlation coefficient evaluates the agreement between the satellite based and gauge stations meteorological estimates. It varies from 0 to 1 which means a high agreement.

The Bias and the coefficient of correlation have no unit and the latter is sometimes expressed in %.

$$\boldsymbol{Bias} = \frac{\sum_{i=1}^{n} S}{\sum_{i=1}^{n} G}$$

$$ME = \frac{\sum_{i=1}^{n} S - \sum_{i=1}^{n} G}{N}$$

$$RMSE = \sqrt[2]{\frac{\sum_{i=1}^{n}(S-G)^2}{N}}$$

$$R^2 = \frac{\sum_{i=1}^{n}(S_i - \bar{S}_i)(G_i - \bar{G}_i)}{\sqrt{\sum_{i=1}^{n}(S_i - \bar{S}_i)^2}\sqrt{\sum_{i=1}^{n}(G_i - \bar{G}_i)^2}}$$

Where $\boldsymbol{S}$ represent satellite based data, $\boldsymbol{G}$; the gauge stations data and $\boldsymbol{N}$ the number of data pairs. These variables are calculated in millimetres as they represent depths of water both rainfall and potential evapotranspiration.

4.5.2. Detection Capability

A detection capability check of the satellite based meteorological products; was conducted to quantify the ability of those products to distinguish information bearing conditions and casual conditions that disturb the information (Nurmi, 2003). This was done by counting event detection components such as the hits, which represent the count for when both gauge station and satellite product record meteorological data, misses; the count of event reported by gauge stations when satellite product report nothing, false alarm;

when the satellite product falsely detect meteorological event, and correct negative; which represent the count for when both gauge station and satellite product records are null.

Further, these event detection components were used to evaluate the satellite products capability of detection for meteorological events. This is done by estimation of the contingency table score which which is a statistical measure to rate the forecast verifications and includes the Frequency Bias (FB), the Probability of Detection (POD), the False Alarm Ratio (FAR) and the Critical Success Index (CSI also called Threat Score) (Moazami, Golian, Hong, Sheng, & Kavianpour, 2014). These are calculated as follow:

$$FB = \frac{\text{hits} + \text{false alarm}}{hits + misses}$$

$$POD = \frac{\text{hits}}{hits + misses}$$

$$FAR = \frac{\text{false alarm}}{hits + false\ alarm}$$

$$CSI = \frac{hits}{hits + false\ alarm + misses}$$

POD, FAR and CSI parameters range from 0 to 1, with 1 being a perfect POD and CSI while 0 is a perfect FAR. The FB ranges from 0 to ∞ and its desirable value is also 1.

4.6. Bias Decomposition and Correction

The satellite based data bias can be split into three components which are hit events bias, missed events bias and false events bias. To assess the source of bias, components of the bias were evaluated for each product and station. These bias are mathematically expressed as shown here,

$$Hit\ events\ bias = \sum_{i=1}^{n} (S_i - G_i)\ (when\ S_i > 0\ and\ G_i > 0)$$

$$Missed\ events\ bias = \sum_{i=1}^{n} G_i\ (when\ S_i = 0\ and\ G_i > 0)$$

$$False\ events\ bias = \sum_{i=1}^{n} S_i\ (when\ S_i > 0\ and\ G_i = 0)$$

Where S represent satellite based data, G; the gauge stations data and these bias components expressed in millimetres.

The satellite based meteorological products were corrected by multiplying their daily estimates to a bias factor of a sequential seven days window, lumped over each of the three sub-basins. So, the time variable bias correction scheme was adopted for each sub-basins, because of its simplicity and the space variable was not totally ignored as the bias was corrected per sub-basin. The seven days' time window was selected based on 2 reasons: previous study by Habib et al. (2014) and the fact coefficient of regression between

satellite data and *in situ* measurement observed for a 7 days' time window lengths was the highest compared to shorter time length see (appendix 4).
Therefore the bias factor was calculated after every seven successive days and multiplied to a daily value in the satellite based products time series within the same time window. The new obtained values were the bias corrected satellite based data which were used in as input for HBV model set up.

4.7. Hydrological Modelling

The hydrological modelling part for this research was done according to the flow chart below:

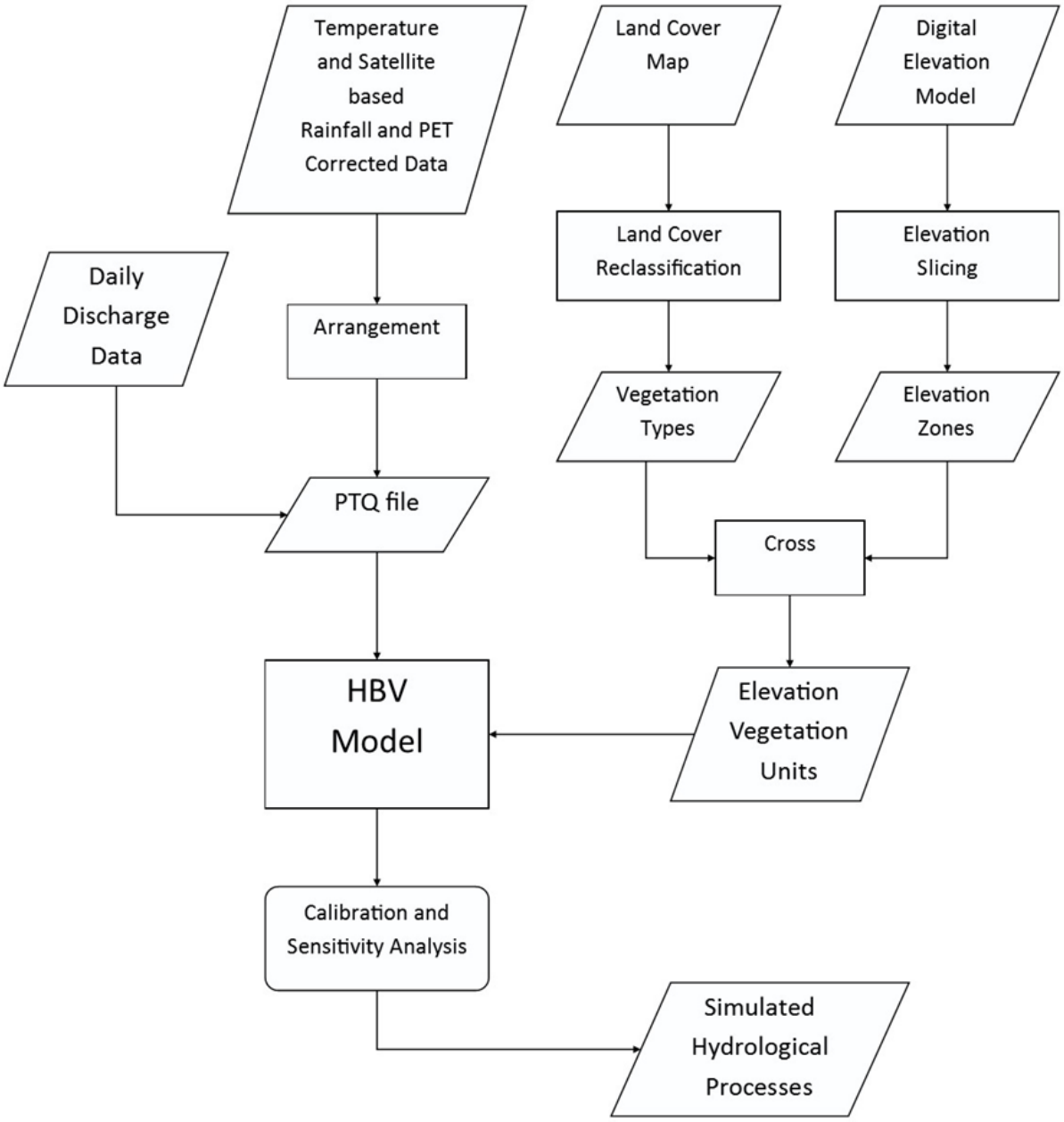

4.7.1. Model Set Up

Model Input Data

For the basic model variant of HBV-light, a Precipitation-Temperature-Discharge (PTQ) textfile is required to set up the model. This file contains daily time series of precipitation (mm), temperature (^oC) per sub-basin and the observed discharge at the outlet (m/day).

The discharges (m^3/s) at the basin outlet, which were obtained by the rating curve (section 4.4), were converted into mm per day by dividing by the area of Nyabarongo Downstream sub-basin.

An evaporation textfile containing potential evapotranspiration time series with a single daily values for each month is required as well.

The file was made by three sets of 12 values for long term monthly mean values for each of the three sub-basins as required in HBV-light model.

A sub-basin file which describe the spatial relation between the different sub-basins was also made and load in the model together with the file mentioned above. This file indicates the water flow direction form one sub-basin to another until the outlet of the entire basin.

The catchment physical characteristics based on elevation zones and vegetation type for the area understudy were defined and incorporated in the HBV-light model as well.

Elevation zones

The Shuttle Radar Topography Mission (SRTM) digital elevation model of 90m resolution of Rwanda was provided from RNRA during fieldwork. It is the same DEM which was used to delineate the catchments in the country. The sub-basins were classified into hydrological units according to the elevation ranges called elevations zones. This was done to allow the HBV model to take into consideration the slope, and the elevation aspect as well as the distribution of the meteorological variables of the area understudy accordingly to the topography.

As aforementioned Nyabarongo basin elevation varies from 1342m above mean see level to 4480m, so this range was sliced using ILWIS into 17 elevation zones of 200m each. The slicing results are shown in Figure 4-7.

Vegetation zones

For this study a land cover map produced in March 2013 by Greenhouse Gas inventories project in East and southern Africa was also provided by RNRA in its Lands and Mapping Department during the fieldwork phase of the study. The land cover map was developed based on a digital version of land cover maps of 2010 which was developed from the Landsat TM and ETM scenes from USGS website and processed by SERVIR Africa (RCMRD-SERVIR Africa, 2013). The classification scheme followed was provide by the Intergovernmental Panel on Climate Change (IPPC) guidelines suggesting of 7 classes and subclasses. The map were assessed and validated in comparison to ground control points and high resolution orthophoto images taken during the 2008-2009 Rwanda National Land Use and Development Masterplan campaign.

The land cover map was reclassified to meet the inputs requirements of the HBV model. As shown in Figure 4-8, the land cover map classes were regrouped into four main classes as HBV allows only three vegetation types, alongside the lakes present in the catchment. Where 1 represents the forestlands which cover 33% of the entire basin, 2; the croplands which cover 63% of the entire basin, 3; the lakes which occupy 3% of the basin and 4 representing the built up areas with 1% of the entire basin.

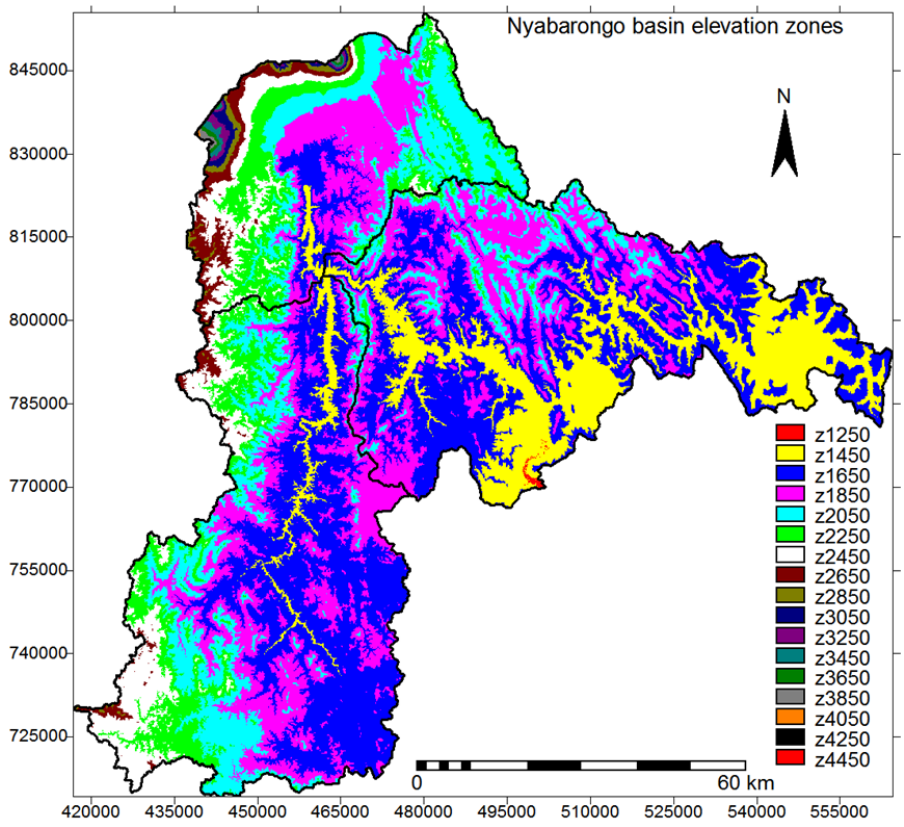

Figure 4-7: Elevation Units of Nyabarongo Basin with 200m range

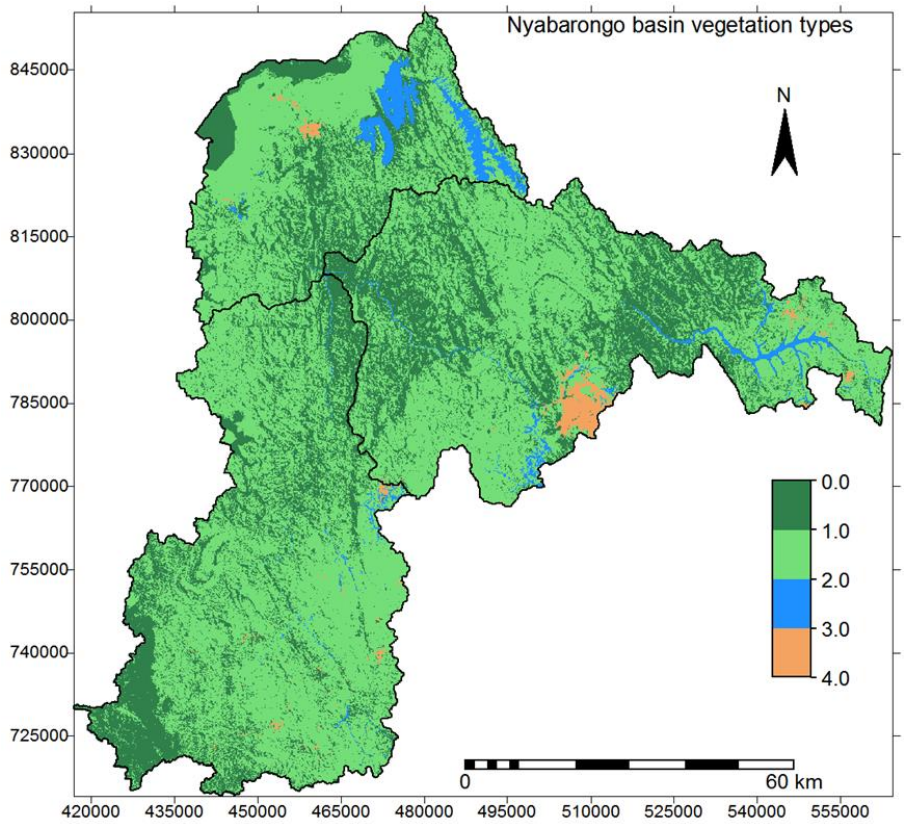

Figure 4-8: Three main vegetation types and Lakes in Nyabarongo Basin

4.7.2. Model Calibration

The model input parameters fine-tuning was applied to the model to reach a certain acceptable model performance for a selected time period. This was done by optimizing values of the model input parameters within their respective predefined ranges.

HBV-light has four identified calibration approaches namely the manual 'trial and error' technique, the genetic calibration algorithm, the calibration by Monte-Carlo simulation and a batch calibration.
Among the four approaches the manual calibration was preferred in this study as it allows a more interactive parameterisation in successive model simulations. During this calibration, the model parameters adjustment was based on visual inspection of the computed and observed hydrographs, and the analyses of two different goodness of fit functions; the model efficiency (Reff) also called the Nash-Sutcliffe coefficient and the mean difference (MeanDiff). The expressions of these goodness of fit functions in the following equations:

$$NSE = 1 - \frac{\sum_{i=1}^{n}\left(Q_{sim\,(i)} - Q_{obs\,(i)}\right)^2}{\sum_{i=1}^{n}\left(Q_{obs(i)} - \bar{Q}_{obs}\right)^2}$$

and

$$MeanDiff = \frac{\sum_{1=1}^{n}\left(Q_{obs(i)} - Q_{sim\,(i)}\right)}{n} * 365$$

where *Qsim* is the simulated flow, *Qobs*; the observed flow, $\overline{Qobs}$;the mean of observed flow and *n* is the number of days.

The Nash-Sutcliffe coefficient ranges from 0 to 1, with 1 representing the perfect performance of the model. The NSE in the range of 0.6 to 0.8 shows a reasonable model performance while values form 0.8 to 0.9 indicates excellent model performance.
While the Nash-Sutcliffe coefficient is more used to assess the predictive power of the model by describing the accuracy of model outputs (Nash & Sutcliffe, 1970). The mean difference emphasize more on quantitative assessment of the simulated flow water volumes compared to the observed flow, it shows the perfect performance when its value is 0.

Furthermore, in terms of the water mass balance error the model can be calibrated and evaluated through other commonly applied goodness of fit measures such as the relative volume error (RVE). The RVE indicates a perfect performance when its value is 0 as well and values which ranges from -10 to -5 and +5 to +10 are indicators of a model with an equitable performance. The equation which express the RVE shown below,

$$RVE = \left(\frac{\sum_{i=1}^{n} Q_{sim(i)} - \sum_{i=1}^{n} Q_{obs\,(i)}}{\sum_{i=1}^{n} Q_{obs(i)}}\right) 100\%$$

where *Qsim* is the simulated flow, *Qobs*; the observed flow and *n*; the number of days

Only the observed water flow derived from the measurements recorded by the automatic gauge were used in the calibration phase, as most of the manually recorded water levels data looked unreliable. Hence the simulation period was from March 2012 to September 2013.

5. RESULTS AND DISCUSSION

5.1. Rainfall Time Datasets Comparison and Bias Correction

As aforementioned the rainfall data used in this study was the data obtained from *in situ* measurements, and three satellite based rainfall estimation products; CMORPH 8km, RFE 2.0 and TRMM 3B42 v7 for a period of five years from 2009 to 2013. The main objective of this comparison to determine which satellite based rainfall products is the most reliable in reference to *in situ* measurements.

The comparison is based on statistical and graphical analysis which includes the calculation of statistical estimator such as the bias, the mean error, the root mean square error, and the coefficient of regression (section 4.6).

5.1.1. Point to Pixel Analysis

The point to pixel analysis was applied to compare time series of rainfall data observed at the selected stations in and close to Nyabarongo Basin with the satellite based counterparts at pixels overlaying the stations. Figure 5.1 shows a diagram where accumulated rainfall estimates are averaged at annual scale of the selected 20 stations are compared to the satellite based rainfall products. Stations are ordered from low elevation (left) to high elevation (right) and the comparison is made for CMORPH 8km, RFE 2.0, and TRMM 3B42 v7 products.

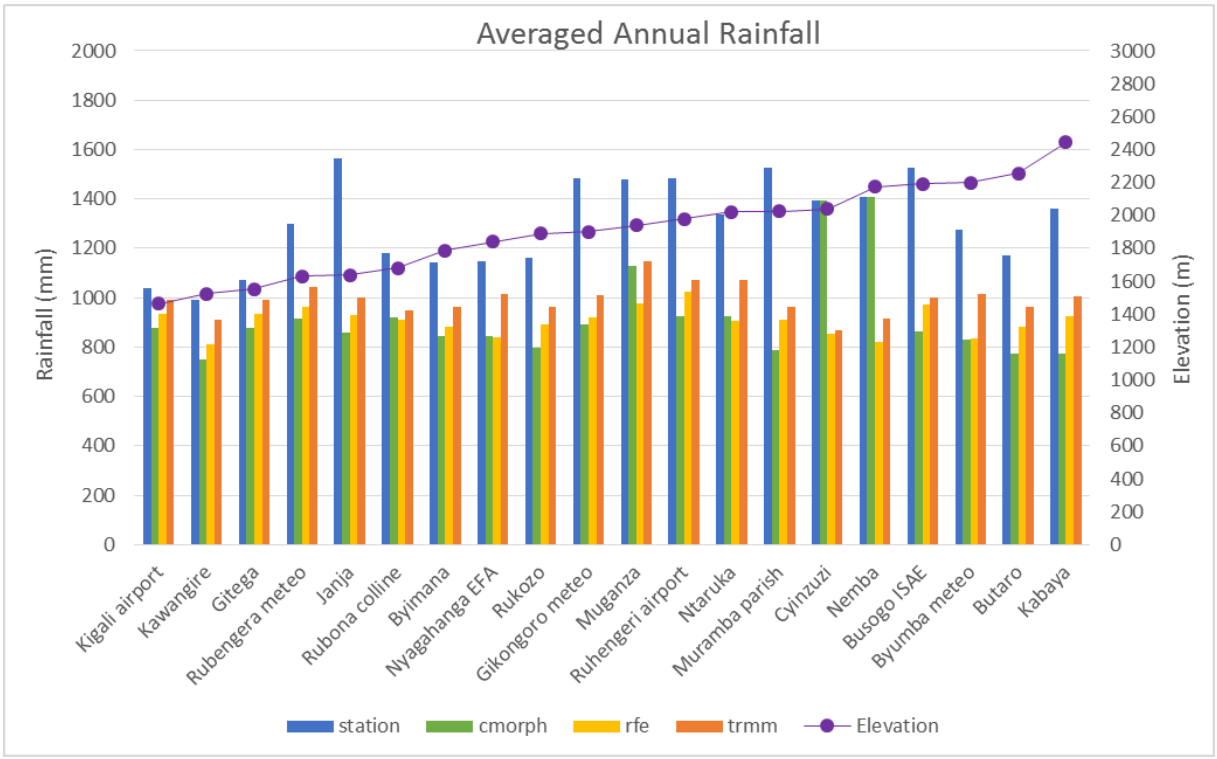

Figure 5-1: Comparison of averaged annual rainfall from satellite products and stations measurements

This figure shows that for the station measurements, the trend of rainfall increase follows the elevation increase in most of the cases except for few stations located in the areas close to the natural forest of Nyungwe, the Volcanoes region and the mountainous regions of the Congo-Nile divide.
That same trend is also shown in the satellite rainfall products even if it not very well highlighted in RFE 2.0.

Rainfall detection

For the rainfall detection analysis, results show that rainfall satellite products used in this study detected rainfall events as given in Table 5-1. Rainfall detection as indicated by the "Hits" ranging from 257 to 749 days, the "Missed" rainfall events counts range from 142 to 563 days, the "False" rainfall events count ranges from 91 to 570 days and the "Correct Negative" rainfall events range from 475 to 1057 days.

Table 5-1: The ranges of the Hits, Missed, False and Correct Negative rainfall events for each satellite rainfall product

Range	Product	Hits		Missed		False		Correct Negative	
		Counts	Station	Counts	Station	Counts	Station	Counts	Station
Minimum	CMORPH	324	Nyagahanga	179	Kigali	91	Janja	616	Ntaruka
	RFE	390	Nyagahanga	142	Kigali	159	Janja	636	Busogo
	TRMM	257	Nyagahanga	294	Butaro	252	Janja	475	Ruhengeli
Maximum	CMORPH	649	Ruhengeri	407	Muramba	311	Butaro	1033	Kigali
	RFE	749	Janja	330	Gitega	456	Butaro	1057	Kigali
	TRMM	567	Ruhengeri	563	Muramba	570	Butaro	821	Nyagahanga

The Minimum indicates the minimum count for each of the detection components and Maximum indicates the maximum for each of the detection components.Ttogether they show the range for each of the detection components.

The highest rainfall event Hits count was found for RFE 2.0 product at Janja station which was has relatively higher averaged annual rainfall. Janja station also showed the lowest False count for the three products. The lowest rainfall event Hits count occurred for TRMM 3B42 v7 product at Nyagahanga EFA station which had also showed minimum rainfall event Hits count for CMORPH 8km and RFE 2.0. The rainfall products used in this study showed highest count of False rainfall events at Butaro station which is the second most elevated station. Lowest Correct Negative rainfall events counts were observed in high elevation areas as well.

Contingency table score

Furthermore, rainfall detection analysis was done based on the contingency table score which is a measure to rate the forecast verifications. It consists of the frequency bias, the probability of detection, the false alarm ratio and the critical success index which are shown in table 5-2. The Frequency bias varies between 0.7 and 1.4 where the minimum was observed for CMORPH 8km at Janja station precisely, and the highest was for RFE 2.0 at Nyagahanga EFA station.
The probability of detection of the rainfall products used in this study was found in a range of 0.4 to 0.8, with the lowest POD for TRMM 3B42 v7 at Kawangire station and the highest for RFE 2.0 at Rubona hill station.
The false alarm ration showed a scale ranging between 0.1 to 0.6 where CMORPH 8km was found with the lowest FAR at Nemba station and the highest was found for TRMM 3B42 v7 at Nyagahanga station.
The critical index success which mixes the information from false alarms and missed events showed lowest value 0.3 at Nyagahanga station and highest value 0.6 at Janja station.

Table 5-2: Satellite rainfall products' contingency table scores at stations inside or at close distance to Nyabarongo basin (2009-2013)

Station	CMORPH 8km				RFE 2.0				TRMM 3B42 v7			
	FB	POD	FAR	CIS	FB	POD	FAR	CIS	FB	POD	FAR	CIS
Busogo	0.767	0.64	0.17	0.56	0.964	0.74	0.23	0.61	0.77	0.50	0.35	0.39
Butaro	1.045	0.60	0.43	0.41	1.372	0.71	0.48	0.43	1.40	0.58	0.59	0.32
Byimana	0.801	0.60	0.25	0.50	1.142	0.74	0.35	0.53	0.86	0.45	0.48	0.32
Byumba	0.805	0.62	0.23	0.52	1.080	0.71	0.34	0.52	0.92	0.47	0.48	0.33
Cyinzuzi	0.761	0.52	0.32	0.41	1.008	0.64	0.37	0.47	0.79	0.42	0.48	0.30
Gikongoro	0.897	0.68	0.24	0.56	1.188	0.77	0.35	0.55	0.91	0.45	0.50	0.31
Gitega	0.771	0.59	0.24	0.50	0.788	0.59	0.26	0.49	0.90	0.48	0.47	0.34
Janja	0.689	0.60	0.13	0.55	0.898	0.74	0.18	0.64	0.74	0.49	0.34	0.39
Kabaya	0.839	0.59	0.29	0.48	1.085	0.73	0.33	0.53	1.07	0.54	0.49	0.35
Kawangire	0.813	0.60	0.27	0.49	1.205	0.75	0.38	0.51	0.93	0.41	0.56	0.27
Kigali	1.027	0.70	0.32	0.53	1.048	0.76	0.27	0.59	1.20	0.49	0.59	0.29
Muganza	0.893	0.67	0.25	0.55	1.136	0.77	0.32	0.57	0.95	0.52	0.45	0.36
Muramba	0.699	0.59	0.15	0.54	0.880	0.71	0.20	0.60	0.69	0.44	0.37	0.35
Nemba	0.718	0.62	0.13	0.57	0.887	0.72	0.19	0.62	0.74	0.48	0.35	0.38
Ntaruka	0.987	0.64	0.35	0.48	1.033	0.72	0.30	0.55	1.06	0.59	0.44	0.40
Nyagahanga	1.040	0.57	0.46	0.38	1.426	0.68	0.52	0.39	1.20	0.45	0.63	0.26
Rubengera	0.908	0.64	0.30	0.50	1.045	0.75	0.28	0.58	0.97	0.52	0.47	0.36
Rubona	0.954	0.68	0.28	0.54	1.254	0.80	0.36	0.55	0.95	0.47	0.50	0.32
Ruhengeri	0.844	0.67	0.20	0.57	0.952	0.76	0.21	0.63	0.99	0.59	0.41	0.42
Rukozo	0.831	0.64	0.24	0.53	1.046	0.74	0.29	0.57	0.92	0.50	0.46	0.35

In general, for all the station, CMORPH 8km is the one that showed the lowest False Alarm Ratio, RFE 2.0 was found with higher Probability of Detection and TRMM 3B42 v7 had lower Critical Index Success which one was higher for RFE 2.0.

Rainfall estimated depth

The depth of rainfall estimated from the satellite products was analysed using statistical analysis and the results are shown in the table 5-3. The statistical measures used include the mean error, the root mean square error all in millimetres of rainfall, the bias and the coefficient of regression (section 4.6.1).

The maximum of the bias was found inferior to 1 which means that all products underestimate the rainfall at all the stations inside or at close distance to Nyabarongo basin; the highest value of the bias was 0.96, and it was for TRMM 3B42 v7 at the Kigali airport station while the smallest value was found for CMORPH 8km at Muramba parish station.

The mean error was found to be in the range of 2.02 mm/day and -1.94mm/day for the five year evaluation period. The lowest and the highest mean error were found for CMORPH 8km at Janja and Muramba stations respectively. Normally the ideal mean error value would be 0 or close to zero and the bias 1 or close to 1. Considering the obtained results, this shows a weak performance of the satellite products in the basin.

Therefore, from these results in general, it was found that depth wise TRMM 3B42 v7 was performing better than RFE 2.0 and CMORPH 8km. CMORPH 8km was underestimating the rainfall in the basin by 1mm/day with an overall of 0.67 bias, RFE 2.0 was also underestimating the rainfall depth in the basin by

0.97mm/day with an overall bias of 0.71. The TRMM 3B42 v7 product was underestimating the rainfall depth in the basin as well by 0.73mm/day with an overall bias of 0.78

Table 5-3: Statistical analysis of satellite rainfall product in reference to stations' data

Station	CMORPH 8km				RFE 2.0				TRMM 3B42 v7			
	Bias	ME	RMSE	R^2	Bias	ME	RMSE	R^2	Bias	ME	RMSE	R^2
Busogo	0.57	-1.81	7.17	17.62	0.64	-1.51	7.47	12.54	0.66	-1.44	8.91	1.04
Butaro	0.66	-1.09	6.75	11.11	0.75	-0.79	6.89	7.83	0.82	-0.57	8.14	0.21
Byimana	0.74	-0.82	7.74	13.58	0.77	-0.71	7.76	9.93	0.84	-0.49	9.68	0.02
Byumba	0.65	-1.22	7.60	19.49	0.65	-1.21	7.63	15.04	0.80	-0.71	9.83	0.99
Cyinzuzi	0.61	-1.49	7.68	6.91	0.62	-1.44	7.24	8.33	0.68	-1.21	8.76	0.14
Gikongoro	0.60	-1.63	7.76	28.95	0.62	-1.55	8.82	13.08	0.68	-1.30	10.79	0.25
Gitega	0.82	-0.53	7.05	17.79	0.87	-0.38	8.67	8.92	0.93	-0.21	8.90	0.31
Janja	0.55	-1.94	7.34	14.99	0.59	-1.74	7.19	14.91	0.64	-1.54	8.75	0.86
Kabaya	0.57	-1.61	7.52	10.03	0.68	-1.20	7.72	8.36	0.74	-0.97	8.82	0.16
Kawangire	0.76	-0.66	5.68	29.55	0.82	-0.50	5.94	14.87	0.92	-0.22	8.04	1.11
Kigali	0.85	-0.44	7.11	19.46	0.90	-0.29	8.14	16.47	0.96	-0.13	9.28	0.06
Muganza	0.76	-0.97	8.37	15.02	0.66	-1.37	8.77	6.93	0.77	-0.92	9.76	0.33
Muramba	0.52	2.02	7.17	21.49	0.60	0.33	7.82	11.73	0.63	0.47	9.41	0.30
Nemba	0.58	-1.60	6.58	17.81	0.65	-1.35	6.83	13.64	0.69	-1.21	8.27	0.69
Ntaruka	0.69	-1.13	7.71	8.10	0.68	-1.18	7.58	8.59	0.80	-0.72	9.02	0.08
Nyagahanga	0.74	-0.82	8.76	6.56	0.73	-0.83	8.49	3.98	0.89	-0.35	10.06	0.27
Rubengera	0.70	-1.05	6.83	19.14	0.74	-0.92	7.18	11.53	0.80	-0.71	8.43	0.48
Rubona	0.78	-0.72	7.08	21.68	0.77	-0.75	7.51	10.14	0.80	-0.63	9.18	0.09
Ruhengeri	0.62	-1.53	7.44	14.09	0.69	-1.25	7.32	16.55	0.72	-1.12	8.93	0.39
Rukozo	0.69	-1.00	5.99	21.64	0.76	-0.75	6.70	11.99	0.83	-0.55	8.01	0.43

The accumulated and the random errors were estimated by the use of the Root Mean Square Error and the correlation coefficient in order to evaluate the agreement between the satellites based and gauge stations rainfall data.
The RMSE was found in the range of 10.8mm/day to 5.7 mm/day, the highest for TRMM 3B42 v7 at Gikongoro station and the lowest for CMORPH 8km at Kawangire station. Generally, RMSE is higher for TRMM 3B42 v7 at the stations in and close to Nyabarongo basin with an overall value of 9mm/day against 7.6mm/day for RFE 2.0 and 7.3mm/day for CMORPH 8km. The higher value of RMSE signify less agreement with the reference dataset.

The correlation coefficient which emphasizes on the deviation observed in the satellite rainfall products vis-a-vis the station rainfall measurements according to the data distribution along a linear trendline in their scatterplots (see appendix 4). R^2 ranges from 0% to 100% with 100 as the perfect correlation.
In Nyabarongo basin the correlation between satellite and station rainfall data was found to be in the range of 0.02% to 29.5% with the minimum value for TRMM 3B42 v7 at Byimana station and the maximum for CMORPH 8km at Gikongoro station. In general the R^2 was found low in all satellite rainfall products however CMORPH 8km had a higher overall R^2 at the stations in and close to Nyabarongo basin with an overall value of 16.7% followed by RFE 2.0 with 11.2% and last TRMM 3B42 v7 with 0.5%.

With results showing considerable systematic errors, satellite estimates were further assessed based on findings on rain detection. Biases estimates were categorized into Hit rainfall bias, Missed rainfall Bias, and False rainfall bias following the description in section 4.7.
These bias components are given in mm/day at each station and for each satellite based rainfall estimates products. Results close to 0 show a good performance of the satellite product at the corresponding station.

Table 5-4: Daily depth of rainfall bias components

Station	CMORPH 8km			RFE 2.0			TRMM 3B42 v7		
	Hit rain	Missed rain	False rain	Hits rain	Missed rain	False rain	Hits rain	Missed rain	False rain
Busogo	-1.00	1.03	0.22	-1.10	0.78	0.36	-0.39	2.02	0.98
Butaro	-0.83	0.98	0.69	-0.99	0.71	0.89	-0.78	1.28	1.47
Byimana	-0.51	0.75	0.44	-0.79	0.45	0.52	0.10	1.88	1.30
Byumba	-0.61	0.85	0.23	-1.16	0.56	0.51	-0.37	1.66	1.32
Cyinzuzi	-0.70	1.48	0.68	-1.17	1.01	0.74	-0.27	2.22	1.28
Gikongoro	-1.26	0.71	0.34	-1.58	0.48	0.51	-0.45	2.23	1.38
Gitega	-0.07	0.78	0.31	0.11	0.89	0.41	0.02	1.44	1.20
Janja	-0.89	1.21	0.16	-1.27	0.76	0.29	-0.43	2.04	0.93
Kabaya	-0.94	1.09	0.41	-1.16	0.69	0.64	-0.52	1.76	1.32
Kawangire	-0.30	0.66	0.29	-0.65	0.46	0.59	0.04	1.51	1.25
Kigali	-0.24	0.58	0.37	0.01	0.60	0.30	-0.22	1.48	1.57
Muganza	-0.50	0.95	0.48	-1.33	0.66	0.60	-0.53	1.91	1.52
Muramba	-1.21	0.98	0.16	-1.27	0.73	0.31	-0.24	2.29	0.99
Nemba	-0.83	0.91	0.13	-0.90	0.73	0.27	-0.21	1.90	0.90
Ntaruka	-0.66	1.07	0.59	-0.92	0.79	0.52	-0.47	1.52	1.27
Nyagahanga	-0.43	1.25	0.85	-0.88	0.93	0.96	-0.37	1.67	1.69
Rubengera	-0.64	0.81	0.37	-0.86	0.55	0.48	-0.19	1.72	1.20
Rubona	-0.34	0.79	0.40	-0.81	0.55	0.60	-0.22	1.80	1.39
Ruhengeri	-0.96	0.86	0.29	-0.80	0.79	0.34	-0.56	1.65	1.08
Rukozo	-0.56	0.76	0.30	-0.68	0.53	0.45	-0.16	1.62	1.23

The bias from the Hit rainfall depth was varying between -1.6 and 0.1 mm/day with the highest value at Gitega station and the lowest at Gikongoro station for RFE 2.0. The overall Hit rainfall bias depth showed that in general the satellite based rainfall estimates products underestimates rainfall depths when the latter is detected both in station measurements and in the satellite products.
The range of the bias from the Missed rainfall depth was found between 0.4 and 2.3mm/day, the lowest value being for RFE 2.0 at Byimana station and the highest for TRMM 3B42 v7 at Muramba station. The overall Missed rainfall bias depth was found less for RFE 2.0 followed by CMORPH 8km.
The bias from the falsely detected rainfall depth was also assessed and found ranging between 0.1 and 1.7mm/day. The highest value was indicated for TRMM 3B42 v7 at Nyagahanga EFA station and the smallest value for CMORPH 8km at Nemba station. Figures5.2 and 5.3 show graphs presenting these findings, the stations were split into two groups according to the elevation of their location for display purposes. It can be seen that the depth of missed rainfall contributes more to the bias than the two other bias components.

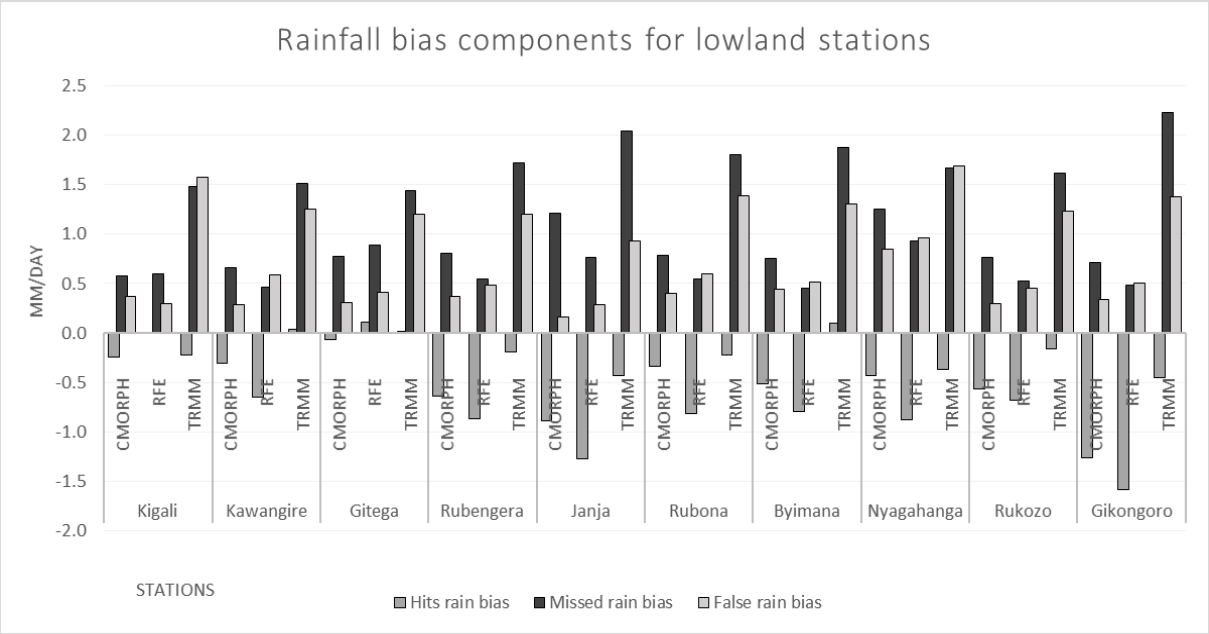

Figure 5-2: Daily depth of rainfall bias components for highland stations

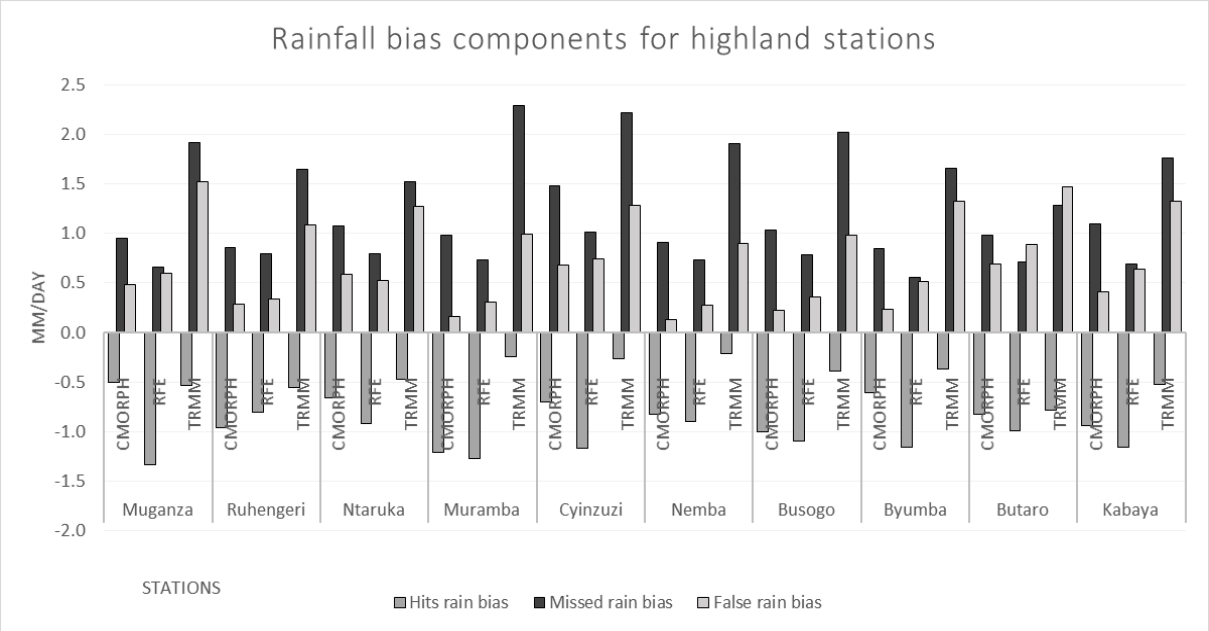

Figure 5-3: Daily depth of rainfall bias components for highland stations

5.1.2. Sub-Basins Scale Analysis

The rainfall depth from satellite based rainfall estimates and the gauges stations were spatially averaged over each of the three catchments of Nyabarongo basin. This was done by Thiessen polygons for station measurements and simple arithmetic mean of the rainfall products pixels values covering the respective catchments.

Rainfall occurrence analysis

The rainfall occurrence analysis of the satellite rainfall products showed good results when the rainfall estimates were summed and averaged by arithmetic mean over the catchments in Nyabarongo basin compared to the detection analysis at stations.

As shown in the table 5-5, in a five year period (2009-2013) the Hits were more than the sum of the Missed and the False rainfall events together, the Corrected Negative events were in the same range around 30%.

The percentage of days with False rainfall events was between 1.6 and 2.7% for CMORPH 8km, and 2.7 to 3.2% for TRMM 3B42 v7 and slightly higher for RFE 2.0 with 5 to 6% days with rainfall wrongly detected.

The number of days for rainfall occurrence are all expressed in percentage of rainfall events occurrence in one catchment following the relation below:

$$\frac{Event\ hits + Missed\ events + False\ events + Correct\ negative\ events}{Number\ of\ Days\ of\ the\ Timeslot} = 100\%$$

Table 5-5: Satellite products' rainfall occurrence in Nyabarongo basin (2009-2013)

Catchment	CMORPH 8km				RFE 2.0				TRMM 3B42 v7			
	Hits	Missed	False	Negative	Hits	Missed	False	Negative	Hits	Missed	False	Negative
Mukungwa	44.1	22	2.5	31.5	52	14	6	27.9	38.3	27.7	2.8	31.1
Nyabarongo Downstream	41.8	22.6	1.6	34	47.5	16.9	5	30.6	45.2	19.2	2.7	32.9
Nyabarongo Upstream	43.4	17.1	2.7	36.9	47.6	12.9	6	33.5	43.2	17.3	3.2	36.3

Contingency table score

The contingency table score was made and the results showed significant improvements in for Critical Success Index (CSI); with all its values superior to 0.5.

RFE 2.0 showed the highest value of CSI whereas the lowest was found for TRMM 3B42 v7, both in the Mukungwa catchment.

The bias frequency was found in the ranges of 0.62 and 0.88, the lowest being for TRMM 3B42 v7 in Mukungwa and the highest for RFE 2.0 in Nyabarongo Upstream catchment. Table 5-6, shows results for the contingency score for rainfall occurrence in the catchments.

Table 5-6: Satellite rainfall products' contingency table scores in Nyabarongo basin (2009-2013)

Catchment	CMORPH 8km				RFE 2.0				TRMM 3B42 v7			
	FB	POD	FAR	CIS	FB	POD	FAR	CIS	FB	POD	FAR	CIS
Mukungwa	0.705	0.667	0.053	0.643	0.879	0.788	0.104	0.722	0.624	0.580	0.069	0.556
Nyabarongo Downstream	0.675	0.649	0.038	0.633	0.816	0.738	0.096	0.684	0.745	0.702	0.057	0.673
Nyabarongo Upstream	0.762	0.717	0.058	0.687	0.887	0.787	0.112	0.716	0.767	0.714	0.070	0.678

The rainfall occurrence analysis of the satellite rainfall products showed more correlation with the *in situ* measurements when the analysis was done per catchments than when it was done per point location.

Rainfall estimated depth

The depth of rainfall in the sub-basins was assessed by use of statistical and graphical analysis as it was done for in section 5.1.1.

The results shown in Table 5-7 indicate smaller values of RMSE compared to the findings in the point to pixel analysis, and they vary from 4 to 5.7mm/day. The highest value of RMSE was found for RFE 2.0 in Nyabarongo upstream catchment, and the smallest was for CMORPH 8km in Nyabarongo downstream.

The bias was found varying from 0.6 to 0.8 with the highest bias being for TRMM 3B42 v7 in Nyabarongo downstream catchment and the lowest value for CMORPH 8km in the Mukungwa catchment.

As all the values of the bias were found inferior to 1 and the mean error was found negative for these rainfall products, it showed that the satellite products were underestimating the rainfall depth in Nyabarongo basin as was also the case in the point to pixel analyses.

The level of agreements of the satellite data with the *in situ* data averaged over the sub-basins, was measured using the R^2 measure. It was found that R^2 was higher for CMORPH 8km with an overall value of 37.3 % against 31 % for TRMM 3B42 v7 and 24.1 % for RFE 2.0

Table 5-7: Statistical analysis of satellite rainfall product in reference to sub-basin scale *in situ* observations in Nyabarongo sub-basins.

Catchment	CMORPH 8km				RFE 2.0				TRMM 3B42 v7			
	Bias	ME	RMSE	R^2	Bias	ME	RMSE	R^2	Bias	ME	RMSE	R^2
Mukungwa	0.601	-1.534	4.539	34.43	0.684	-1.216	5.046	24.52	0.716	-1.094	5.525	25.05
Nyabarongo Downstream	0.687	-1.026	4.098	38.38	0.728	-0.892	4.668	26.99	0.799	-0.658	4.317	34.43
Nyabarongo Upstream	0.649	-1.285	4.754	39.28	0.687	-1.148	5.718	20.98	0.739	-0.957	5.061	33.63

The bias was divided into its three components (Hit, Missed rainfall and False rainfall biases). It was revealed that the main bias source was the Hits rainfall bias depth for CMORPH 8km and RFE 2.0 while it was the Missed rainfall bias depth for TRMM 3B42 v7. The false rainfall bias depth is small for the 3 satellite rainfall products as shown in Figure 5-4.

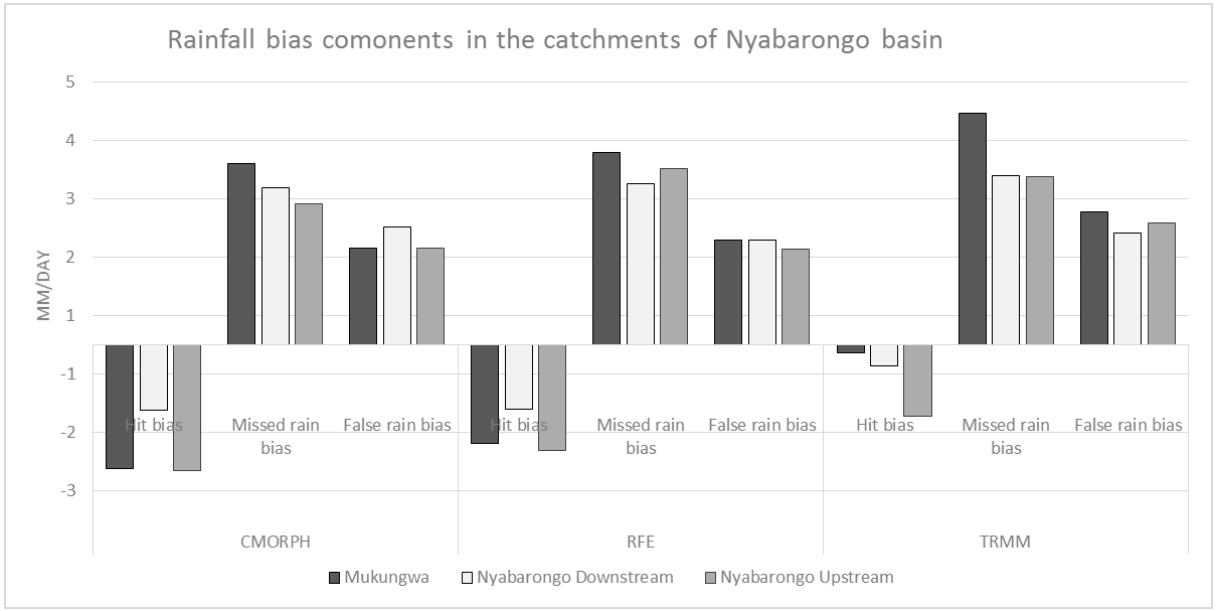

Figure 5-4: Daily depth of rainfall bias components in the sub-basins of Nyabarongo

5.1.3. Rainfall Data Bias Correction

Different techniques of error determination showed strong disagreements between *in situ* measurements at the stations and satellite rainfall products. Therefore, to correct systematic errors found in the previous section, bias correction was applied to the data extracted from the satellite rainfall products for further use in the hydrological modelling.

The bias correction was done per sub-basins and, in reference to the *in situ* measurements, a significant increase of rainfall depth was denoted in the bias corrected time series compared to the uncorrected data from the satellite rainfall products.

This is illustrated in the different kind of graphical analysis done as shown in the Figure 5-5 and Figure 5-6.

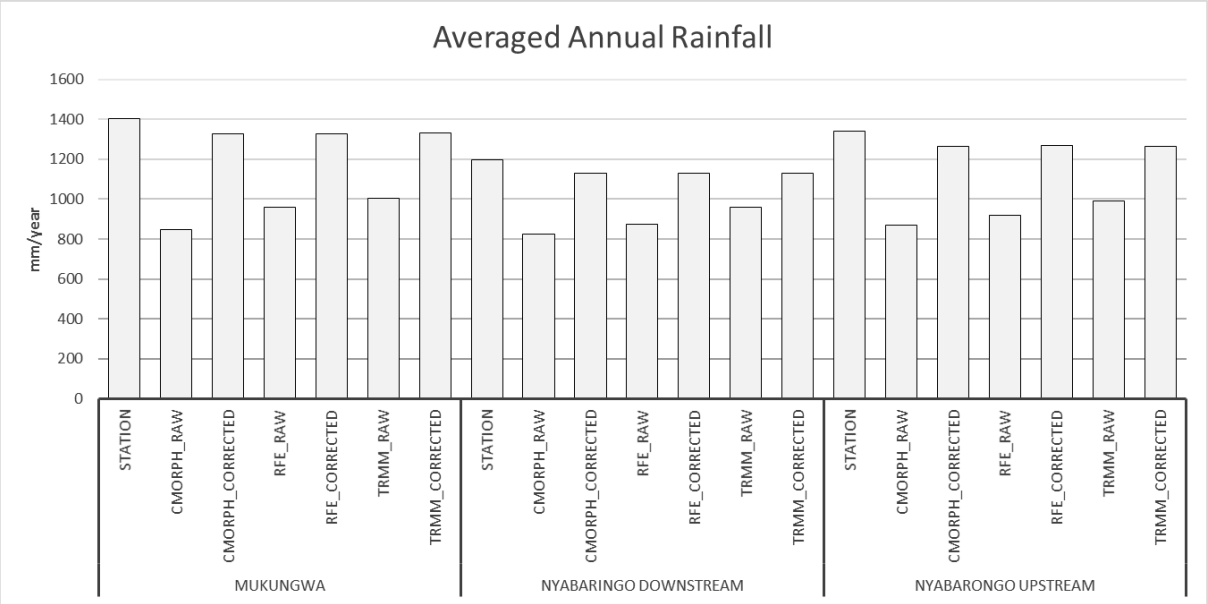

Figure 5-5: Sub-basin scale comparison of averaged annual rainfall from satellite products and *in situ* observations

The graph of averaged annual rainfall show that after the bias correction was applied to the uncorrected data directly extracted from the satellite rainfall products, the obtained bias corrected time series roughly matched up with the *in situ* measurements

Not surprisingly, statistical analysis of the rainfall depths of the bias corrected time series revealed a RMSE and R^2 indicating a better correlation with the *in situ* measurements compared with the uncorrected satellite data. For example RMSE decreased considerably up to 4.1mm/day and R^2 increased up to 56% for the bias corrected CMORPH 8km time series.

The accumulated mass curve plot of the areal rainfall representation of the sub-basins, the uncorrected and the bias corrected satellite based datasets in Figure 5-6, showed a strong agreement between the bias corrected time series from the different products used for this study among them, and with the *in situ* measurements.

The rainfall depth underestimation from the uncorrected satellite products was also denoted.

CMORPH 8 km was the one found to underestimate the rainfall depths the most, as compared to the *in situ* measurements, followed by RFE 2.0 and TRMM 3B42 v7.

The short intervals between the successiveness of the two rain seasons in the basin, the short rainy season (September, October, November and December) and the long rainy season (March, April and May), don't allow a very clear differentiation of the two dry seasons situated in between.

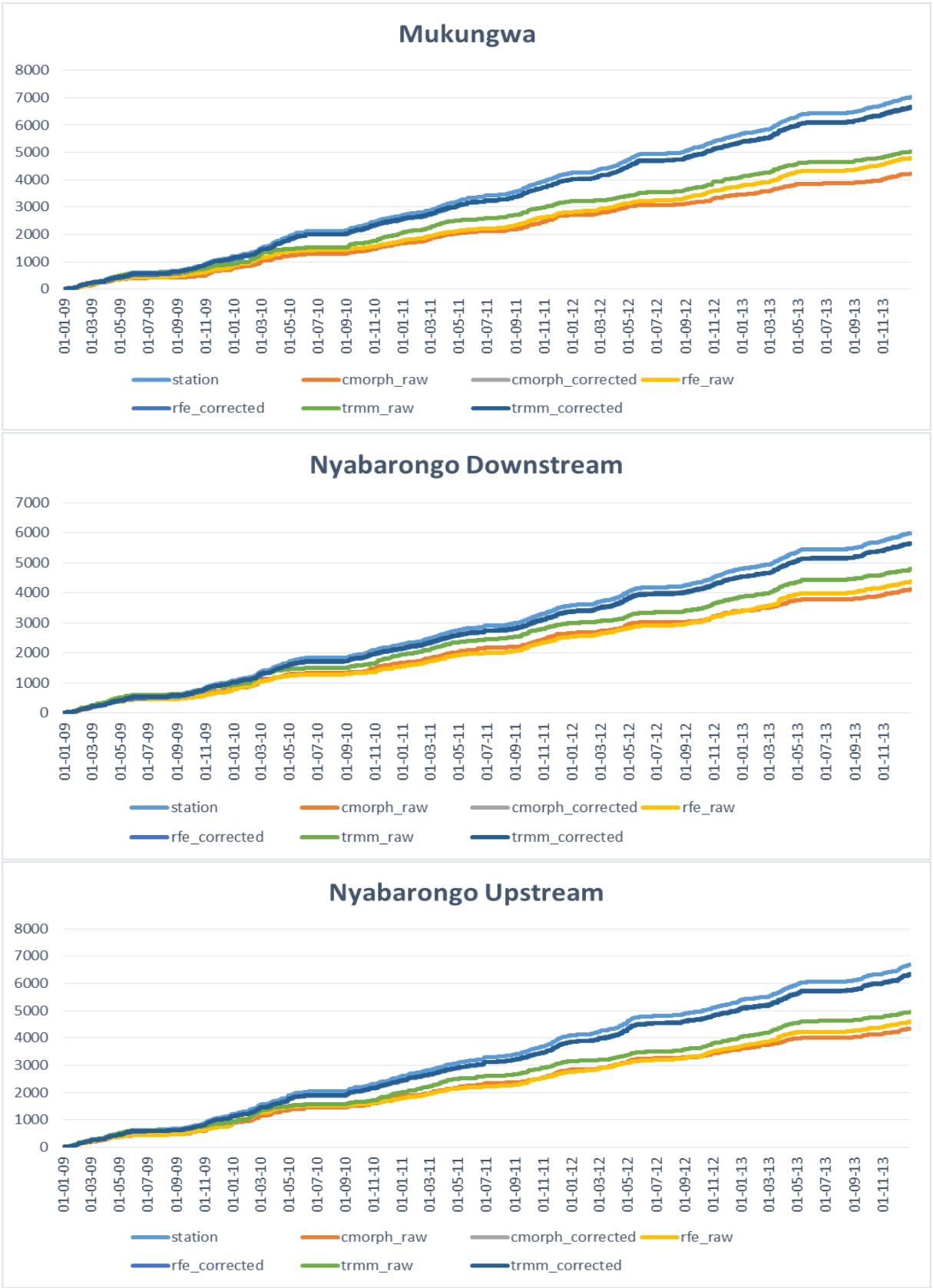

Figure 5-6: The accumulated mass curve plots of the sub-basin scale rainfall from the *in situ*, the uncorrected and the bias corrected satellite products observations

5.2. Potential Evatranspiration Datasets Comparison and Bias Correction

The potential evapotranspiration product used in this study was also compared to the *in situ* measurements from 5 Agro Synoptic stations operated by RMA Comparison aimed to evaluate estimates of evaporation from FEWSNET satellite estimates (i.e. FEWSNET PET product) at daily base for the period 2009-2013. The comparison was based on both statistical and graphical analysis.

5.2.1. Point to Pixel Analysis

A point to pixel analysis showed that the FEWSNET PET averaged annual PET was found having higher values than 4 out of 5 stations with the exception of Gisenyi airport station. There was no clear relation with the elevation in both the stations and the FEWSNET PET datasets.

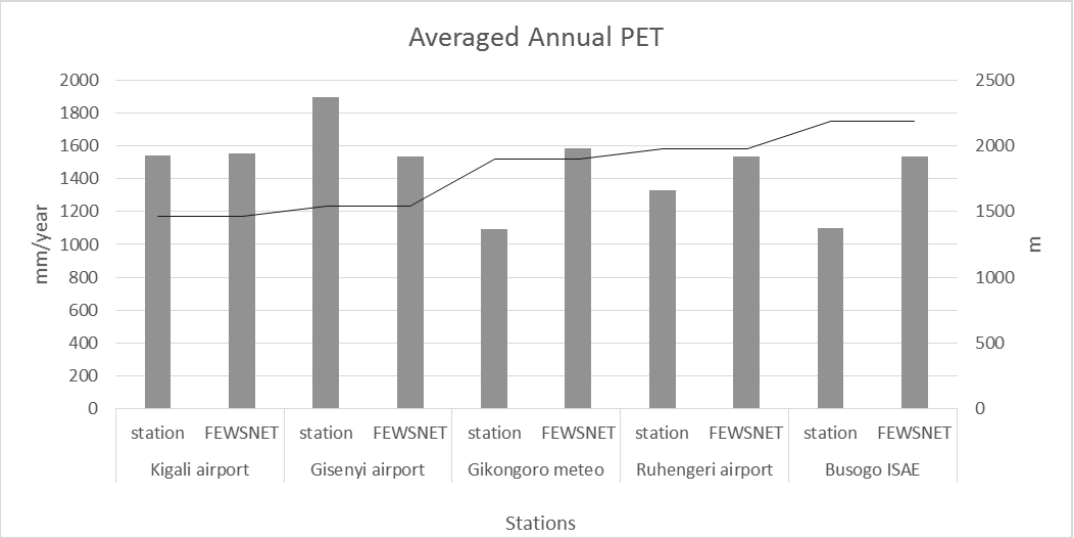

Figure 5-7: Comparison of averaged annual PET from FEWSNET and stations estimates

PET estimates depth

The analysis of the FEWNET PET product, depth wise at daily basis for the period of 2009-2013, was done by the same statistical analysis as for assessing the satellite based rainfall products. The agreement on the depth of the PET between the satellite product and the *in situ* measurements at the evaporation gauge stations showed a RMSE varying from 1.7 to 2.3 and R^2 in the range of 3.2% to 10.5%.

For a 5 year timeslot selected for this study, the mean error and the bias showed that the FEWSNET PET was overestimates with respect to counterparts' stations measurements, apart from the Gisenyi airport station. The bias was found varying between 0.8 and 1.4, the latter found at Gikongoro meteo station.

Table 5-8: Statistical analysis of FEWSNET PET estimates in reference to stations data.

Stations	ME	RMSE	R^2 [%]	Bias
Busogo Isae	1.204	2.136	3.325	1.400
Gikongoro Met	1.340	1.971	10.522	1.447
Kigali Aero	0.044	1.761	9.053	1.010
Ruhengeri Aero	0.573	2.115	3.294	1.157
Gisenyi Aero	-0.979	2.378	6.242	0.811

5.2.2. Sub-Basins Scale Analysis

Estimates from the FEWSNET PET product and the gauge stations estimates were spatially averaged over the sub-basins of Nyabarongo by the use of the Thiessen polygons for the *in situ* data and simple arithmetic mean of the pixels values covering the respective catchments.

The same scheme of analysis was conducted and the findings summarized in Table 5-9 showed that the PET depth assessment over sub-basins shows better agreement to the *in situ* estimates comparing to the point to pixel analysis done in section 5.2.1. The mean error was found varying between 0.1 and 1.2 respectively in Nyabarongo downstream and Nyabarongo Upstream catchments. The bias was varying from 1 to 1.4 as shown in Table 5-9.

Table 5-9: Statistical analysis of FEWSNET PET estimates in reference to sub-basin scale *in situ* estimates in Nyabarongo sub-basins.

Catchments	ME	RMSE	R^2 [%]	Bias
Mukungwa	0.840	1.904	4.88	1.249
Nyabarongo Downstream	0.169	1.623	10.15	1.041
Nyabarongo Upstream	1.251	1.821	11.87	1.405

5.2.3. Potential Evapotranspiration Data Bias Correction

Bias correction was applied to the FEWSNET PET product before usage in hydrological modelling with HBV-light. Similar to the procedure to correct the satellite rainfall product data, the PET date were corrected based on the accumulation of 7 days' time window for the PET estimates spatially averaged over the 3 Nyabarongo sub-basins.

The averaged annual PET estimates from the stations, the uncorrected and the bias corrected FEWSNET PET product time series are plotted together for graphical analysis as shown in Figure 5-8.

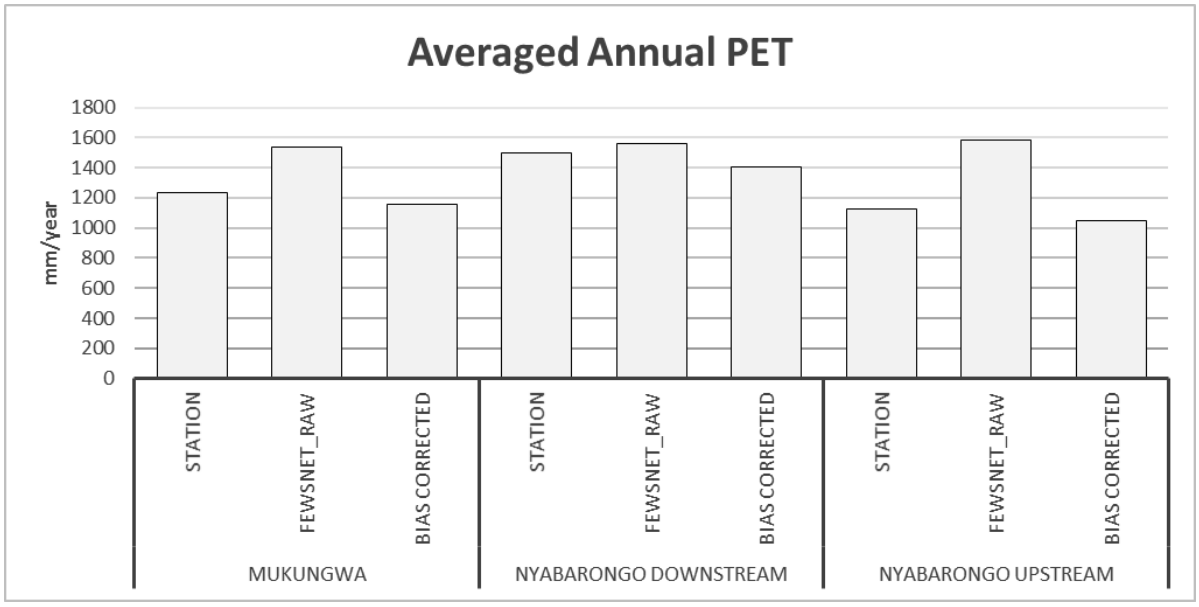

Figure 5-8: Sub-basin scale comparison of averaged annual PET from *in situ*, uncorrected and bias corrected FEWSNET estimates

The bias corrected time series roughly matches up with the *in situ* measurements, although underestimation of the depth of the PET estimates is now denoted.
Statistical analysis of the bias corrected PET estimates time series in reference to the *in situ* estimates showed a stronger correlation than the uncorrected satellite data. R^2 was found at 21% in Mukungwa catchment, at 36% in Nyabarongo downstream catchment and at 38% in Nyabarongo upstream catchment. RMSE was varying from 1.27 to 1.52.

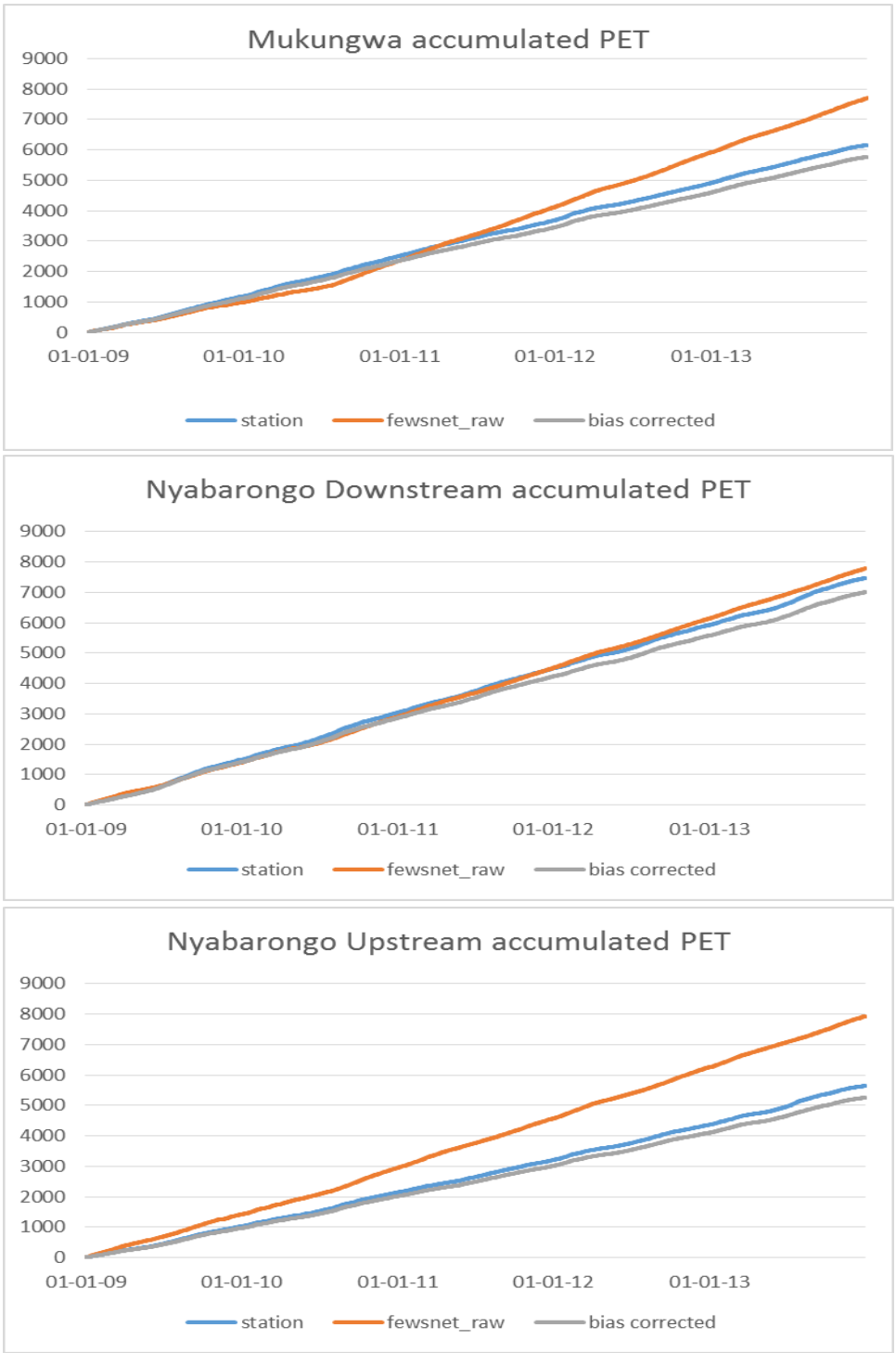

Figure 5-9: The accumulated mass curve plots of the sub-basins averaged PET from the stations, the uncorrected and the bias corrected FEWSNET PET product.

In Figure 5-9, the accumulated mass curve plots of the sub-basins aggregates of the *in situ*, the uncorrected and the bias corrected FEWSNET PET product time series shows a linear pattern with visible differences of the accumulated PET depth over time. Less differences are noted in Nyabarongo downstream catchment as it was also found with a smaller bias value (1.041)

5.3. Hydrological modelling

The hydrological modelling in HBV-light was done using different meteorological input datasets. Firstly the *in situ* measurements were incorporated into the model as the reference data in this study and assumed to be true. Daily hydro-meteorological input data were set into the model together with other sub-basins characteristics as required by the basic model variant of HBV-light.

For daily stream flow simulation in HBV-light, daily mean sub-basins time series of the forcing data were used. The observed discharge measurements at Ruliba station were set into the model as well, for calibration purposes.

5.3.1. Elevation Vegetation Zones of Nyabarongo Basin

The elevation vegetation zones were obtained by crossing the elevation zones map, the vegetation type map and the sub-basin boundaries. From this operation, a weight for every vegetation type per elevation zone within each sub-basin was determined and loaded into the model.

It was found that the Mukungwa sub-basin had 16 elevation zones of 200m ranging from the 1450m to the 4450m elevation zone, with 3 vegetation type and some lakes, where the cropland occupies 59.8% of the sub-basin against 31.9% for the forestland, 7.7% for the lakes, and 0.6% of built up areas.

Nyabarongo downstream catchment was found with 8 elevation units of 200m each from the 1250m to the 2650m elevation zone, also it has 3 main vegetation types, a lake and a number of water ponds; the cropland was found leading again with 60.3% of the sub-basin, the forestland occupies 35% and 2.4% occupied by water. The built up area in this sub-basin had a higher percentage than in the other sub-basins, with 2.3%.

The third sub-basin, the Nyabarongo upstream catchment, had also 8 elevation units of 200m as well from the 1450m to the 2850m elevation zone and the main vegetation type were ranked as follow, the cropland with 67% of the sub-basin area, followed by the forestland with 31.7%, then 0.7% covered by water and 0.4 % of the built up areas.

5.3.2. HBV model runs and parameterization

For assessment of the model performance, the model efficiency known as the Nash-Sutcliffe coefficient (NSE) and the mean difference (MeanDiff) objective function are used as described in section 4.8.2. Visual inspection of the simulated and the observed stream flow was considered as well to decide of the best fit of the hydrographs patterns. Model calibration was performed by "trial and error" optimization procedure where model parameters are optimized to adjust the simulated to the observed stream flow hydrographs. The calibration target is to 1 or values close to 1 for the NSE objective function which determines the best overall performance of the model, and a MeanDiff equal to zero or close to 0 is the target value. This is applicable to the RVE which most of the time preferred to the MeanDiff even though, they are all focalized on the volume of water in the system as described in section 4.8.2.

First the basic model variant was selected with the standard model type of HBV-light. This was done using *in situ* measurements of the meteorological variables and the model behavior showed an accumulation of water in the system increasing over the whole period of simulation.

As it was obvious that water release from the system was to slow, another HBV-light model type using routing response with delay under the same basic model structure was adopted for this study.

It is said (Seibert, 2005) the structure is used for catchments with deep groundwater as it is the case for Nyabarongo basin according to the Water Resources Master Plan in Rwanda (SHER Ingénieurs-Conseils s.a., 2012).

The difference between the two model types is that, for the standard response routine, the whole amount of the recharge water is directly conveyed from the soil moisture store to the soil upper zone, then from the soil upper zone water reaches the lower zone store through percolation. While for the response routine with delay model type; the recharge coming from the soil routine is divided into two parts, where one portion of the recharge is directly conveyed to the storage in the lower zone and the other one goes to the storage in the upper zone as illustrated in figure 5-11 and 5-12 (Seibert, 2005).

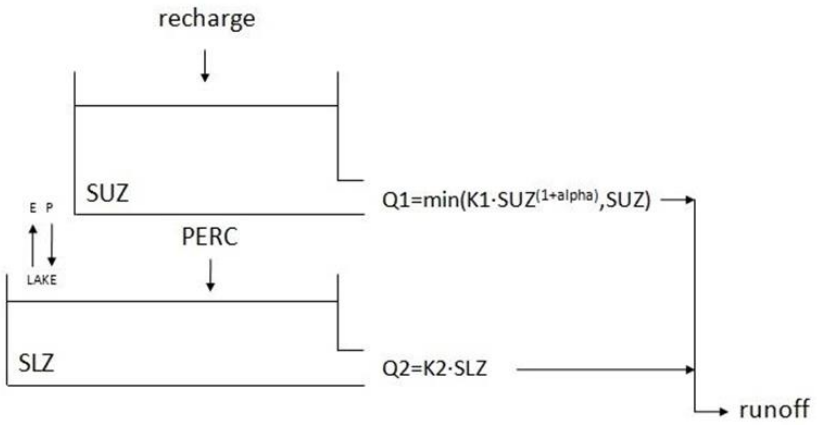

Figure 5-10: Standard model response routine

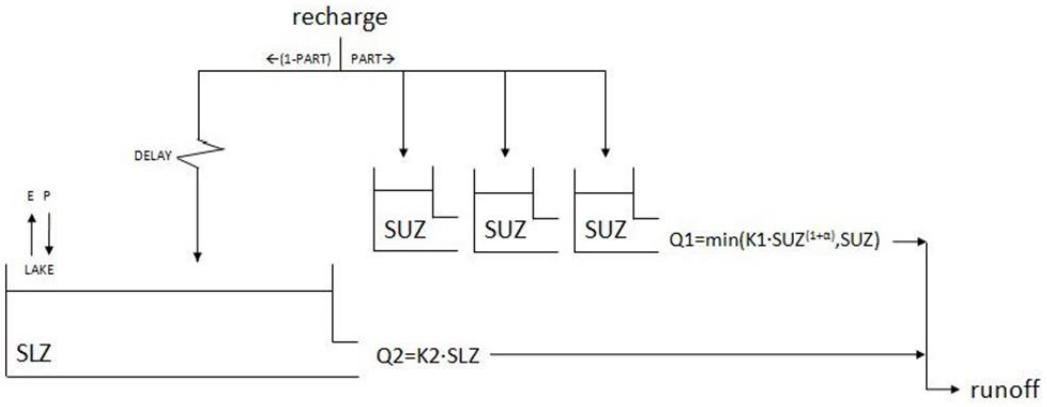

Figure 5-11: Response routine with delay model type

Where, E and P are respectively the evaporation and the precipitation from the Lakes, the SUZ is the storage in the upper zone, the SLZ is the storage in the lower zone, K1 and K2 are the recessions coefficients for the discharges form the upper (Q1) and the lower (Q2) zones respectively. Alpha is a parameter for the non-linearity of the Q1 in both cases and the PERC is the parameter for percolation.

In the standard structure model type percolation is a water flux from the upper zone to the lower zone whereas in the Response routine with delay model type, percolation is replaced and based on the parameter PART which redistributes recharge water from the soil moisture zone. Recharge portion added to the upper zone is estimated recharge flux multiplied by PART whereas the portion added to the lower zone reads recharge multiplied by 1-PART.

5.3.3. Model sensitivity analysis using *in situ* datasets.

As part of the calibration of the model, a sensitivity analysis was applied to evaluate the sensitivity of the model to changes of model parameter values. The objective of the sensitivity analysis, was to identify and separate sensitive model parameter and insensitive parameter which are ignored from extensive optimization. This was done by increasing and decreasing the values of one model parameter at a time by 10% up to 100%.

The influence of each model parameter was analyzed based on NSE, RVE and RMSE objective functions using graphical plots for visualization, hence, the parameters with abrupt slopes, are therefore considered to be more sensitive, as compared to those that have gentle slope, which are considered to be less sensitive.

The parameters at which the model performance was sensible the most in this study were found to be the PART parameter, K1, K2 and Beta, while Alpha, FC, LP and the MaxBas were found moderately sensible. The sensitivity of model performance to the Delay parameter was found relatively weak with a constant value of the NSE, a RVE ranging between 5.26 and 5.22 and a RMSE between 13.97 and 13.87. The figures below show the sensitivity of the model to each of the parameters sited above. The model parameter analysis helped in finding which parameters to optimize extensively to attain the highest possible accuracy.

For this study two classes of model parameters were defined according to their sensitivity.

After some "trial and error" calibrations, a satisfactory fit of the hydrographs patterns between the simulated and observed stream flow was reached, but the objective functions values were still modest. The model sensitivity was initiated by changing the value of each parameter, one at a time by reducing and increasing it to evaluate its effect on the model behavior which is expressed by the objective functions. The parameter was returned to its original (initial) value before changing another one.

On the graphs in Figure 5.12, the original values of the parameters when satisfactory fit is reached are shown in the middle (at zero change) of the horizontal axis (abscissa) and the change objective functions are shown on the vertical axis (ordinates). Curves of the changes of the objective functions when the original values of the parameters are increased or decreased are plotted.

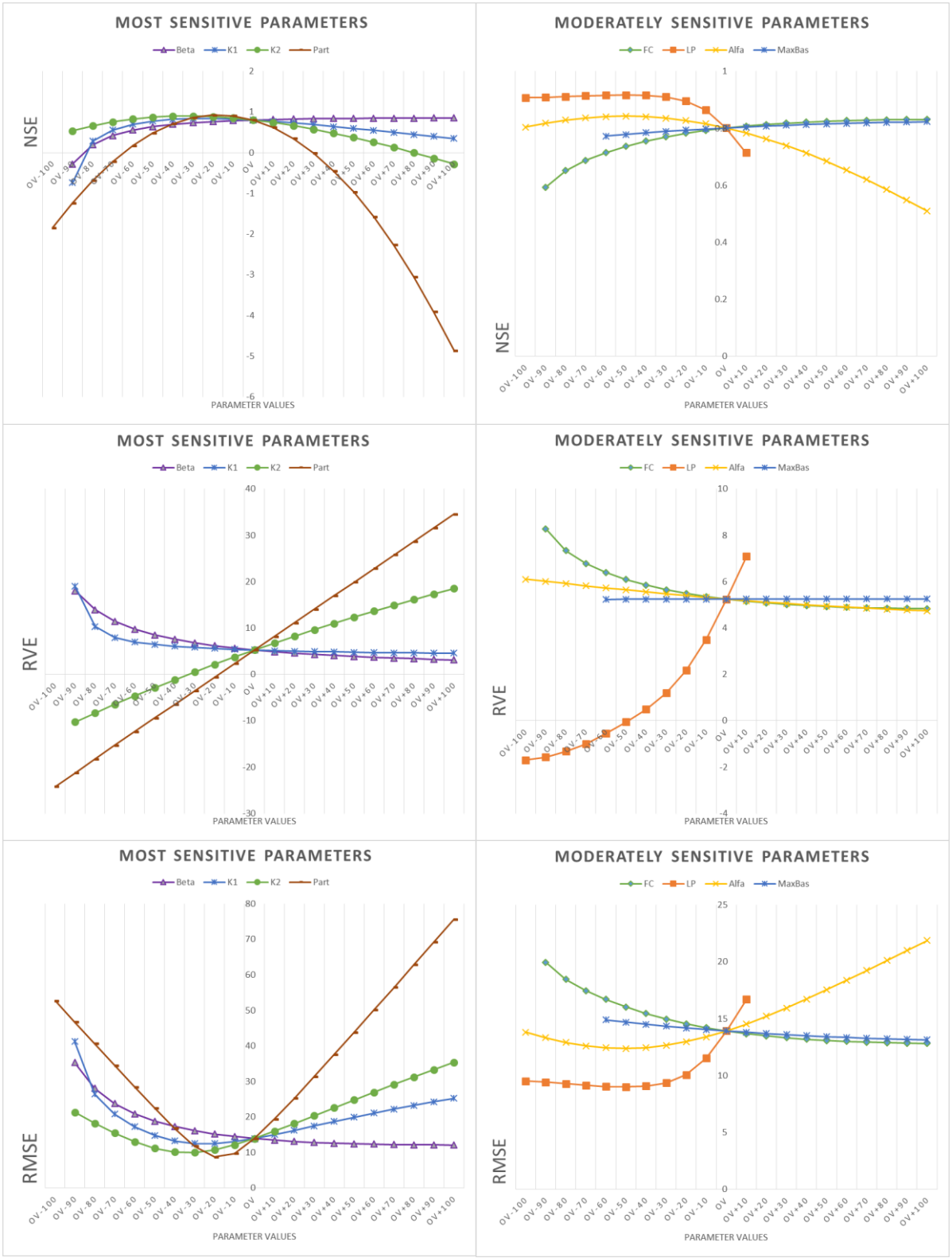

Figure 5-12: Model Parameter sensitivity analysis

The parameterization was done prior to the model parameter range taken from Rientjes (2014) but for some parameters, it was not found to be the best match for Nyabarongo basin, probably due to fact that the model structure selected in this study was different and the study areas were different too. The HBV model optimum parameter set for Nyabarongo River is presented in table 5.12.

Table 5-10: HBV optimized model parameter set for Nyabarongo river stream flow.

	HBV-light valid range		Prior model parameter range		Nyabarongo basin
Model parameter	Minimum	Maximum	Minimum	Maximum	Optimized model parameter
FC (mm)	0	∞	125	800	600
LP	[0	1]	0.1	1	0.9
BETA	0	∞	1	4	1.5
ALFA	[0	∞	0.1	3	0.001
K1 (/Δt)	[0	1	0.0005	0.15	0.019
K2 (/Δt)	[0	1	0.0005	0.15	0.0003
MAXBAS (Δt)	[1	100]	-	-	3
PART	[0	1]	-	-	2.555
DELAY (Δt)	[0	∞	-	-	1

5.3.4. Comparison of simulated stream flow and water balance closure

The model was found performing very well with the *in situ* time series of rainfall and potential evapotranspiration, the Nash-Sutcliffe coefficient was very close to one and the relative volumetric error close to zero as shown in Table 5-13.

Table 5-11: Model simulation results using *in situ* and bias corrected meteorological datasets input.

Objective function	*In situ* measurements	CMORPH 8km Bias corrected	RFE 2.0 Bias corrected	TRMM 3B42 v7 Bias corrected	FEWSNET PET Bias corrected
NSE	0.958	0.884	0.884	0.890	0.950
RVE	-0.019	-5.031	-4.775	-4.787	1.344
RMSE	6.411	10.627	10.626	10.382	6.963

The optimized model parameter set was then used to simulate Nyabarongo stream flow using bias corrected time series from satellite based meteorological products. The calibration results showed good model performance for all of the time series as well. However the stream flow measurements were not sufficient for the validation of the model.

The bias corrected time series from different products were found with high NSE and RVE but not as much as the *in situ* measurements time series. For the bias corrected satellite based data best results were found when the FEWSNET PET product replaces the *in situ* PET estimates as input to the model.

The bias corrected satellite rainfall product that showed a better performance as input to the HBV model in Nyabarongo basin was TRMM 3B42 v7 followed by RFE 2.0 and CMORPH 8km. That coincide with the analyses done comparing those three products in section 5.1, where TRMM 3B42 was found with less bias than RFE 2.0 and CMORPH 8km (in that order). And as the rainfall estimates from the satellite products were underestimated compared to the *in situ* measurements, even after bias correction, this was reflected in the simulated discharge as well.

The simulated stream flow from the *in situ* measurements was higher than the other simulated stream flow when the bias corrected rainfall estimates from the satellite products were used as inputs to the model. This is illustrated in figure 5.13.

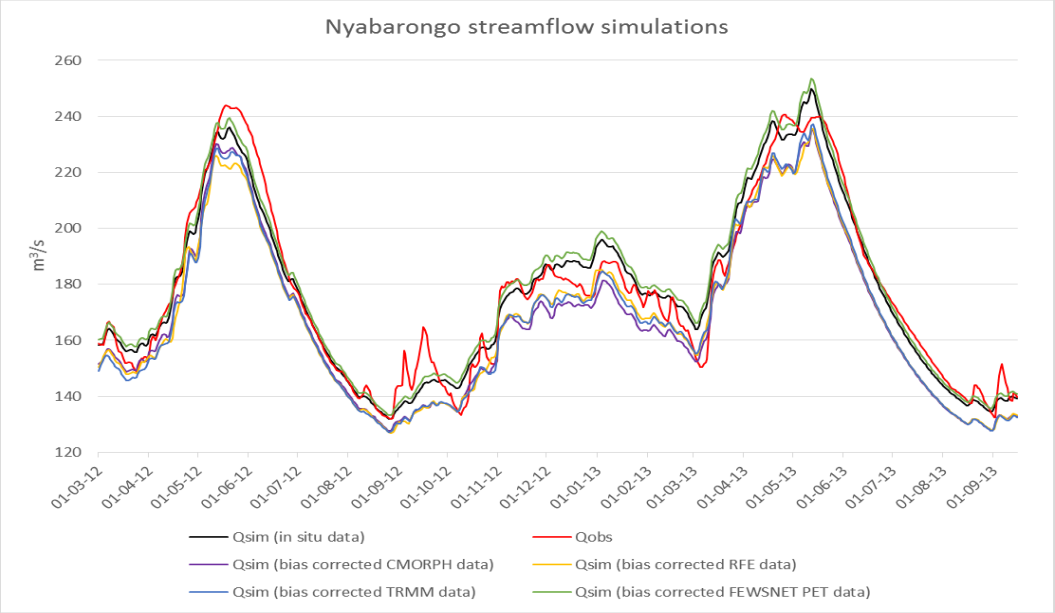

Figure 5-13: Nyabarongo stream flow simulated using *in situ* measurements data and bias corrected satellite based data

The stream flow simulation using bias corrected satellite based meteorological time series looks a lot like to the stream flow using the *in situ* measurements time series as the bias has been corrected in reference to the *in situ* data.

The stream flow modelling was also done using the uncorrected (raw) data extracted from the satellite based meteorological products as shown in Figure 5.14. Apart from the FEWSNET PET product the optimized parameter set obtained using *in situ* measurements was found not valid to the uncorrected satellite data and each satellite product required its own calibration. .

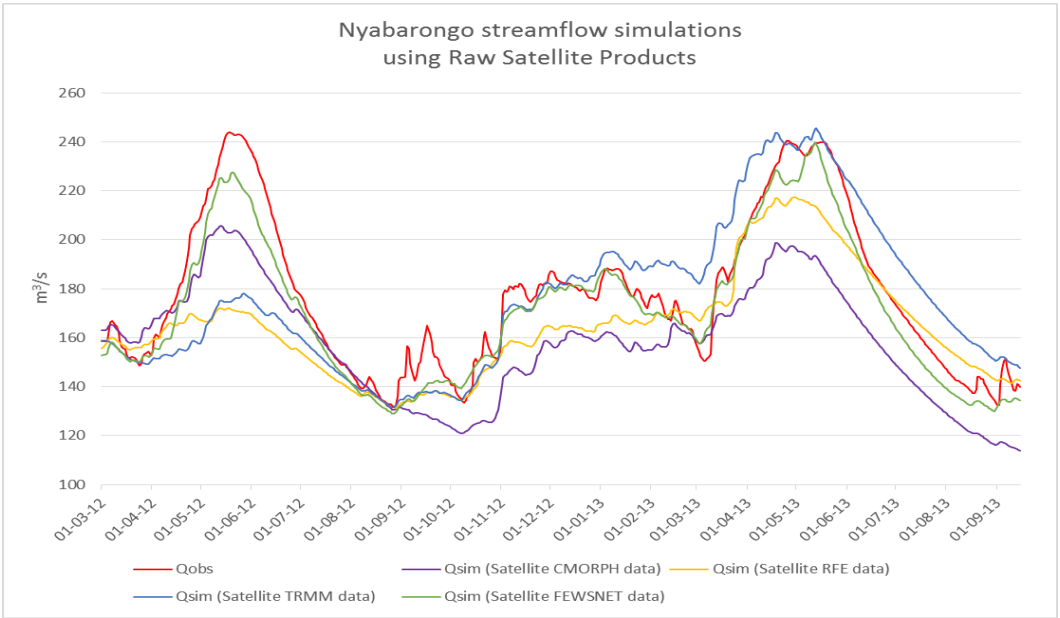

Figure 5-14: Nyabarongo stream flow simulated using uncorrected satellite based data

The calibration of the model for the satellite products was done prior to the *in situ* measurements parameter set but for the most sensitive model parameters this was not possible as shown in Table 5-12.

Table 5-12: HBV-light optimized parameter set for each of the satellite meteorological input dataset for Nyabarongo stream flow modelling

Model parameter	*In situ* Measurements	CMORPH 8km	RFE 2.0	TRMM 3B42 v7	FWESNET PET
FC (mm)	600	600	600	600	600
LP	0.9	0.9	0.9	0.9	0.9
BETA	1.5	1.5	1.5	1.5	1.5
ALFA	0.001	0.001	0.001	0.001	0.001
K1 (/Δt)	0.019	0.009	0.007	0.008	0.019
K2 (/Δt)	0.0003	0.0003	0.0003	0.0003	0.0003
MAXBAS (Δt)	3	3	3	3	3
PART	2.555	0.61	0.46	0.53	2.555
DELAY (Δt)	1	1	1	1	1

The model results were not satisfactory as the model performance was weak, except for the FEWSNET PET product which showed high values of the objective functions; NSE at 0.9 and RVE at -3.548. The results of the model when the uncorrected satellite data are used are shown in Table 5-13

Table 5-13: Model simulation results using uncorrected satellite based products' input datasets

Objective function	CMORPH 8km Uncorrected data	RFE 2.0 Uncorrected data	TRMM 3B42 v7 Uncorrected data	FEWSNET PET Uncorrected data
NSE	0.385	0.471	0.482	0.918
RVE	-11.134	-7.294	-8.84	-3.548
RMSE	24.515	22.738	22.500	8.932

The stream flow simulation of Nyabarongo River using uncorrected satellite based rainfall products showed low values of the NSE below 0.5 and a high RMSE values than the ones observed when the *in situ* rainfall data were used. The model showed weaker performances when CMORPH 8km is used as forcing data even though it shows a better pattern of the simulated discharge hydrograph. This can be associated to the fact that in this study CMORPH 8km was found with higher coefficient of correlation (R^2) but with the lowest value of the bias; which means that CMORPH 8km agrees more with the station data than the other products according to the data distribution in the scatterplots, but also underestimates more the observed rainfall depth.

Model water balance components comparison

The assessment of the water balance components was done to compare the model outputs for the five input datasets used in HBV model.

For this purpose the hydrological year 2012/2013 was used, starting from the end of the dry season in September 2012 till September 2013.

The results are summarized in the Table 5-14 where, besides the accumulated depth of simulated actual evapotranspiration and discharge time series, the change in storage of the soil moisture, the soil upper zone and the soil lower zone are shown when different forcing data are used in the model.

When accumulated all over the hydrological year, the *in situ* observations were found with greater rainfall depth and simulated actual evapotranspiration estimates. The high simulated stream flow and big change in the soil lower zone were found when the FEWSNET product replaces *in situ* estimates in the model. The high change in the lower zone water storage can be explained by the interconnectivity of the groundwater basins in Rwanda.

Table 5-14: Nyabarongo downstream catchment water balance components after simulation in HBV-light (2012/2013)

Water balance components [mm]	*In situ* measurements	CMORPH 8km Bias corrected	RFE 2.0 Bias corrected	TRMM 3B42 v7 Bias corrected	FEWSNET PET Bias corrected
Rainfall	1263.4	1160.9	1185.4	1182.3	1263.4
Actual ET	1159.7	1135.6	1140.8	1141.1	1100.9
Q simulated	1718.8	1615.7	1629.9	1629.5	1742.9
Δ Soil moisture	-18.5	-12.8	-15.4	-10.4	-18.6
Δ Soil upper zone	-5.8	-6.1	-6.0	-5.5	-5.8
Δ Soil lower zone	527.2	359.4	403.3	397.5	550.2

6. CONCLUSION AND RECCOMENDATION

6.1. CONCLUSION

In this study, considerable differences between *in situ* observations and satellite meteorological products were found present as it has been reported in several previous studies.
Four satellite products CMORPH 8km, RFE 2.0 and TRMM 3B42 v7 and FEWSNET PET were assessed in this study. The systematic differences found in these products were corrected based to *in situ* measurements before being used as forcing data in stream flow simulation in the HBV-light model.
The *in situ* data were collected from 21 stations in or at close distance to Nyabarongo basin, one relatively well gauged basin in Rwanda.

The satellite based rainfall product were found to underestimate the depth of rainfall compared to the *in situ* measurements. CMORPH 8km was found to have a larger bias error with an overall of 0.67 and a mean error up to -1mm/day. Although TRMM 3B42 v7 revealed a slightly better performance in retrieving quantities of rainfall during the timeslot selected, (0.78 of bias and 0.73mm/day of mean error), it exposed a weak correlation with the *in situ* data than the other products as indicated by the overall values of R^2 (0.5%) and RMSE (9mm/day).

These biases could be due to the mechanisms of the generation, but also to errors linked to the spatial and temporal discretization during meteorological variables estimation from space. Nonetheless in situ measurements are not exempt of inherent errors as well.
Whereas all the rainfall bias components significantly contribute to the total bias, most of the bias was due to the missed rain bias. This can be explained by the complex topography of the study area as orographic rainfall effects are not included in RFE as reported by Thiemig et al.(2012) and Dinku et al.(2010) for the CMORPH and TRMM performances over mountainous regions.
The rainfall occurrence detection in Nyabarongo basin was analyzed and as results, the Critical Success Index (CSI), which typically combines information from the Probability of Detection (POD) and the False Alarm Ratio (FAR) found below 0.5 for the 3 satellite based rainfall products.

The systematic errors found in the satellite rainfall products were corrected. In this way, the time variant bias correction scheme was applied, for a sequential time window of 7 days, to the areal rainfall representation for each of the 3 sub-basins of Nyabarongo.
The data retrieved from FEWSNET PET product were also corrected following the same scheme, as the product assessment through the statically analysis revealed systematic errors and weak correlation with *in situ* data. In short, the overall bias was found varying between 0.8 and 1.4. Except for one station, FEWSNET was found overestimating the quantities of PET comparing to the *in situ* data. The agreement with the *in situ* data indicated a R^2 of 6.5%.

For all the products, the bias corrected time series showed resemblance to the *in situ* time series, and yet underestimation of the measurements was observed, when accumulated over the entire period. These bias corrected satellite products and the *in situ* time series were used for daily stream flow modelling of Nyabarongo River, in HBV model for the period of 19 months (March 2012- September 2013).

Initially, HBV model was calibrated using the *in situ* meteorological inputs data, and model parameter sensitivity analysis was carried out using the same *in situ* time series to identify sensitive model parameter for a more thorough optimization. In summary, the PART parameter, which controls the recharge portion conveyed to the groundwater, was found to be the most sensitive model parameter. However the stream flow measurements were not sufficient for the validation of the model.

Very good results were obtained from the model calibration for Nyabarongo stream flow simulations in HBV-light. Since, for *in situ* measurements, the goodness of fit functions of 0.958 for the NSE and a RVE of -0.019 were obtained after calibration. Furthermore, the optimized model parameter set was used for simulations using bias corrected meteorological variables. Best results were found when the bias corrected FEWSNET PET input data replaces the *in situ* measured PET in the model (NSE at 0.95 and RVE at 1.344) and among the rainfall products, it was the bias corrected TRMM 3B42 v7 data with NSE at 0.89 and RVE at -4.787.

The uncorrected satellite based meteorological data was used to simulate Nyabarongo stream flow and the hydrological model failed to capture the observed hydrograph patterns and volumes when the optimized parameter set from *in situ* time series was used. Therefore, prior to that parameter set, for each uncorrected satellite product dataset, a calibration was done in HBV for the most sensitive model parameters to achieve a higher model performance. Still, the model results showed weak performances with small values of the NSE (below 0.5) and a high RMSE values, except for the FEWSNET PET product with a NSE reduced to 0.91 and a RVE of -3.548.

6.2. RECOMMENDATIONS

- The study accentuates on the importance of assessing and correcting the systematic errors residing in the satellite based meteorological products, before use in any hydrological application. As this study assessed the satellite based meteorological products for a period of 5 years, further studies should assess the seasonal variability of these meteorological variables in the satellite products over the basin.

- The number of meteorological gauge stations should be increased in the country, especially for PET estimates. It is also recommended to install more automated water level gauge stations in the basin, since most of the manually recorded water levels of the Nyabarongo River were found unreliable for the use in streamflow modelling.

- Due to limited availability of gauged stream flow data in Nyabarongo basin, only the downstream sub-basin was calibrated in HBV model. Therefore, a regionalization should be applied in reference to other gauged catchments surrounding the two left sub-basins, in order to find their physical catchments characteristics for streamflow quantification purposes.

- The calibration of HBV-light resulted in particularly good model performances for Nyabarongo basin stream flow simulation, especially when *in situ* measurements are used as forcing inputs. Despite that, model validation using different hydrological stress conditions is recommended in order to prove the reliability of the model.

LIST OF REFERENCE

Artan, G., Gadain, H., Smith, J. L., Asante, K., Bandaragoda, C. J., & Verdin, J. P. (2007). Adequacy of satellite derived rainfall data for stream flow modeling. *Natural Hazards*, *43*(2), 167–185. doi:10.1007/s11069-007-9121-6

Barbalho, F. D., Silva, G. F. N. da, & Formiga, K. T. M. (2014). Average Rainfall Estimation: Methods Performance Comparison in the Brazilian Semi-Arid. *Journal of Water Resource and Protection*, *06*(02), 97–103. doi:10.4236/jwarp.2014.62014

Bell, T. L., & Reid, N. (1993). Detecting the Diurnal Cycle of Rainfall Using Satellite Observations. *Journal of Applied Meteorology*, *32*(2), 311–322. doi:10.1175/1520-0450(1993)032<0311:DTDCOR>2.0.CO;2

Beven, K. J. (2011). *Rainfall-Runoff Modelling The Primer* (2nd ed., pp. 1–49). West Sussex: Wiley-Blackwell.

Bizimana, J. P., & Schilling, M. (2010). Geo-Information Technology for Infrastructural Flood Risk Analysis in Unplanned Settlements: A Case Study of Informal Settlement Flood Risk in the Nyabugogo Flood Plain, Kigali City, Rwanda. In P. S. Showalter & Y. Lu (Eds.), *Geospatial Techniques in Urban Hazard and Disaster Analysis*. Dordrecht: Springer Netherlands. doi:10.1007/978-90-481-2238-7

Brutsaert, W. (2005). *Hydrology: An Introduction* (pp. 21–151). New York: Cambridge University Press.

DHV Consultants BV & Delft Hydraulics with Halcrow, Tahal, Ces, O. & J. (1999a). *How to correct and complete rainfall data*. New Delhi.

DHV Consultants BV & Delft Hydraulics with Halcrow, Tahal, Ces, O. & J. (1999b). *How to establish stage discharge rating curve* (p. 43). New Delhi. Retrieved from http://www.cwc.nic.in/main/HP/download/29 HOW TO ESTABLISH STAGE DISCHARGE RATING CURVE.pdf

Dinku, T., Ceccato, P., Grover-Kopec, E., Lemma, M., Connor, S. J., & Ropelewski, C. F. (2007). Validation of satellite rainfall products over East Africa's complex topography. *International Journal of Remote Sensing*, *28*(7), 1503–1526. doi:10.1080/01431160600954688

Dinku, T., Connor, S. J., & Ceccato, P. (2010). Comparison of CMORPH and TRMM-3B42 over Mountainous Regions of Africa and South America. In M. Gebremichael & F. Hossain (Eds.), *Satellite Rainfall Applications for Surface Hydrology* (pp. 193–204). New York: Springer Netherlands. doi:10.1007/978-90-481-2915-7_11

Duan, Q., & Gupta, V. (1992). Effective and Efficient Global Optimization for Conceptual Rainfall-Runoff Models. *Water Resources Research*, *28*(4), 1015–1031. doi:10.1029/91WR02985

Ebert, E. E. (2010). Neighborhood Verification of High Resolution Precipitation Products. In M. Gebremichael & F. Hossain (Eds.), *Satellite Rainfall Applications for Surface Hydrology* (pp. 127–143). Melbourne: Springer Netherlands. doi:10.1007/978-90-481-2915-7_8

Ebert, E. E., Janowiak, J. E., & Kidd, C. (2007). Comparison of Near-Real-Time Precipitation Estimates from Satellite Observations and Numerical Models. *Bulletin of the American Meteorological Society*, *88*(1), 47–64. doi:10.1175/BAMS-88-1-47

ENTREM Ltd. (2012). *Feasibility Study for the Rehabilitation of Yanze Watershed* (p. 137). Kigali.

Gleick, P. H. (2000). A Look at Twenty-first Century Water Resources Development. *Water International*, *25*(1), 127–138. doi:10.1080/02508060008686804

Gupta, S. K. (2010). *Modern Hydrology and Sustainable Water Development. Chapter 5: Surface and groundwater flow modelling* (1st ed., pp. 20–63). Hoboken: Wiley. Retrieved from http://ezproxy.utwente.nl:2163/patron/FullRecord.aspx?p=792631

Habib, E., Haile, A. T., Sazib, N., Zhang, Y., & Rientjes, T. (2014). Effect of Bias Correction of Satellite-Rainfall Estimates on Runoff Simulations at the Source of the Upper Blue Nile. *Remote Sensing*. doi:10.3390/rs60x000x

Herman, A., Kumar, V. B., Arkin, P. A., & Kousky, J. V. (2010). Objectively determined 10-day African rainfall estimates created for famine early warning systems. Retrieved from http://www.tandfonline.com/doi/abs/10.1080/014311697217800#.VKp32CvF8m0

Huffman, G. J., Adler, R. F., Bolvin, D. T., & Nelkin, E. J. (2010). The TRMM Multi-Satellite Precipitation Analysis (TMPA), 3–22. doi:10.1007/978-90-481-2915-7

Joyce, R. J., Jonowiak, J. E., Arkin, P. A., & Xie, P. (2004). CMORPH : A Method that Produces Global Precipitation Estimates from Passive Microwave and Infrared Data at High Spatial and Temporal Resolution. doi:10.1175/1525-7541

Kidd, C., & Kniveton, D. (2003). Satellite rainfall estimation using combined passive microwave and infrared algorithms. *Journal of* …, 1088–1104. doi:10.1175/1525-7541

Kummerow, C., & Giglio, L. (1994). A Passive Microwave Technique for Estimating Rainfall and Vertical Structure Information from Space. Part I: Algorithm Description. *Journal of Applied Meteorology*, *33*(1), 3–18. doi:10.1175/1520-0450(1994)033<0003:APMTFE>2.0.CO;2

Levizzani, V. (2003). Satellite rainfall estimates: new perspectives for meteorology and climate from the EURAINSAT project. *Annals of Geophysics*, *46*(April). Retrieved from http://www.earth-prints.org/handle/2122/947

Levizzani, V., Schmetz, J., Lutz, H. J., Kerkmann, J., Alberoni, P. P., & Cervino, M. (2001). Precipitation estimations from geostationary orbit and prospects for METEOSAT Second Generation. *Meteorological Applications*, *8*(1), 23–41. doi:10.1017/S1350482701001037

Lindström, G., Johansson, B., Persson, M., Gardelin, M., & Bergström, S. (1997). Development and test of the distributed HBV-96 hydrological model. *Journal of Hydrology*, *201*(1-4), 272–288. doi:10.1016/S0022-1694(97)00041-3

Maathuis, B., & Mannaerts, C. (2012). *In Situ and Online Data Toolbox*. University of Twente, Enschede. Retrieved from http://www.itc.nl/library/Papers_2012/general/ISOD_Toolbox.pdf

Maathuis, B., & Mannaerts, C. (2013). *In Situ and Online Data Toolbox*. University of Twente.

Mikova, K., Wali, U. G., & Nhapi, I. (2010, March 15). Infilling of Missing Rainfall Data from a Long Term Monitoring Records. *International Journal of Ecology & Development™*. Retrieved from http://www.ceser.in/ceserp/index.php/ijed/article/view/411

Moazami, S., Golian, S., Hong, Y., Sheng, C., & Kavianpour, M. R. (2014). *Comprehensive evaluation of four high-resolution satellite precipitation products over diverse climate conditions in Iran*. *Hydrological Sciences Journal* (p. 141217125340005). doi:10.1080/02626667.2014.987675

Nash, J. E., & Sutcliffe, J. V. (1970). River Flow Forecasting Through Conceptual Models Part I - A Discussion of Principles*. *Journal of Hydrology*, *10*, 282–290. doi:10.1016/0022-1694(70)90255-6

Nurmi, P. (2003). *Recommendation on the verification of local weather forecasts*. Retrieved from http://www.eumetcal.org/resources/ukmeteocal/temp/msgcal/www/english/msg/library/TechnicalMemorandum430.pdf

RCMRD-SERVIR Africa. (2013). *Land Cover Mapping For Green House Gas Inventories Development Project in East and Southern Africa Region*. Kigali.

Rientjes, M. (2014). *Modelling in Hydrology*. University of Twente, Enschede.

Searcy, J. K., & Hardison, C. H. (1960). Double-Mass Curves. *WaterSupply Paper 1541B*, 66. doi:http://udspace.udel.edu/handle/19716/1592

Seibert, J. (2005). *HBV Light User ' s Manual*. Stockholm University. Retrieved from http://people.su.se/~jseib/HBV/HBV_manual_2005.pdf

Seibert, J., & Vis, M. J. P. (2012). Teaching hydrological modeling with a user-friendly catchment-runoff-model software package. *Hydrology and Earth System Sciences*, *16*, 3315–3325. doi:10.5194/hess-16-3315-2012

SHER Ingénieurs-Conseils s.a. (2012). *Rwanda National Water Resources Master Plan-Exploratory Phase Report* (p. 263). Kigali.

Solomatine, D. P., & Shrestha, D. L. (2009). A novel method to estimate model uncertainty using machine learning techniques. *Water Resources Research*, *45*(12), n/a–n/a. doi:10.1029/2008WR006839

Sun, Z., Gebremichael, M., Ardö, J., Nickless, A., Caquet, B., Merboldh, L., & Kutschi, W. (2012). Estimation of daily evapotranspiration over Africa using MODIS/Terra and SEVIRI/MSG data. *Atmospheric Research*, *112*, 35–44. doi:10.1016/j.atmosres.2012.04.005

Thiemig, V. (2014). *The development of pan-African flood forecasting and the exploration of satellite-based precipitation estimates* (Utrecht St., p. 131). Ispra: CPI-W¨ohrmann Print Service, Zutphen.

Thiemig, V., Rojas, R., Zambrano-Bigiarini, M., Levizzani, V., & De Roo, A. (2012). Validation of Satellite-Based Precipitation Products over Sparsely Gauged African River Basins. *Journal of Hydrometeorology*, *13*(6), 1760–1783. doi:10.1175/JHM-D-12-032.1

Wagner, S., Kunstmann, H., Bárdossy, A., Conrad, C., & Colditz, R. R. (2009). Water balance estimation of a poorly gauged catchment in West Africa using dynamically downscaled meteorological fields and remote sensing information. *Physics and Chemistry of the Earth, Parts A/B/C*, *34*(4-5), 225–235. doi:10.1016/j.pce.2008.04.002

APPENDIX

Appendix 1: Agro-climatic zones in Rwanda

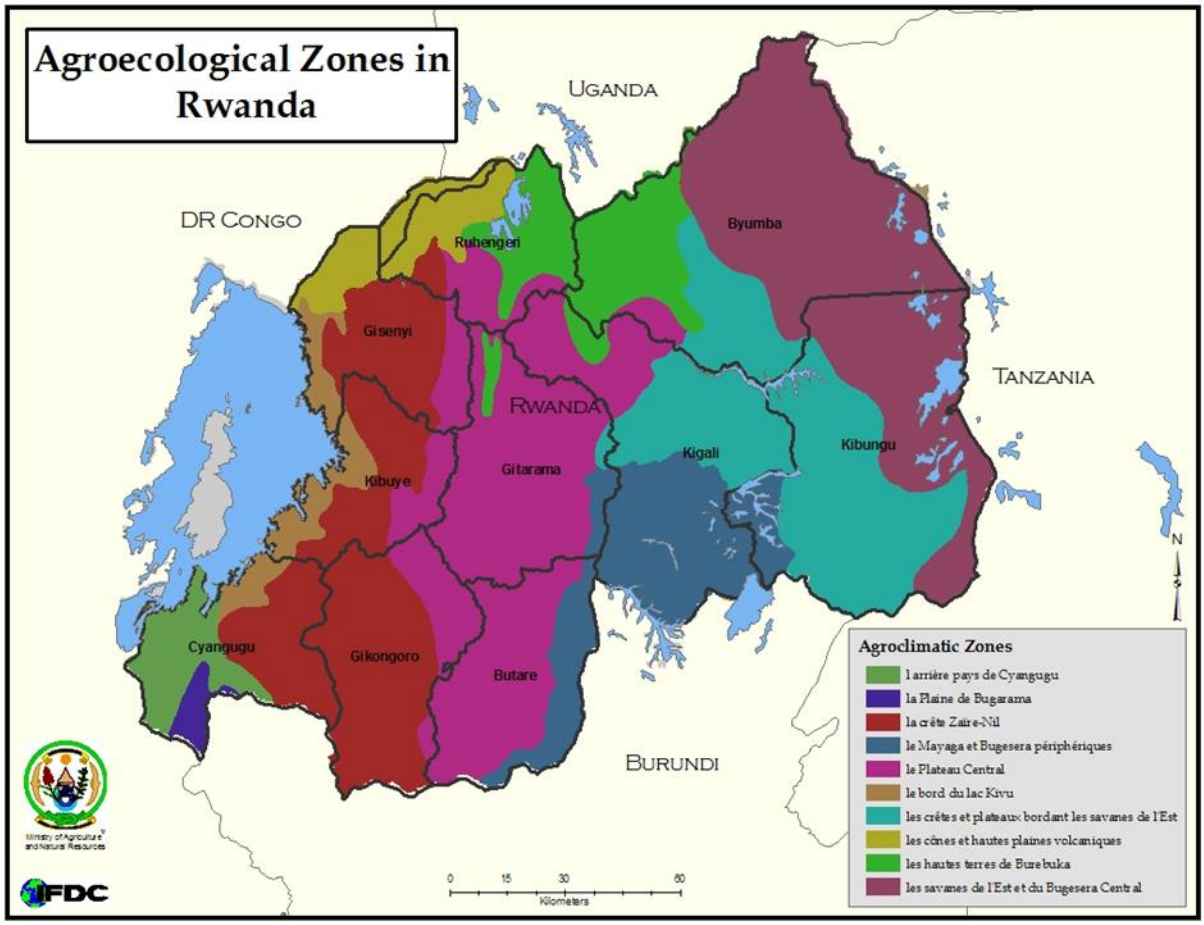

Appendix 2: Weighting of meteorological stations in Nyabarongo basin

Station ID	Station Name	Rainfall station weight in the basin		Temperature station weight in the basin		Evaporation station weight in the basin	
		Polygon Area (m^2)	Weight in the basin	Polygon Area (m^2)	Weight in the basin	Polygon area (m^2)	Weight in the basin
1	KAWANGIRE	628750000	0.074119	714750000	0.0843487		
2	JANJA	381250000	0.044943				
3	BUTARO	210500000	0.024814				
4	MUGANZA	39000000	0.004597				
5	RUBONA_COLLINE	294000000	0.034658				
6	BYIMANA	1098750000	0.129524	1194000000	0.1409057		
7	GIKONGORO_MET	1108750000	0.130703	1412750000	0.1667208	2553000000	0.301257
8	NYAGAHANGA_EFA	215750000	0.025433				
9	KIGALI_AERO	236250000	0.027850	1055250000	0.1245316	2959250000	0.349195
10	CYINZUZI	677500000	0.079866				
11	MURAMBA PAROISSE	552250000	0.065101	1354000000	0.1597876		
12	BYUMBA_ MET	124000000	0.014617	998750000	0.1178640		
13	BUSOGO_ISAE	311750000	0.036750	391000000	0.0461425	1645500000	0.194171
14	GITEGA	557000000	0.065661				
15	NEMBA	347000000	0.040905				
16	RUKOZO	318250000	0.037516				
17	RUBENGERA_MET	514250000	0.060621	525000000	0.0619560		
18	KABAYA	329250000	0.038813				
19	NTARUKA	250000000	0.029471				
20	RUHENGERI_AERO	288750000	0.034039	828250000	0.0977430	1234500000	0.145672
21	GISENYI_AERO					82250000	0.009706

Appendix 3: Rating Curve Double Logarithmic Plot for optimized *a* parameter (a=-1.7)

Appendix 4: Sampling time window lengths considered for bias correction of Satellite products

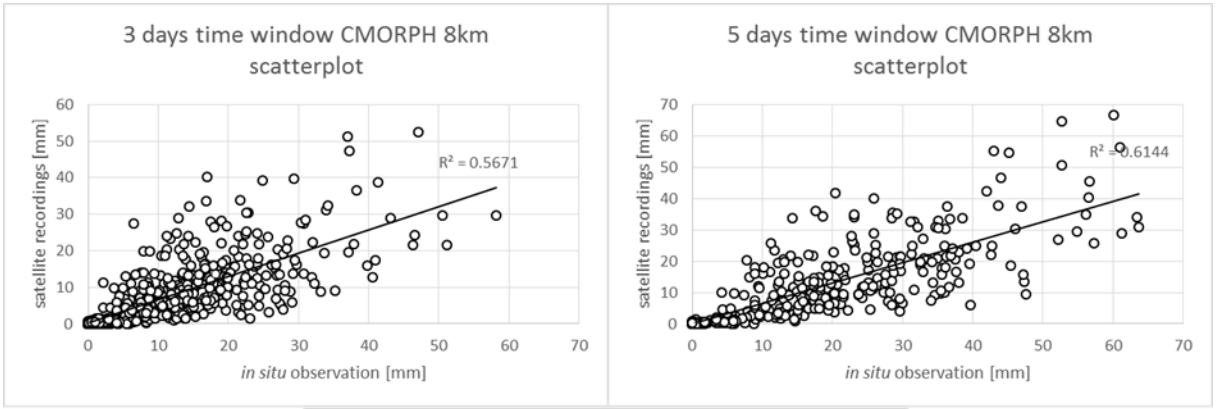

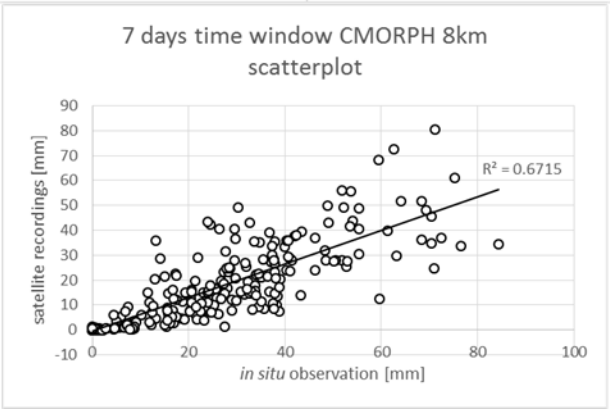

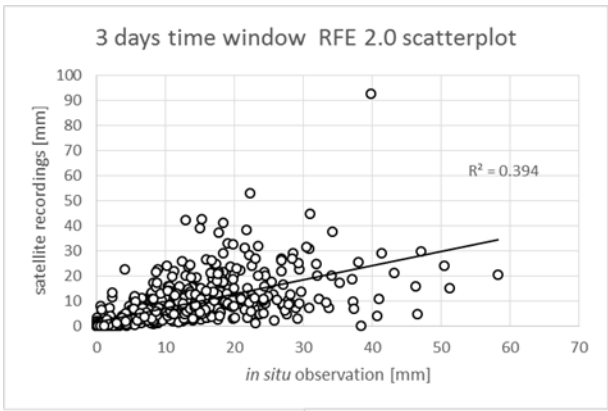

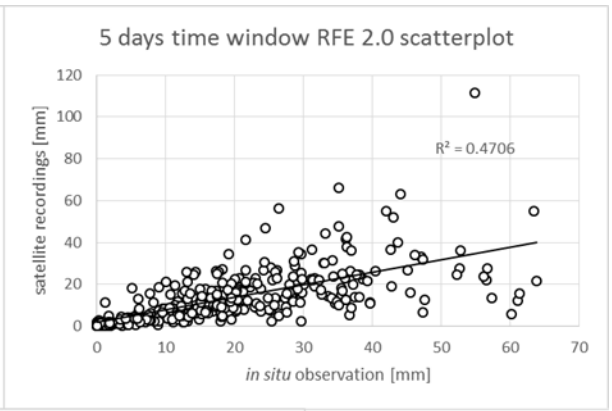

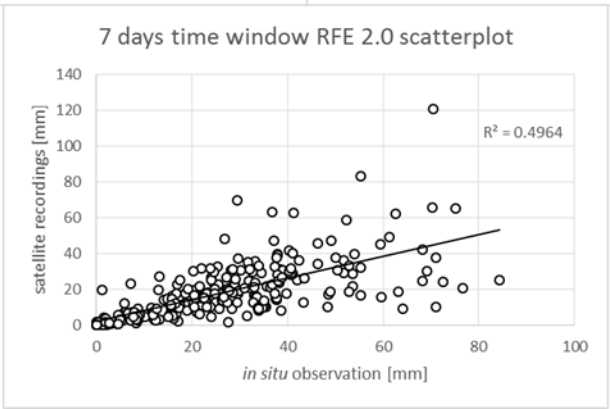

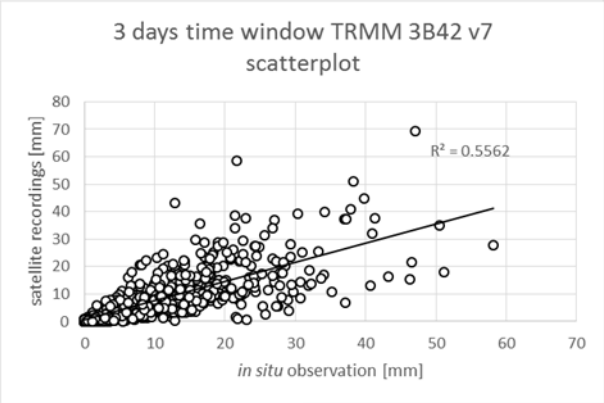
3 days time window TRMM 3B42 v7 scatterplot
satellite recordings [mm]
in situ observation [mm]
R² = 0.5562

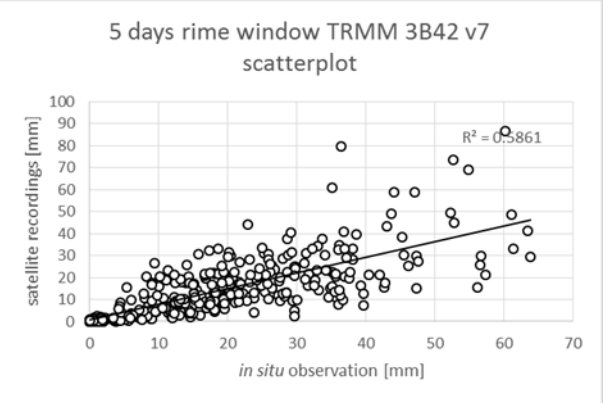
5 days rime window TRMM 3B42 v7 scatterplot
satellite recordings [mm]
in situ observation [mm]
R² = 0.5861

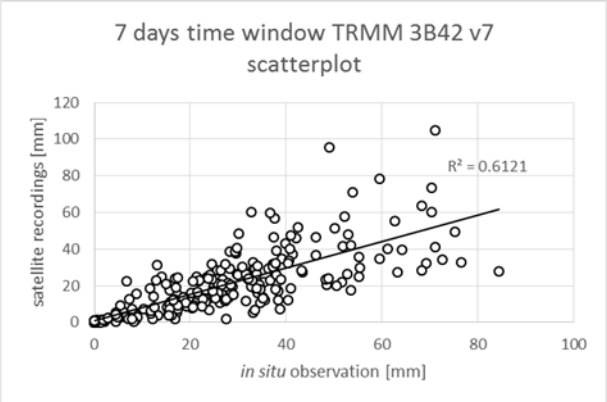
7 days time window TRMM 3B42 v7 scatterplot
satellite recordings [mm]
in situ observation [mm]
R² = 0.6121

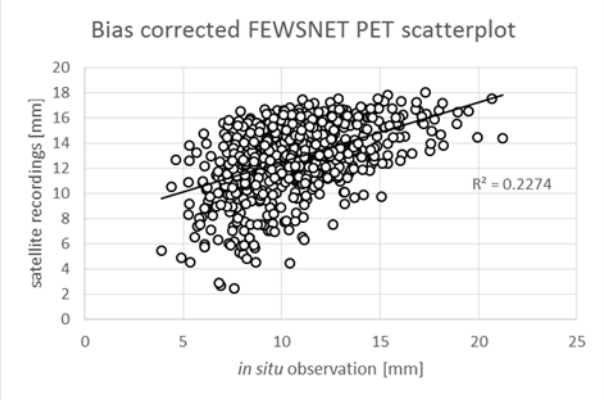
Bias corrected FEWSNET PET scatterplot
satellite recordings [mm]
in situ observation [mm]
R² = 0.2274

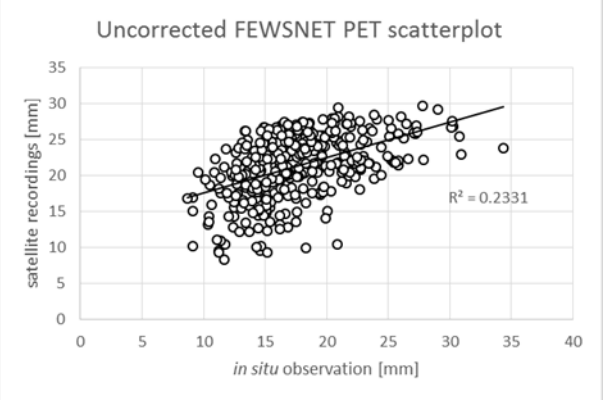
Uncorrected FEWSNET PET scatterplot
satellite recordings [mm]
in situ observation [mm]
R² = 0.2331

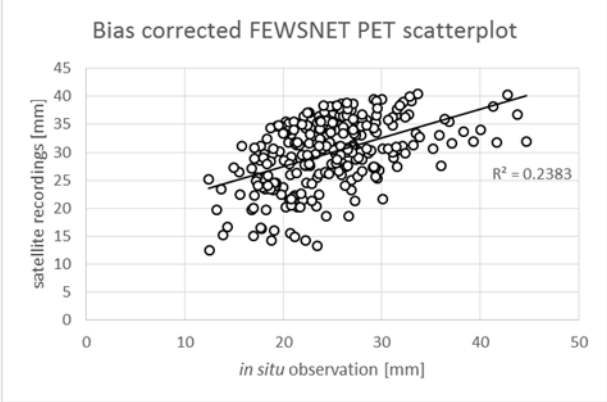
Bias corrected FEWSNET PET scatterplot
satellite recordings [mm]
in situ observation [mm]
R² = 0.2383

Appendix 5: Scatterplots and Double mass curve of satellites meteorological products and *in situ* measurements in Nyabarongo basin

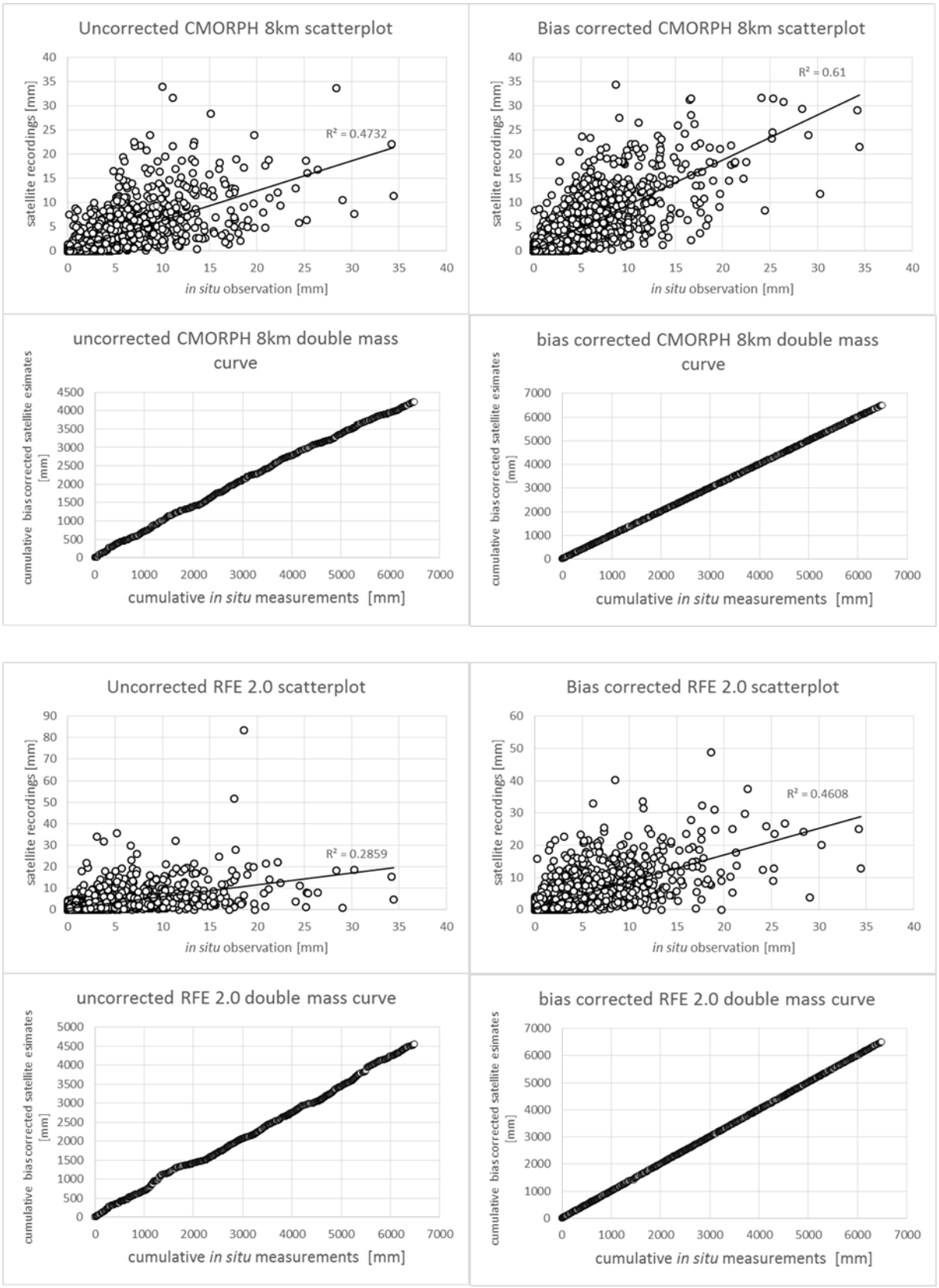

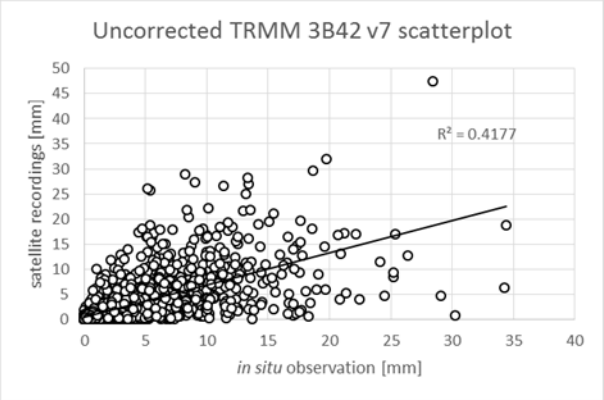
Uncorrected TRMM 3B42 v7 scatterplot
satellite recordings [mm]
in situ observation [mm]
R² = 0.4177

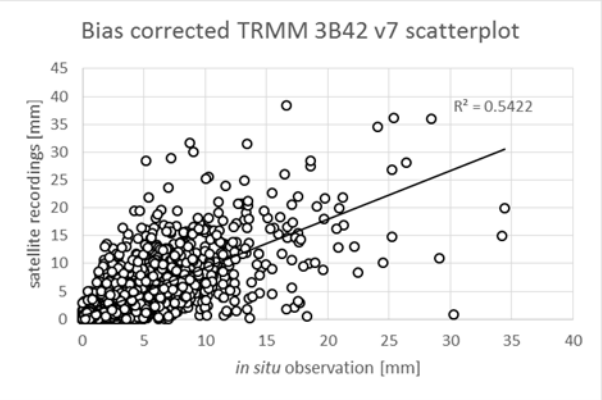
Bias corrected TRMM 3B42 v7 scatterplot
satellite recordings [mm]
in situ observation [mm]
R² = 0.5422

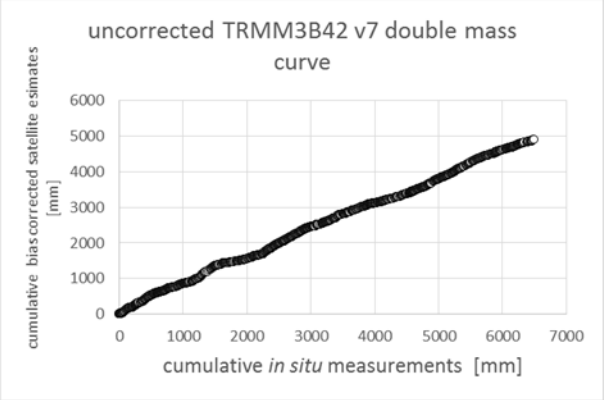
uncorrected TRMM3B42 v7 double mass curve
cumulative bias corrected satellite esimates [mm]
cumulative in situ measurements [mm]

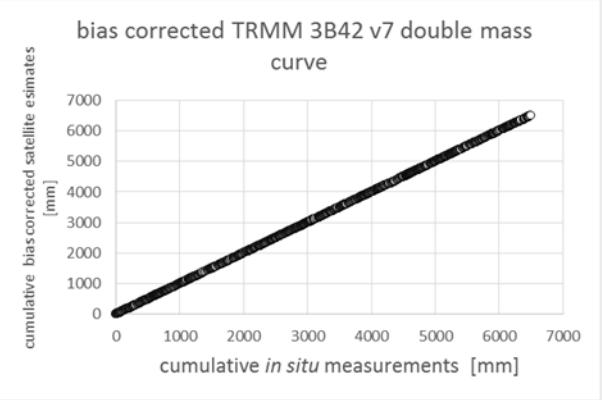
bias corrected TRMM 3B42 v7 double mass curve
cumulative bias corrected satellite esimates [mm]
cumulative in situ measurements [mm]

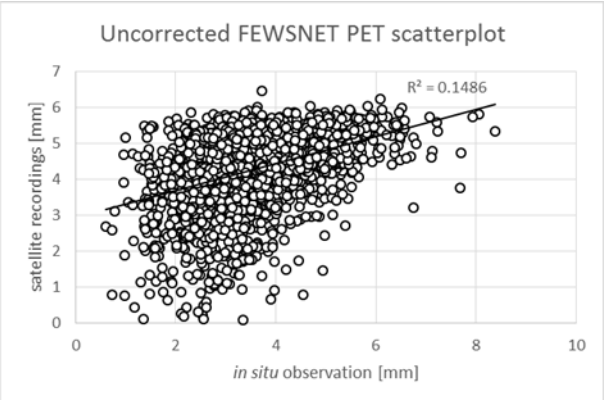
Uncorrected FEWSNET PET scatterplot
satellite recordings [mm]
in situ observation [mm]
R² = 0.1486

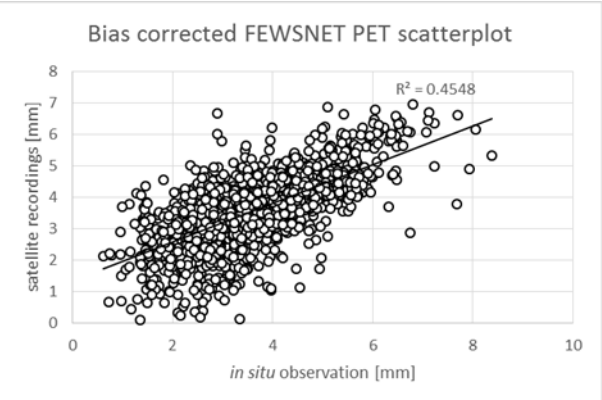
Bias corrected FEWSNET PET scatterplot
satellite recordings [mm]
in situ observation [mm]
R² = 0.4548

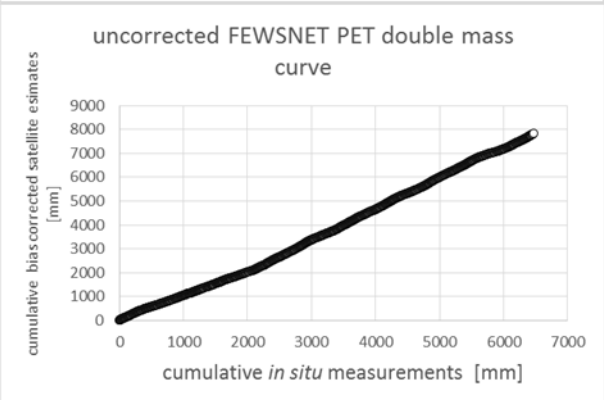
uncorrected FEWSNET PET double mass curve
cumulative bias corrected satellite esimates [mm]
cumulative in situ measurements [mm]

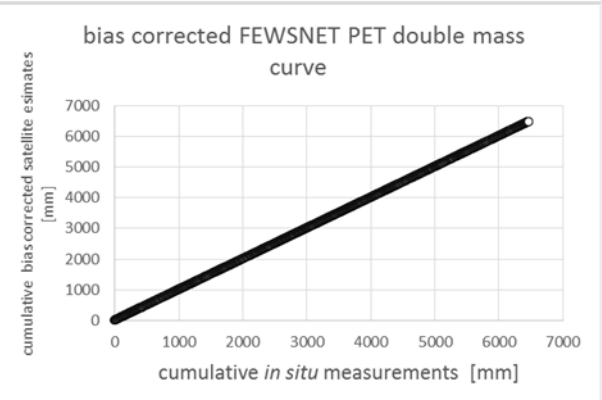
bias corrected FEWSNET PET double mass curve
cumulative bias corrected satellite esimates [mm]
cumulative in situ measurements [mm]